ISSN 1068-3755, Surface Engineering and Applied Electrochemistry, 2008, Vol. 44, No. 4, pp. 253–256. © Allerton Press, Inc., 2008.
Original Russian Text © A.P. Malyushevskaya, P.P. Malyushevskii, 2008, published in Elektronnaya Obrabotka Materialov, 2008, No. 4, pp. 4–8.

ELECTRICAL PRECISION TREATMENT OF MATERIALS

Electrodischarge Cavitation Intensification in the Processes of Fibrous Material Treatment

A. P. Malyushevskaya and P. P. Malyushevskii

Institute of Pulse Processes and Technologies, National Academy of Sciences of Ukraine, pr. Oktyabr'skii 43-a, Nikolaev, 54018 Ukraine

E-mail: iipt@iipt.com.ua

Received January 31, 2008

Abstract—The results of experimental research of the method of electrodischarge cavitation at interaction of electric explosions in parallel discharge gaps are represented. The practical use of electrodischarge cavitation for activation of the processes of waste paper processing for application in preparation of qualitative gypsum–concrete products is proposed.

DOI: 10.3103/S1068375508040017

For some time, studies focused on the enhancement of the application of the electrodischarge treatment method for activation and regeneration of fibrous materials used for different purpose, including those used in structural engineering, have been carried out. It is found that, in this application, the electrodischarge method contributes to an efficient process of splitting and fiber separation in wastes of cardboard and paper; it allows obtaining of activated pulp applicable for tempering of gypsum–concrete solutions in the production of gypsum–concrete separating slabs and other products. It is necessary to emphasize the possibility to control the required final product fractional yield with minimization of the overgrinding, maximum activation, and stability for the obtained solutions. However, the control of electrodischarge treatment of paper–cardboard wastes requires further improvement, as well as the electrodischarge method of treatment of low-dimensional objects in general.

At the same time, it is necessary to solve a number of problems for the building industry attributed to the determination of the efficiency of discharge–pulse technology application in operations of raw material preparation, especially for recycled materials and industrial wastes. This would allow significant enlargement of the raw–material base of the corresponding branches with a simultaneous increase of the quality and operational characteristics of the prepared products.

Fibrous materials used in production of textile, thermal insulation materials, fiberglass products, in the papermaking industry, etc., consist of single fibers with cross dimensions of 1–50 μm. In the process of production of these low-dimensional fibers or products of them, they may be subjected to pulse treatment for modification, activation, coloring, or decontamination [1]. In these cases, the frontage of the acting compression waves must correspond to the cross dimensions of the treatment object; the primary shockwave, even of low-power electric explosions, has a leading edge that exceeds the fiber cross dimensions by a factor of 10–100.

METHODIC PRINCIPLES

Earlier there was proposed a method for transformation of broad shock fronts into short ones, which is applicable for the treatment of low-dimensional objects [2], due to excitation of bulk cavitation by tensile waves, which are formed at reflection of electrodischarge shockwaves. The given paper presents data on the development of the electrodischarge method for separation of fibers of paper–cardboard wastes and preparation of activated binding agent tempering solutions on their basis. The following types of paper-making industry wastes were selected as the research object: paper waste (newsprint fibers), industrial writing paper, and high-quality drawing paper (Whatman paper).

The initial operating environment in the studied electrodischarge reactors was main water with a resistivity of 8–10 Ohm m. The experiments were carried out in chamber-type electrodischarge reactors of different volumes; their characteristic feature was a coupled electrode system (see Fig. 1). A surge–current generator ensured series connection of a couple of electrode gaps or of a single discharge gap at identical energy in the pulse. The series connection allowed strict synchronism of all the stages of the electric explosions in the parallel discharge gaps. The following parameters of the external discharge circuit were set constant: the operation voltage U_0 = 50 kV, the inductance $L = 4 \times 10^{-6}$ H, and the pulse repetition frequency f = 1 and 2 Hz. The following parameters were variable: the unit pulse energy E_0 = 1.25–2.5 kJ, the interelectrode discharge gap length l_p = 40–60 mm, the solid percentage

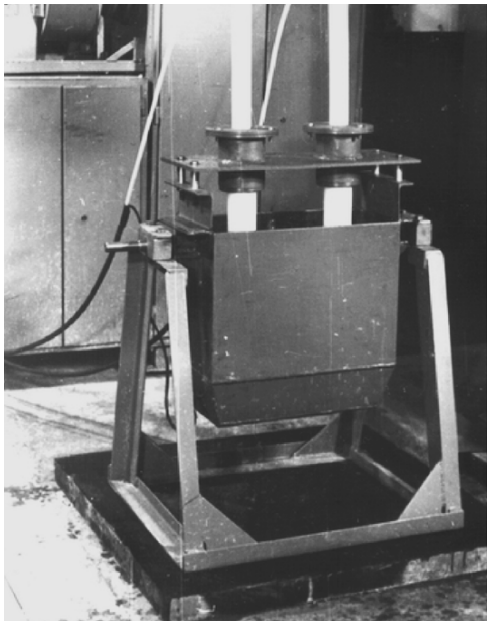

Fig. 1. General view of the electrodischarge two-electrode chamber.

in the liquid phase (in terms of bulk) was selected to be 1–5, and the time of the unit bulk treatment $\tau = 2$–15 min.

The optimization parameter was selected to be the stability of the colloid system obtained as a result of the treatment, its degree being determined according to the bottom settling in the measuring cylinder. Visual examination of the obtained fibers was carried out by means of a biological MBI-3 microscope. The checking points were photographed for subsequent analysis.

Separated fibers of paper-making industry wastes in the form of activated pulp were used for obtaining of reference samples of the building products. Herein, a gypsum binding agent of the G-4 and G-5 grades was used as the cementing component. Studies on obtaining of lightened gypsum rock were carried out with introduction of electrodischarge-activated paper suspension (pulp) of various concentrations as "tempering water" into gypsum. Checking and test samples were prepared by the techniques of GOST 6428-83; the properties of the gypsum dough and rock were measured according to the same requirements.

The following was applied for the measurements: a slide-wire bridge R-38 with a flask Kh-38, a Suttard viscosimeter, a Vicat apparatus, a stopwatch timer, scales, forms for preparation of the test beams, pressure plates for compression testing of the beams, supports for the bending test of the beams, a graduated jar, and a drying box.

The power losses at the prebreakdown stage of the electric discharge significantly depend on the environment conductivity. Therefore, the research objects were divided into two groups. The first group, which does not contain a chemical component capable of leaching at treatment in water, is writing paper and Whatman paper; the second group, which consists of materials capable of leaching various soluble chemical substances in water, is newspaper waste with chemical components of printing black.

As is shown in [1, 2], the main contribution to the process of electrodischarge dispersion of low-dimensional initial particles in water is made by nonlinear bulk cavitation. Paper, being cellulose fibers compacted in a certain manner, in the course of watering and underwater discharge exposure looses at first, then separation of the fibers takes place. From this moment on, the main operation of cavitation begins in the whole reactor volume.

Therefore, taking into account [3], for the study of the processes of electrodischarge fiber separation and activation of the obtained pulp, energetically identical modes of the initial paper stock treatment with discharge series were compared: separate ones in a single discharge gap (the weak-cavitation mode, or WC) and in a couple of the same discharge gaps connected in parallel in similar discharge circuits (strong-cavitation mode, or SC). Herein, the identical total energy was released at each pulse in both the single discharge gap and the couple of discharge gaps. The SC mode of the electrodischarge treatment is provided by interaction of synchronously parting (at joining) walls of afterdischarge cavities, which form a dynamic zone of decreased pressure between two parallel discharge gaps.

OPTIMUM TREATMENT MODE SELECTION

The criterion of optimization was the stability of the disperse system depending on the degree of the paper fiber separation. Here, an appreciable influence of the energy stored in the capacitor on the process was found. As this value increased, the exposure process proceeded more efficiently; therefore, for the further studies, the energy in the pulse was fixed on the upper level.

Now, four parameters remain variable: the interelectrode gap value, the solid phase concentration in the suspension, the treatment time or the number of exposure pulses (at constant pulse repetition frequency), and the treatment mode cavitation level (weak or strong). At the initial stage, the value of the interelectrode discharge gap was found to be 50 and 40 mm for the first and second groups of materials, respectively. It was difficult to optimize level of the remaining variable factors, because it is unknown how the concentration and dispersion of the solid phase of the obtained suspension influence the physicomechanical properties of gypsum rock. There appeared the necessity to carry out two additional research stages: determination of the dependence of the stability degree in suspensions of different concentrations on the treatment time (the total pulse energy consumed for the treatment) and the determination of variations in the physicomechanical characteristics of the gypsum rock formed on different tempering suspensions.

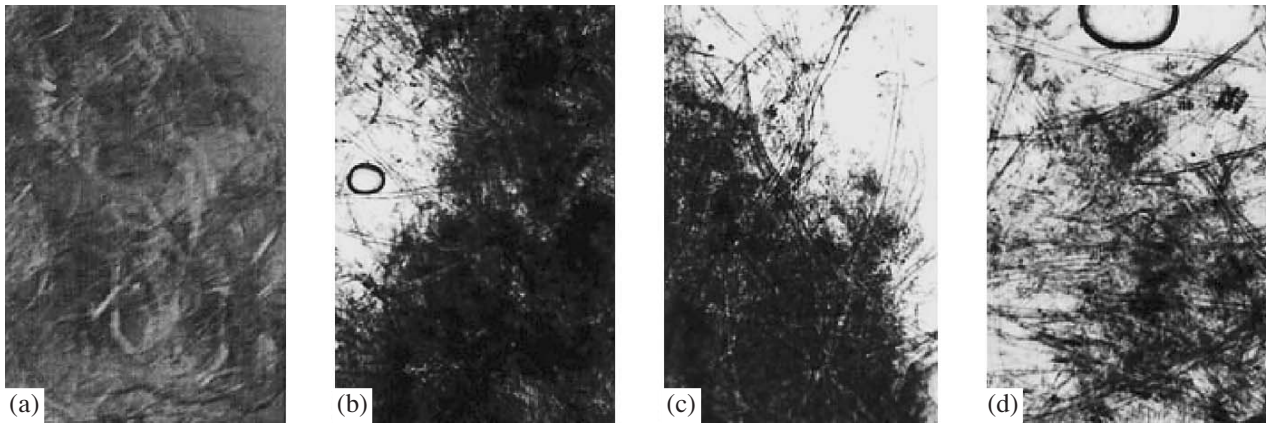

Fig. 2. Samples of electrodischarge separation of fibers of paper wastes: (a) treatment for 3 min, WC mode; (b) treatment for 5 min, WC mode; (c) treatment for 7 min, WC mode; (d) treatment for 1.5 min, SC mode.

STABILITY OF THE OBTAINED SUSPENSIONS

In proportion to the disintegration and separation of the fibers of paper wastes, the increase in the number of solid phase particles and their interaction with the water determine the degree of the suspension stability. One can see the interrelation between the system stability and the degree of solid phase disintegration into separate particles.

The dispersion dynamics are observed at all the process stages. At first, there occurs splitting of large pieces into smaller ones, and then another process begins at once—final fluffing of the material particles to fibers. Then, dispersion is observed in the boundary zone between the paper pieces that have not been split yet and cellulose fibers that have been already fluffed. This is the place where the most importance role of electrodischarge cavitation is shown, as one can see from Fig. 2, which illustrates the results of the paper waste treatment with identical energy in the pulse and ceteris paribus, except for the characteristic of cavitation modes.

The simplest analysis of these experimental materials allows stating that the SC mode, which is achieved by parallel connection of discharge gaps and which ensures proper interaction of pulsing afterdischarge cavities [3], is undoubtedly advantageous.

The test of the stability of the suspensions obtained in modes a, b, c, and d has shown that settling of the "a-suspension" took place after 12 h with water isolation in the upper part of the graduated jar up to 20% of the total volume; settling of the "b-suspension" occurred after 48 h with water isolation up to 10%; settling of the "c-suspension" became apparent only in the fifth day of the retention. It should be noted in particular that the "d-suspension" had a homogeneous structure even after 25 days of retention.

PHYSICOMECHANICAL CHARACTERISTICS OF THE GYPSUM ROCK USING DIFFERENT TEMPERING SUSPENSIONS

The studies determined the dependence of the variation of the physicomechanical characteristics of the gypsum rock at gypsum tempering with suspensions of various concentrations and the change of the suspension-to-gypsum ratios.

One of the basic criteria for preparation of cast mixtures is the flowability of the gypsum dough. The standard consistence was determined at the gypsum binding agent tempering with water and water–cellulose suspensions of various concentrations by means of a Suttard viscosimeter by the standard technique. These experiments made it possible to determine the influence of the colloidal cellulose contained in the suspension (1.5–4.5%) on the variation of the gypsum dough flowability. As the colloidal cellulose in the tempering suspension increases, the gypsum dough flowability appreciably decreases; the higher the concentration, the more appreciable the decrease.

A comparative analysis of the setting time for the gypsum dough prepared depending on the water and various suspensions was made. For gypsum of the G-5 grade, at tempering with water, the initial setting time is 8 minutes; the final setting time is 13 minutes. At tempering with a suspension of 3% colloid *cellulose*, which was obtained in the WC mode of dispersion, the initial setting time is 9 minutes, and the final setting time is 16 minutes; for the one obtained in the SC mode, the initial setting time is 11 minutes, and the final setting time is 20 minutes. This gaging of the tempering interval makes it possible to effectuate the technological operations with gypsum dough for a longer time and to obtain products of higher quality. Analogous results with respect to the setting time were obtained in studying gypsum of the G-4 grade.

Parameters of the sample properties

Fiber weight, g	Gypsum weight, g	Density, kg/m^3	Bending strength, MPa	Compression strength, MPa	Cavitation mode
In 2 h after preparation					
3.91	240	1011	2.0	2.6	SC
4.14	227	1011	1.25	1.80	WC
5.45	190	850	2.0	1.06	WC
After drying until constant weight					
3.91	240	1011	4.98	8.18	SC
4.14	227	1011	4.10	7.30	WC
5.45	190	850	1.83	3.07	WC

The physicomechanical characteristics of the gypsum concrete prepared at tempering with a water–paper suspension were determined by testing of beams fabricated by the standard (the ultimate bending strength and the ultimate compressive strength were determined) method. The tests were carried out 2 h after the preparation and drying until constant weight. The table presents data for gypsum of the G-5 grade.

One can see a decrease in the strength properties of the gypsum rock with increasing the relative content of fiber. This is attributed to the fact that the major part of the water in the suspension is in the bound state and it decreases the gypsum dough flowability; it does not interact with the gypsum binding agent at the hydration moment; at the same time, it produces excess moisture that evaporates in the course of the gypsum rock drying. As a result, in the process of drying, pores appear in this gypsum rock that decrease the weight characteristics and physicomechanical parameters of the rock. In the samples tempered with suspensions obtained in the SC mode, great amounts of moisture are not formed, a less porous structure appears in the course of the drying, and high physicomechanical characteristics are preserved.

Thus, by this practical example, we have demonstrated the technique of efficient control of underwater electric discharges due to intensification of one of the afterdischarge factors, pulse cavitation. This technique, at identical energy in the pulse, allowed obtaining of 10–20% higher strength of the dried gypsum–concrete separating slabs fabricated of gypsum dough tempered with the suspension of fibrous wastes of the paper-making industry, which was prepared in the SC mode. This, in turn, decreases the required thickness of building separating slabs, saves construction materials, and contributes to the improvement of a number of processing methods for gypsum concrete products.

REFERENCES

1. Malyushevskaya, A.P., Study of Pulse Electrodischarge Cavitation in the Processes of Treatment of Phytogenous Fibrous Polymers, *Extended Abstract of Cand. Sci. (Eng.) Dissertation*, Nikolaev–Kherson, 2006.
2. Malyushevskii, P.P., On Procedure of Fine Comminution of Materials at Electric Explosion in Restricted Volume, *Elektron. Obrab. Mater.*, 1982, no. 3, pp. 58–63.
3. Malyushevskaya, A.P. and Malyushevskii, P.P., A Novel Method to Control Electrical–Discharge Nonlinear Bulk Cavitation, *Elektron. Obrab. Mater.*, 2007, no. 1, pp. 76–81 [*Surf. Eng. Appl. Electrochem.* (Engl. Transl.), vol. 43, no. 1, pp. 59–64].

ISSN 1068-3755, Surface Engineering and Applied Electrochemistry, 2008, Vol. 44, No. 4, pp. 257–263. © Allerton Press, Inc., 2008.
Original Russian Text © V.F. Gologan, Zh.I. Bobanova, S.Kh. Ivashku, 2008, published in Elektronnaya Obrabotka Materialov, 2008, No. 4, pp. 9–16.

ELECTRICAL SURFACE TREATMENT METHODS

Peculiarities of Chromium Deposition with Application of an Induction–Capacitance Device

V. F. Gologan, Zh. I. Bobanova, and S. Kh. Ivashku

Institute of Applied Physics, Academy of Sciences of Moldova,
ul. Academiei 5, Chisinau, MD-2028 Republic of Moldova
E-mail: bobanova@phys.asm.md

Received January 17, 2008

Abstract—The experimental data obtained at various parameters of an inductance–capacitor device are presented. It is possible to change the kinetics and efficiency of the chromium plating process by varying the inductance *L* and the capacity *C* of the device while keeping the other conditions of the electrolysis identical.

DOI: 10.3103/S1068375508040029

Due to their high wear resistance and anticorrosion properties, electrochemical coatings of chromium are widely applied in industrial enterprises, particularly, coatings deposited from a multipurpose electrolyte, which satisfy the requirements of modern industry [1]. However, due to low power yield at optimum electrolysis conditions, the chromium coating deposition rate is not high (~30 μm/h).

As was mentioned in previous works, in order to influence the deposition process and the properties of electrodeposited coatings, special inductance–capacitance devices (*LC* devices) may be applied that are embedded or connected in series to power supplies utilized in the electroplating industry, since the variation of the parameters of these devices influences the cathode polarization and the deposit structure [2–4]. The variation of these parameters in the power supply–bath circuit results in changes of the amplitude and frequency of the alternating current components. Their sources are under researched; therefore, it is of interest to study the chromium plating process with application of *LC* devices, in particular, for the reason that the chromium deposition mechanism has peculiarities different from other metals [1].

RESEARCH TECHNIQUE

Coatings were deposited from a multipurpose electrolyte for chromium plating of the following composition: 250 g/l of chromic anhydride and 2.5 g/l of sulfuric acid; t_{el} = 55°C at a cathode current density of 5.5–12.0 kA/m^2.

A three-phase rectifier (model VSZh-303) and an accumulator (12CT-180 Ah type) were used as the power supplies.

Inductance–capacitance devices were connected to the power supply; the inductance of the devices was formed by series and parallel connections of special throttles allowing its variation within 0.006–0.456 mH. The required capacitance within the range of 0.004–0.104 F was obtained by parallel connection of the electrolytic capacitors. For control of the circuital current, a ballast resistor (model RB-302U2) was applied.

The polarization curves were measured using the compensation method in a standard electrochemical cell (YaSE-2) on as-deposited chromium on a platinum cathode with a surface area of 1 cm^2 [1]. A silver chloride electrode (EVL-1M1) was used as the reference electrode. The cell was connected after the device in parallel with the ballast. The latter was used to provide passing of current up to 25 A through the device. At measurement of the polarization curves, the current value was varied in steps by means of a resistance box (model R33) and registered by a voltammeter (M2044 type). The potentials were measured using a high-ohmic voltmeter (model B7–27/A1).

The alternating current components in the power supply–bath circuit were studied using an SK4–56 spectrum analyzer.

The chromium power yield was determined by the coulometric and gravimetric methods [1]. The thickness of the chromium coatings was measured by means of an SR level snap gage with a division value of 0.002 mm; on the transverse microsections, the thickness was measured by virtue of a metallographic microscope (NEOPHOT-2).

The roughness of the surface of 180-μm-thick coatings was determined by means of a Taylor Hobson Form Talysurf Intra Series 50 profilometer–profilograph.

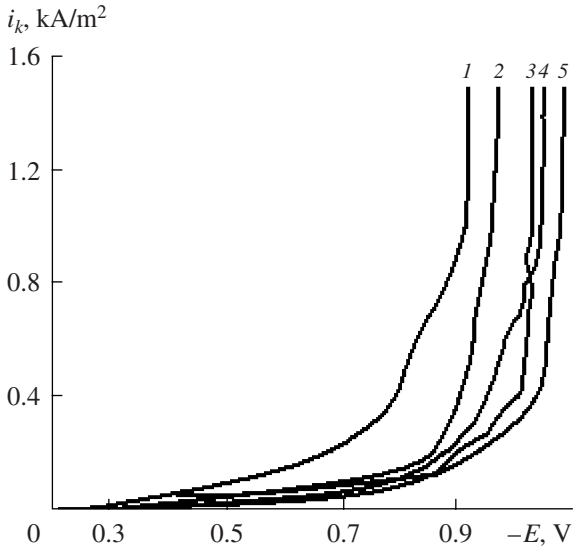

Fig. 1. Variation of the polarization characteristics versus the inductance L (at t_{el} = 55°C, C = 0.024 F). L, mH: (*1*) 0.119; (*2*) 0.06; (*3*) without the *LC* device; (*4*) 0.027; (*5*) 0.456.

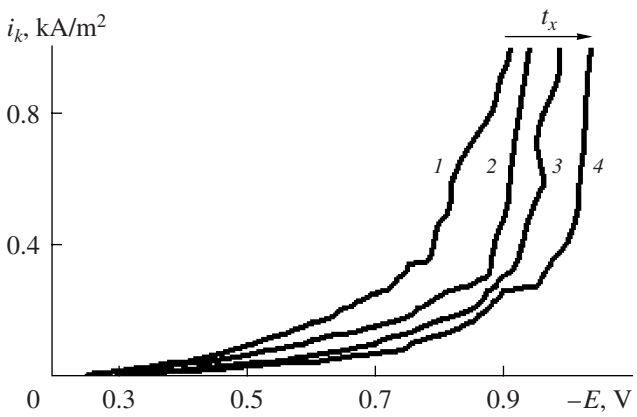

Fig. 2. Polarization curves of chromium deposition from the preliminarily electrolyzed solution with application of the *LC* device: (*1*) at optimum parameters of the *LC* device; (*2*) without the *LC* device; (3) after the solution electrolyzing without the *LC* device for 40 min; (*4*) after the solution electrolyzing without the *LC* device for 1 h.

RESULTS AND DISCUSSION

In preliminary studies, variation limits for the inductance L of the device and the optimal values of the capacitance C were determined, since the cathode polarization depends, to a great extent, on the inductance.

At variation of the determined values of the inductance L, the electrode potential varied within 160 mV at a current density of 1.5 kA/m^2 (C_{op} = 0.024 F): it deviated by 110 mV (L = 0.119 mH) into the positive range and by 50 mV (L = 0.456 mH) into the negative range from its values with the device absence (Fig. 1). These deviations of the electrode potential testify to the significant influence of the device parameters on the chromium deposition process. Thereafter, the values of the inductance and capacitance at which the greatest polarization of the cathode takes place were assumed to be optimum (L_{op} = 0.119 mH, C_{op} = 0.024 F).

For determination of the deposition condition influence on the electrolyte properties with the *LC* device connected, the polarization curves were measured after the solution electrolyzing with the circuit connection (L_{op}, C_{op}) for one hour; then, the experiment continued with the circuit disconnected. These studies have revealed that, immediately after the disconnection of the circuit, the electrode potential appreciably deviated into the positive region from its value in the experiments with fresh electrolyte without the device connected; however, it did not achieve the potential values obtained with the application of the circuit at L_{op} and C_{op} (Fig. 2).

As the time of the solution operation after the circuit disconnection grew, the cathode potential approached the values found in the experiments without the solution electrolyzing with the connected circuit. This may count in favor of variations in the electrolyte structure.

At the above-given parameters of the *LC* device, the spectrum of alternating current components in the circuit was studied (Figs. 3, 4). In the case of the bath substitution by equivalent active resistance with an identical voltage drop (U = 4.1 V), the highest values of the alternating current component amplitude were observed in the range of 0–1 kHz (Fig. 3a).

The connection of the bath to the voltaic circuit instead of the active resistance resulted in a significantly different spectrum of alternating components (Figs. 3b, 4); that is, the amplitude ΔI increased by several times and the frequency achieved a value of 4.3 kHz.

When the *LC* device is connected, its parameters exert an appreciable influence on the value and the amount of alternating components in the spectrum. At optimum values of the inductance and capacitance, the amplitude of the alternating components increased and their frequency achieved 6.5 kHz (Figs. 3c, 4).

Both a decrease of the inductance (L = 0.027 mH) and its increase (L = 0.456 mH) led to a decrease of both the alternating component amplitude and the spectrum width (Figs. 3d, 3e, 4). Comparison of these results with the ones obtained earlier has shown that a wider spectrum corresponds to the parameters L_{op} and C_{op} at which the electrode polarization shifted to a more positive range in comparison with the cathode potential in the case of deposition without the circuit. Under the other

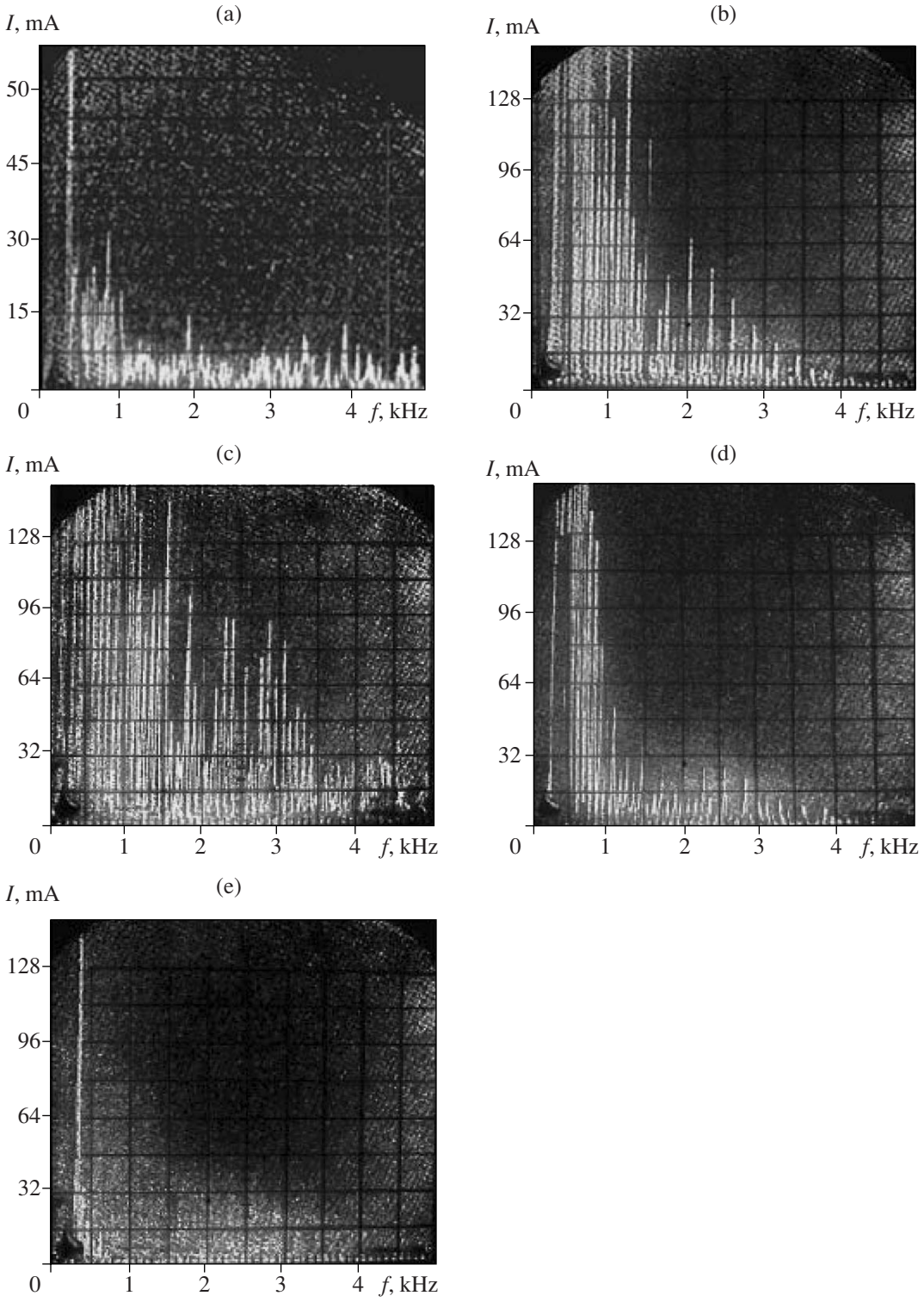

Fig. 3. Influence of the inductance L on the alternating component spectrum at application of a three-phase rectifier (i_k = 5.5 kA/m^2, I = 25 A, C = 0.024 F): (a) without the bath, with the active resistance only; (b) without the LC device. L, mH: (c) 0.119; (d) 0.027; (e) 0.456.

considered conditions of the deposition (L = 0.027 mH, L = 0.456 mH, and C = 0.024 F), a shift of the cathode potential to a more negative range took place (Fig. 1).

For the determination of the influence of the power supply type on the spectrum of the alternating components, the experiments were carried out with the accu-

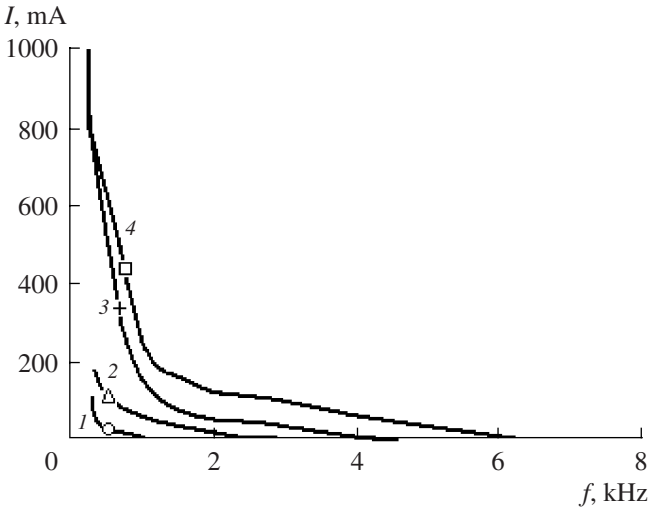

Fig. 4. Influence of the inductance L on the amplitude–frequency characteristics of alternating components at application of a three-phase rectifier (i_k = 5.5 kA/m^2, I = 25 A, C = 0.024 F): (1) 0.456; (*2*) 0.027; (*4*) 0.119; (*3*) without the *LC* device.

mulator connected. In this case, the alternating components significantly decreased in comparison with their values found in the previous tests; in addition, the optimum deposition conditions changed as well (Figs. 5, 6). In the experiments with the connection of the active resistance, the alternating components were at the background level (Fig. 5a).

The connection of the bath resulted in an appreciable increase of their amplitude; the resistance often achieved 5 kHz (Figs. 5b, 6). The greatest increase of the alternating component amplitude was found at L = 0.09 mH and C = 0.01 F; the components were registered up to 8 kHz (Figs. 5c, 6). As well as in the previous experiments, the inductance increase (L = 0.456 mH) led to a decrease in both the amplitude and frequency values of the alternating components (Figs. 5d, 6). Thus, the power supply type exerts a significant influence on the alternating component spectrum and the optimum values of the device parameters. This is also confirmed by experiments with application of a single-phase power supply, wherein the optimum inductance value exceeded the values used in the present tests by dozens of times [2, 3].

Variation of the inductance–capacitance device parameters appreciably influences the rate of the chromium deposition (Table 1; Figs. 7, 8). The greatest influence on the process efficiency at the current density i_k = 5.5 kA/m^2 was exerted by the earlier found optimum values of the inductance and capacitance: L = 0.09 mH and C = 0.01 F.

Under these conditions, the deposition rate increased by a factor of 1.6 (Table 1, Fig. 8); that is, the maximum effect is shown under the deposition conditions when the greatest polarization of the cathode takes place. The capacitance variation at L_{op} exerts less influence on the chromium deposition rate (Fig. 7). A decrease in the coating thickness at the current I = 12.75 A (i_k = 8.5 kA/dm^2) is apparently due to the device sensitivity at low currents.

These experiments have shown that the values of the optimum parameters of the *LC* device can be determined by measurement of the total value of the alternating current components by means of a B7-27/A1 voltmeter with application of a standard resistance (75-A shunt resistor) (Fig. 7).

An increase in the current density contributes to an increase of the power yield and the deposition rate; the latter is 82 μm/h at i_k = 8.5 kA/m^2 (Table 1, Fig. 8). The efficiency of the process increased by a factor of 2.7 in comparison with the generally accepted conditions of deposition without the device (i_k = 5.5 kA/m^2) (Fig. 8). The coatings obtained at this current density are characterized by the highest wear resistance [5].

In the case when an accumulator is applied as the power supply, the highest deposition rate is also

Table 1. Influence of the inductance–capacitance device parameters on the process efficiency ν, μm/h

Power supply	I, A	i_k, kA/m^2	ν, μm/h			
			Inductance, mH			
			0.027	0.09	0.119	0.456
Rectifier (C = 0.024 F)	12.75	5.5	27	40	46	24
	12.75	8.5	44	50	74	40
	25	5.5	30	42	50	26
Accumulator (C = 0.01 F)	25	8.5	47	52	82	43
	25	5.5	34	48	42	30

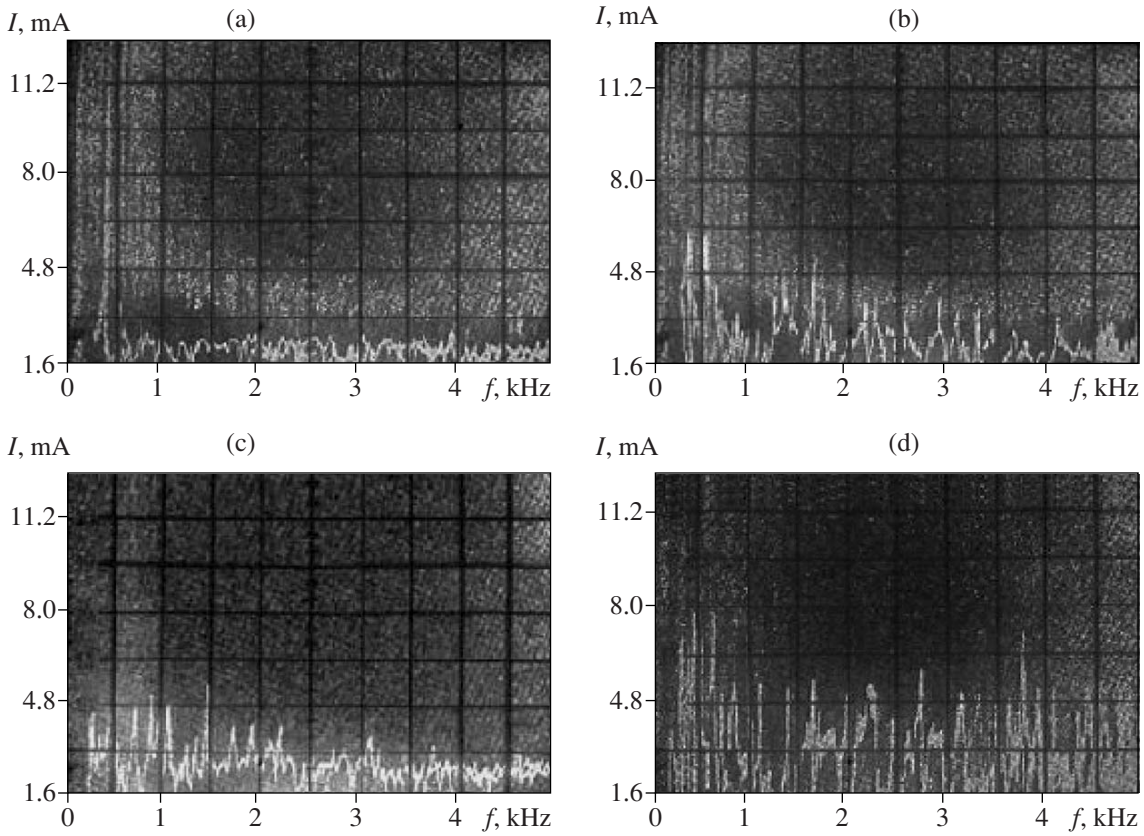

Fig. 5. Influence of the inductance L on the alternating component spectrum at application of an accumulator (i_k = 5.5 kA/m^2, I = 25 A, C = 0.01 F): (a) without the bath, with the active resistance only; (b) without the LC device. L, mH: (c) 0.456; (d) 0.09.

observed at optimum parameters of the device (Table 1); that is, there is the same influence as in the formation of the alternating component spectra (Figs. 5, 6).

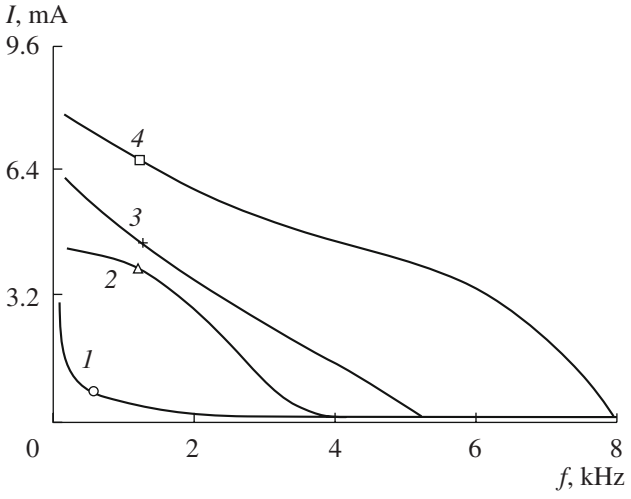

Fig. 6. Influence of the inductance L on the amplitude–frequency characteristics of alternating components at application of an accumulator (i_k = 5.5 kA/m^2, I = 25 A, C = 0.01 F): (*1*) without the bath, with the active resistance only; L, mH: (*2*) 0.456; (*4*) 0.09; (*3*) without the device.

A certain difference in the deposition rates under selected electrolysis conditions is due to the peculiarities of the power supplies.

Application of the inductance–capacitance device positively influenced the roughness of the coatings obtained from a three-phase power supply (Table 2). The roughnesses of the coatings obtained without the LC

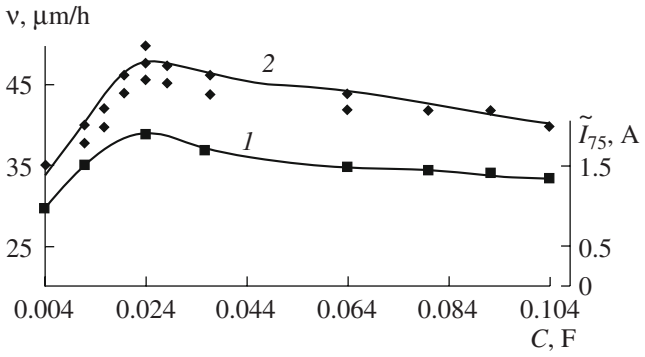

Fig. 7. Influence of the capacitance (L = 0.119 mH, i_k = 5.5 kA/m^2) on the following: (*1*) the total value of the alternating current components; (*2*) the chromium deposition rate.

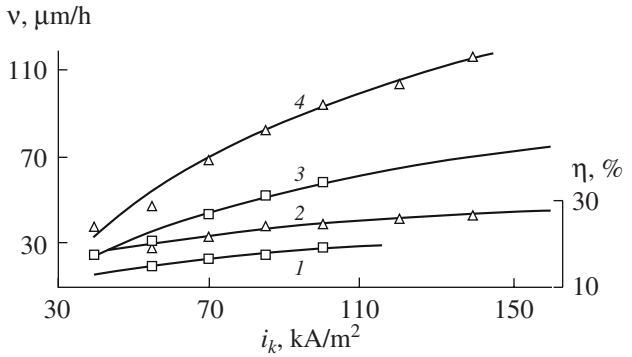

Fig. 8. Influence of the current density on the chromium power yield (*1*, *2*) and the deposition rate (*3*, *4*) under the following deposition conditions: (*1*, *3*) without the *LC* device connection; (*2*, *4*) with the *LC* device ($L = 0.119$ mH, $C = 0.024$ F).

device at current densities of 5.5 and 8.5 kA/m^2 significantly differed (Table 1). At connection of the circuit with the parameters L_{op} and C_{op}, for the coatings deposited at 5.5 kA/m^2, the roughness insignificantly decreased; as the current density increased up to 11.0 kA/m^2, it increased by a small value and the coatings were lustrous.

The inductance increase ($L = 0.456$ mH) resulted in an increase of the coating roughness (Table 2).

Thus, as a result of the studies carried out, the interrelation of the cathode potential value, the character of the alternating component spectrum, the chromium deposition rate, and the inductance–capacitance device parameters has been found. At the same time, the optimum values of the inductance and capacitance with the other deposition conditions being equal depend on the peculiarities of the power supplies.

Table 2. Influence of the inductance–capacitance device parameters on the coating roughness

Mode	i_k, kA/m^2	R_a, μm	R_z, μm
Substrate	–	0.078	0.605
Device disconnected	5.5	0.76	3.8
″	8.5	2.6	8.68
Device connected $L = 0.456$ mH, $C = 0.024$ F	5.5	0.86	3.94
Device connected $L = 0.119$ mH, $C = 0.024$ F	5.5	0.51	2.5
″	8.5	0.12	1.1
″	10.0	0.628	3.16
″	12.0	0.66	3.8

The mentioned parameters apparently influence the power supply–bath system operation, thus resulting in variation of the deposition conditions.

It is known that, at imposition of the alternating current on the direct one, due to the double layer capacitance, there appears a reactive resistance that depends, as well as the active one, on the frequency [6, 7]. In this case, at variation of, for example, the current, the voltage is late in the achievement of its stationary value [6]. Therefore, the phase boundary is a complex resistance, and the electrode equivalent is a circuit with nonlinear lumped parameters.

At the same time, the Faraday process is usually attributed to active resistance only, and the double layer recharging, to capacitance, despite the fact that these processes are dependent [6].

In order to influence the deposition process under these conditions, in work [8], the circuit was connected to the inductance calculated from the resonance conditions with differential capacitance for a specified frequency of the alternating current; this contributed to the growth of smaller and more homogeneous crystals in comparison with the ones obtained at direct current only and/or with imposition of alternating current.

Taking into account that the probability of a unit event and the rate of the electrochemical processes mainly depend on the state of the reagents in the solution, the electrode properties, and the electric field [9]; that the sources of the alternating components can be a slow discharge; the fluctuations of the reagents in the near-cathode space; the intense evolution of gases (hydrogen, oxygen) on the electrodes; the conditions of the electrolyte stirring; etc. [10], the interrelation of the cathode polarization and the alternating component spectra in our experiments becomes clear.

Therefore, we may suppose that, at optimum parameters of the inductance–capacitance device, the electrochemical process activity increases; this is confirmed by the depolarization of the cathode and the form of the spectrum containing a great number of alternating components, which differ in both their amplitude and frequency [10].

These conditions of the deposition contribute to an increase in the chromium power yield and deposition rate, to a decrease in the roughness and irregularity of the coating thickness, to formation of a more perfect structure, and to improvement of the physicomechanical properties of the deposits [5]. This effect is caused by the influence of the chromium deposition conditions on the electrolyte structure, on the formation and properties of the near-cathode film, and on the electrode surface state [1].

REFERENCES

1. Vagramyan, A.T. and Zhamagortsyan, M.A., *Elektroosazhdenie metallov i ingibiruyushchaya adsorbtsiya* (Electrodeposition of Metals and Inhibiting Adsorption), Moscow: Nauka, 1969.
2. Gologan, V.F., Bobanova, Zh.I., Ivashku, S.Kh., Popov, V.A., and Mazur, V.A., Particularities of the Electroplating Process in the Case of Single–Phase Power Supply with an Embedded Induction–Capacitance Device, *Elektron. Obrab. Mater.*, 2007, no. 2, pp. 12–16 [*Surf. Eng. Appl. Electrochem.* (Engl. Transl.), vol. 43, no. 2, pp. 83–86].
3. Gologan, V.F., Bobanova, Zh.I., Ivashku, S.Kh., Mazur, V.A., and Pushkasu, B.M., Features of How the Parameters of an Induction–Capacitance Device Affect the Nickel Plating Process, *Elektron. Obrab. Mater.,* 2007, no. 5, pp. 4–8 [*Surf. Eng. Appl. Electrochem.* (Engl. Transl.), vol. 43, no. 5, pp. 307–311].
4. Gologan, V.F. and Unguryanu, V., USSR Inventor's Certificate no. 1621559, 1990.
5. Gologan, V.F. and Ivashku, S.Kh., Peculiarities of Chromium Plating at Connection of the Inductance–Capacitance Device to Power Supply, in Electrolytic and Electrolytic–Plasma Methods of Metal Surface Modification, *Materialy II Mezhdunarodnoi nauchno–tekhnicheskoi konferentsii* (Proc. II Int. Nauchno–Tekh. Conf.), Kostroma–Moscow, 2007, pp. 167–169.
6. Delimarskii, Yu.K., *Elektrokhimiya ionnykh rasplavov* (Electrochemistry of Ion Melts), Moscow: Metallurgiya, 1978.
7. Gamburg, Yu.D., *Elektrokhimicheskaya kristallizatsiya metallov i splavov* (Electrochemical Crystallization of Metals and Alloys), Moscow: Yanus–K, 1997.
8. Antonyan, S. Influence of Common Action of Alternating and Direct Currens on Morphology, Submicrostructure, and Physicomechanical Properties of Nickel and Copper, *Extended Abstract of Cand. Sci. (Eng.) Dissertation*, Vilnyus, 1979.
9. Frumkin, A.N., Andreev, V.N., Boguslavskii, L.I. et al., *Dvoinoi sloi i elektrodnaya kinetika* (Double Layer and Electrode Kinetics), Moscow: Nauka, 1981.
10. Tyagai, V.A., Noises of Electrochemical Systems (Review), *Elektrokhimiya*, 1974, vol. 10, issue 1, pp. 3–24.

ISSN 1068-3755, Surface Engineering and Applied Electrochemistry, 2008, Vol. 44, No. 4, pp. 264–270. © Allerton Press, Inc., 2008.
Original Russian Text © E.D. Pleshka, 2008, published in Elektronnaya Obrabotka Materialov, 2008, No. 4, pp. 17–24.

ELECTRICAL SURFACE TREATMENT METHODS

Iron Coatings from Multicomponent Methyl Sulfate Chloride Electrolyte

E. D. Pleshka

Institute of Applied Physics, Academy of Sciences of Moldova, ul. Academiei 5, Chisinau, MD-2028 Republic of Moldova
E-mail: bortzoi_tudor@yahoo.com

Received January 16, 2008

Abstract—Results of investigations of the influence of the conditions of electrolysis in methyl sulfate chloride (MSC) electrolytes on the hardness, structure, and chemical composition of doped iron coatings are presented. It is found that, by varying the electrodeposition mode, it is possible to obtain coatings with hardness of 4.5–7.2 GPa characterized by fibrous–columnar, granular, and layered structures with a carbon content up to 0.9%, nickel content up to 2–6%, and manganese content up to 2–4%.

DOI: 10.3103/S1068375508040030

INTRODUCTION

Iron based electrodeposited coatings can be promising for recovery and hardening of machine pieces and mechanisms. Therefore, it is of interest to study the properties of doped iron coatings obtained in methyl sulfate chloride (MSC) electrolytes, which possess efficiency, stability, and other technological parameters adoptable for industry [1–4].

For a reasonable choice of components that improve the quality of iron coatings more efficiently, the influence of doping elements on the properties of metallurgical and electrodeposited materials has been considered [1, 5, 6]. It is noted in the literature that interstitial elements (carbon, nitrogen, and boron) significantly increase the yield point, hardness, and other properties of steels, cast irons, and electrodeposited coatings. In ferrite doping steels, the forming substitution elements W, Mo, and V harden austenites to a greater degree than the austenite formers Co and Ni [6]. The efficiency of the doping element influence on the steel properties is determined by the basic composites of the Fe–Ni, Fe–Mn, Fe–Cr–Ni, and Fe–Gr–Mn types with parameters of 15–20 nm and more. It was also noted that, due to the strain strengthening, the hardness and hardening properties of nickel-containing materials increase by a factor of 1.5 and those containing manganese, by a factor of 2.6 in comparison with low-carbon steels.

The mentioned attributes of the properties may be shown in iron coatings doped with nickel, manganese, molybdenum, and carbon obtained in an MSC electrolyte containing salts of these metals. Due to the close values of the potentials of electrodeposition of iron, nickel, manganese, and cobalt, they can be deposited on a cathode forming a particular crystalline structure. According to the stated factors, the presence of the mentioned doping elements in the electrodeposited iron coatings may contribute to the improvement of their physicomechanical properties and wear resistance, especially under conditions of contact deformations in surface layers of mating pieces.

The aim of the present paper is to study the process of electrodeposition in the MSC electrolyte and to find conditions for obtaining doped iron coatings with improved physicomechanical properties, which determine the operating capability of recovered and hardened pieces.

RESEARCH TECHNIQUE

With the view to obtain doped iron coatings for recovery and hardening of pieces, the influence of the electrolyte composition and the electrolysis modes on the deposition rate of the coatings, their hardness, structure, and other properties was studied.

Iron plating was realized in an MSC electrolyte [1] containing 250 g/l of methyl sulfate iron and 150 g/l of iron chloride, and in a multicomponent (MSC 3) electrolyte [2, 3] that, in addition to the mentioned salts, contained 30 g/l of nickel chloride, 30 g/l of manganese sulfate, and 10 g/l of molybdenum sulfate.

The electrolytes were prepared of reagents of the "CP" and "AP" grades according to technological recommendations [1, 3]. The content of iron and other components in the electrolyte was determined by the volume titration method [11].

The coatings were obtained using the electrolytic method by applying direct current from a rectifier (VU-42/70 A) and devices for measurement of the current and voltage of class 0.2 and 0.5.

The coatings were deposited on samples prepared of steel 45. The anodes were plates or pins of armco iron and steel 10. The distance between the anode and cathode was 0.1 m, and the ratio of their surface areas was

2 : 1. The iron plating was carried out according to the technological recommendations in [1, 3].

The cathode polarization was studied in the galvanostatic mode using the method of A.T. Vagramyan [20] with application of a cell with a volume of 350 ml. The cathode surface area was 1 cm^2. The values of the potential–time, potential–current, and potential–voltage on the cell terminals were registered by oscillographs (C1-19B and C1-20) and by a thyratron device [12].

The microhardness of the coatings was determined using a PMT-3M device according to GOST 9450-75 at a load on the indenter of 0.98 N. The hardness of the thick-layer coatings (1–3 mm) on the samples and pieces was measured using a device of the T K-2 type.

The microstructure of the coatings was studied on sample microsections with application of microscopes (MBI-6 and MIM-8) and a scanning electron microscope (REM 200). The particularities of the structure, the characteristic growth habits, the structure of the deposits, and the distribution of the doping elements were revealed by chemical treatment of sample microsections with solution–indicators.

The carbon content was determined according to GOST 2331-63 by applying a gas analyzer (GOU-1) and gas measuring burets (0–0.25 t 0.001% C, 0–1.5 ± 0.05%). The nickel content was determined by the gravimetric method and deposition by virtue of dimethylglyoxime, and the manganese content was determined by the silver persulfate titrimetric method [16].

The parameters of the submicrostructure of the electrodeposited coatings were studied using a diffractometer (DRON-3). The size of the coherent-scattering regions and the values of the crystal lattice microdistortions were determined by analysis of diffraction curves by the second order method [13, 14, 15].

The experiment results were treated by the methods of mathematical statistics according to GOST 11.004.74 and were estimated using basic parameters of the electrolysis process and properties of the coatings.

RESULTS AND DISCUSSION

In the course of studying the parameters of the iron plating process in MSC electrolytes, it was found that the influence of the electrolysis conditions on the coating deposition rate is described by dependences characteristic of other electrolytes [1, 7, 20]. Introduction of salts of doping elements into the MSC electrolyte contributes to an increase in the coating deposition rate in the current density range of 5–8 kA/m^2 (Fig. 1). The deposition rate significantly depends on the current density and acidity. The obtained deposition rate dependences on the current density allow estimating the efficiency of the process and selecting modes of iron plating of pieces.

Electrodeposition in the MSC 3 electrolyte resulted in obtaining of qualitative coatings characterized by different hardness and structure. At low and mean current densities, smooth deposits with homogeneous surfaces at significant thicknesses are obtained. For the coatings deposited at a temperature of 333 K and a current density of 6–8 kA/m^2, the roughness increases with the growing thickness.

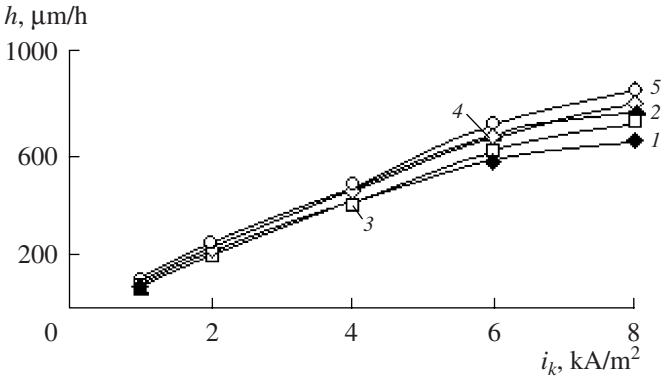

Fig. 1. Current density influence on the iron coating deposition rate in MSC 1 and MSC 3 electrolytes.

Variation of the modes within pH = 0.6–1.6, T = 298–333 K, and a current density of 1–8 kA/m^2 (see Figs. 2a–2d) appreciably influences the microhardness of the doped iron deposits by varying it within 4.5–7.2 GPa. Viscous deposits of doped iron with a hardness of H_m = 4.5–5.3 GPa are obtained at pH = 0.6–0.8, T = 333 K, and a current density of 1–8 kA/m^2 (Figs. 2a–2b, curve *3*). A decrease in the temperature to 313 and 298 K contributes to the formation of harder deposits (H_m = 5.4–6.5 GPa) (Fig. 2; curves *1*, *2*) with a granular structure. A decrease in the electrolyte acidity to pH = 1.2–1.6 at temperatures of 313 and 298 K leads to an increase in the microhardness up to 6.6–7.2 GPa. The microhardness of the doped coatings deposited at pH = 1.2 and 1.6 and at the above given temperatures is practically identical (Figs. 2a, 2d).

It is possible to obtain the required values of the coating hardness by stabilization of the acidity and temperature modes in the electrolysis process. Formation of deposits with identical hardness in a wide range of current densities may be considered to be a positive factor of the reproducibility of the properties in the process of iron plating in industry.

Iron coatings of a thickness up to 2–3 mm with a microhardness of 4.4–7.2 GPa obtained in the MSC 3 electrolyte at pH = 0.8–1.6 and T = 298–333 K are comparable in hardness with quenched steels and may be applied for recovery and hardening of pieces.

Metallographical tests have revealed that the current density increase significantly influences the growth habit and structure formation of the deposits. At variation of the modes within pH = 0.9–1.6 and T =298–333 K and the current density within 1–8 kA/m^2, deposits with fibrous–columnar, granular, and layered structures are formed (Figs. 3–5).

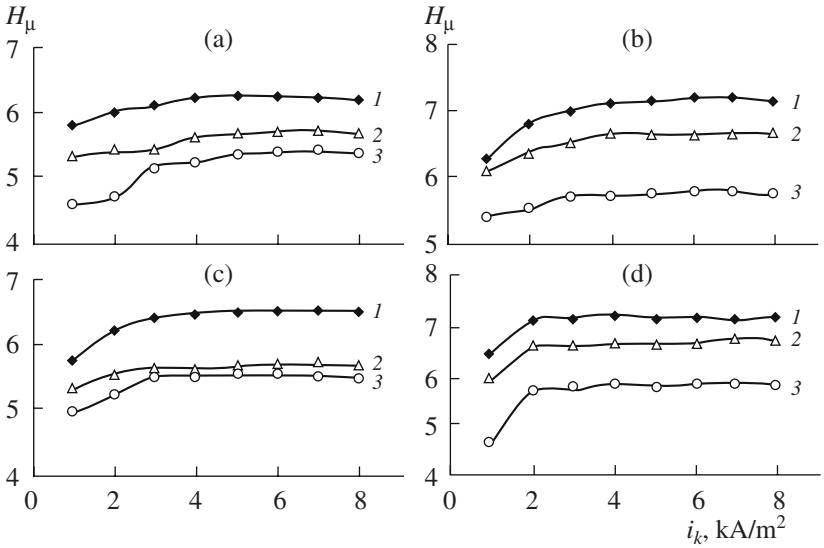

Fig. 2. Cathode current density influence on the coating microhardness in MSC 3 electrolyte. pH: 0.6 (a); 0.8 (b); 1.2 (c); 1.6 (d). *T*, K: 298 (*1*); 313 (*2*); 333 (*3*).

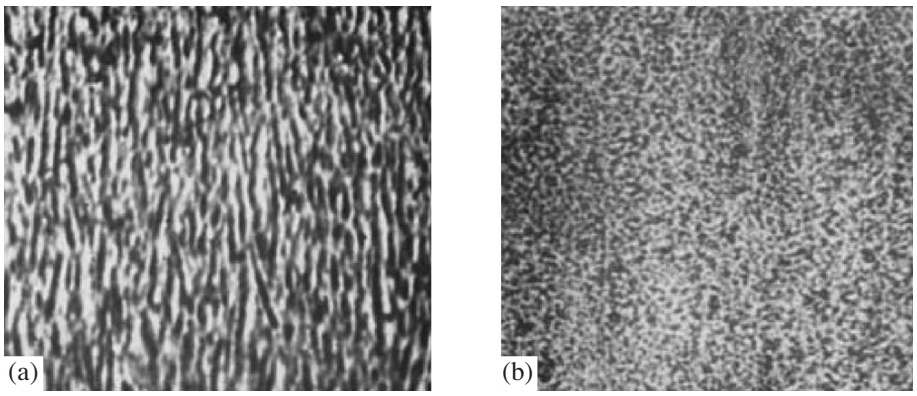

Fig. 3. Fibrous–columnar structure of iron deposits obtained from MSC electrolytes: (a) transverse microsection of the deposit; (b) morphology of the deposit surface.

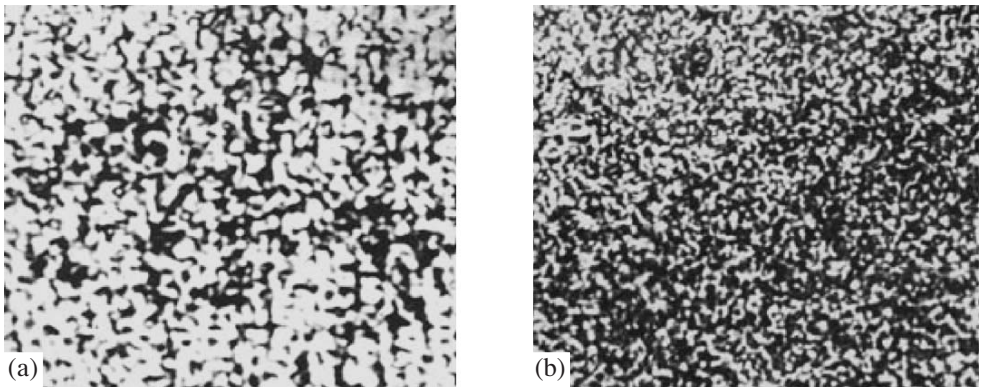

Fig. 4. Granular structure of iron deposits obtained from MSC electrolytes: (a) transverse microsection of the deposit; (b) morpho–logy of the deposit surface (×1000).

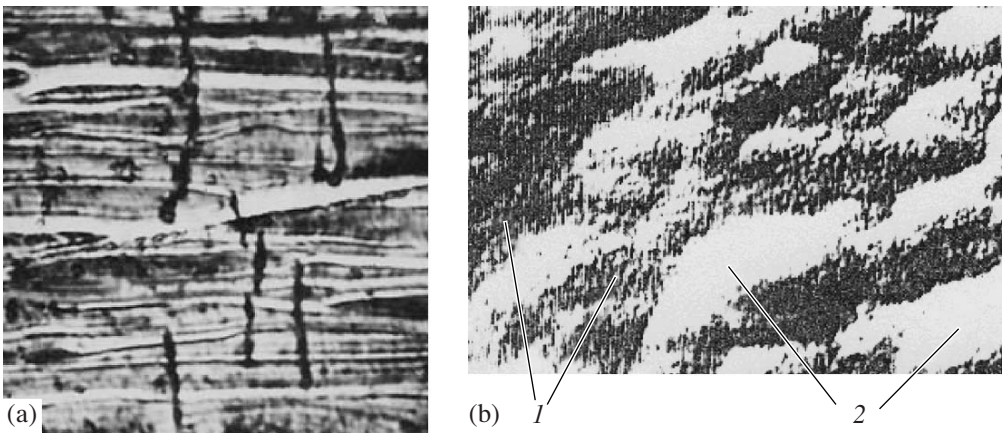

Fig. 5. Layered structure of iron deposits obtained from MSC electrolytes: (a) transverse microsection of the deposit (×1000); (b) morphology of the deposit surface (×30 000): (*1*) zones of crystal formations with high carbon content; (*2*) formations of grains with a more perfect metal structure.

Formation of deposits with a fibrous–columnar structure in the MSC 3 electrolyte (Fig. 3a) may be explained by adsorption of organic compounds on the cathode surface and by the influence of the electromagnetic and hydrodynamic conditions contributing to nucleation and predominant crystal growth in the direction normal to the substrate. The surface morphology preserves peculiarities at significant (0.8–1.2 mm) thicknesses of the coatings (Fig. 3b, 4b). In the course of the microstructure study using the method of electron microscopy (magnification up to 30 000 times), it was found that the deposit morphology is characterized by microcrystals of the spheroid type that form greater crystal formations (fibers, grains) of the same type (Fig. 5b) with a metal structure. The zones between the grains (fibers) are formed by metal crystal formations with a more defective structure and a higher content of carbon.

The microstructure of the deposits obtained at low current densities is characterized by greater blocks and longer fibers in comparison with those formed at high current densities. An increase in the current density changes the deposit structure from a pronounced fibrous–columnar one (Fig. 3) characterized by great mosaic blocks (D = 1380 Å) at a current density of 2–3 kA/m^2 to a granular structure (Fig. 4) with the block dimension D = 900–1160 Å at 4–6 kA/m^2. Formation of coatings of a granular structure with blocks D = 430–320 Å corresponds to pH = 1.6 and T = 313 K. As the temperature decreases to 298 K at high current density (5–8 kA/m^2), the dimension of the crystal blocks decreases to D = 270–120 Å and the deposits become layered and harder. In the pH range of 1.6 and more with the current density increasing, due to the intensification of the adsorption of organic compounds and concentration restrictions with respect to metal ions, layers with a high carbon content are periodically formed on the cathode. Layers of polycrystals with a metal structure and an appreciably lower carbon content are formed on their surface. One can judge the cyclic nature of the crystallization process by the revealed characteristic regions (bands) at chemical treatment of the sample microsections with various solutions (Figs. 5a, 6) and by the increase of the carbon content in the deposits (Fig. 8).

Analyzing the mentioned peculiarities of the growth and formation of the dense metal layers *2* on more "defect" layers *1* (Fig. 6), one should suppose their high electron conductivity contributing to the normal proceeding of the electrocrystallization process. This may confirm that the layered structure is due to carbon inclusion into the deposit and, to a lesser degree, hydroxide metal compounds characterized by appreciably lower conductivity.

Formation of various structure types results from the influence of methyl sulfate ions, the electrolyte acidity, and factors varying the cathode polarization (Fig. 7). Acidity lowering leads to a decrease in the current densities of the critical crystallization conditions corresponding to the formation of the layered deposit structure (layer *4*) (Fig. 6). These conditions can be determined by comparison of the cathode polarization variation dependence on the electrolysis current density with the form of the appearing structures of the coating layer (Fig. 6).

Analysis of the research results has shown that the conditions of fibrous–columnar structure formation (Fig. 3) correspond to a cathode potential of 740–870 mV. Coatings with a layered structure (Fig. 5) are formed at low electrolyte acidity and the cathode polarization above 950–970 mV. Intermediate values of the cathode polarization correspond to conditions of formation of deposits with a granular structure (see Fig. 4).

In the range of low temperatures, variation of the electrolyte viscosity and worsening of the ion diffusion lead to an increase in the cathode polarization (Fig. 6, curve *1*). This contributes to the formation of hard dis-

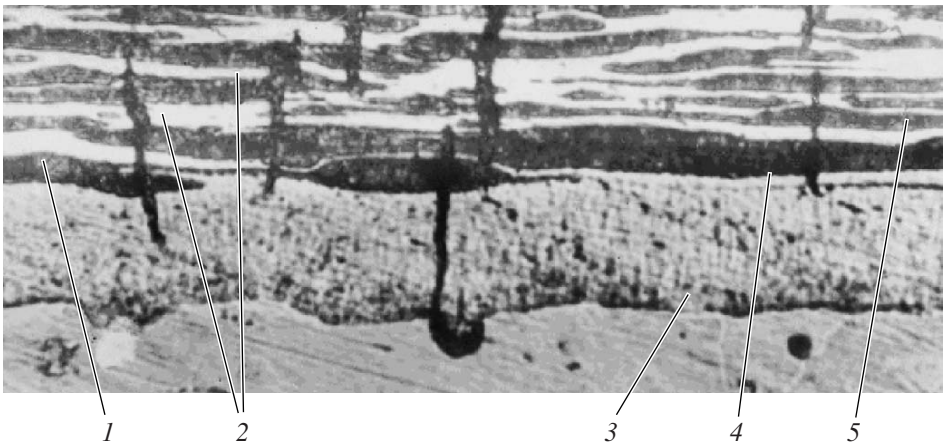

Fig. 6. Structure of the coating layer (×1000) obtained in MSC electrolyte at the following modes: i_k = 6 kA/m^2, T = 313 K, pH = 1.5. (*1*) Layer with high carbon content; (*2*) layer with a more perfect metal structure; (*3*) zone of the initial current density, 0.2 kA/m^2; (*4*) zone of the critical current density (≈ 4 kA/m^2), transition from the granular structure to the layered one; (*5*) subsequent coating layers, current density of 6 kA/m^2.

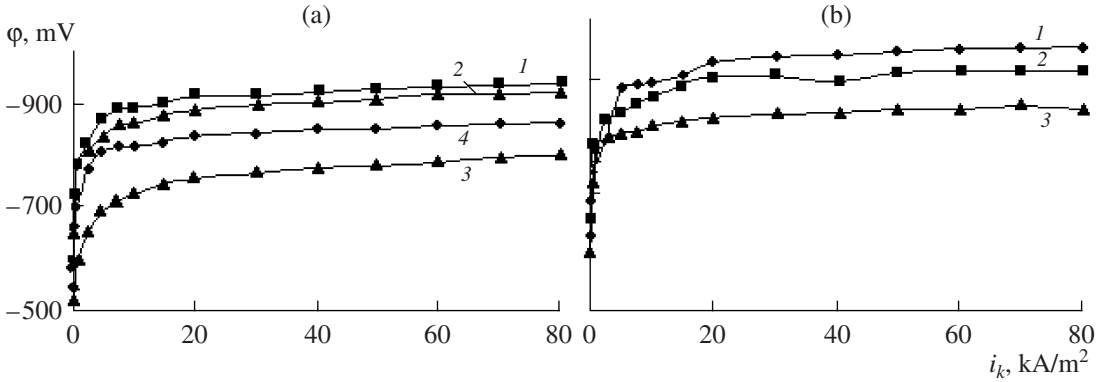

Fig. 7. Polarization curves obtained in the course of iron plating in the MSC 3 electrolyte at the following electrolysis modes: the pH = (a) 0.5 (*4*), 0.9 (*1–3*); (b) 1.6 (*1–3*); *T*, K: 298 (*1* and *4*), 313 (*2*), and 333 (*3*).

perse deposits with a block dimension of 450–470 Å (Fig. 2) and a higher carbon content (Fig. 7). According to present-day theories, significant variation in the hardness of electrodeposits is due to change of their elastic and plastic properties depending on the dimensions of the mosaic blocks (D = 1380–120 Å) and the content of doping elements. As was mentioned earlier, they influence the improvement of the physicomechanical properties due to the strain strengthening effect and the potential formation of base composites of the Fe–Ni and Fe–Mn types and in the presence of carbon in electrodeposited coatings of the $Me_{(n)}$–C type too. Taking into account the probability of formation of the mentioned intermetallic compounds and composites containing carbon, the increase in hardness of the coatings can also be explained by the precipitation strengthening effect [6, 8]. The conditions of its manifestation can be confirmed by the significant (almost by an order of magnitude) decrease in the mosaic block parameter characterizing the degree of dispersion of the crystalline formations of the doped iron coating structure.

The analysis of the research results allows concluding that, in MSC and MSC 3 electrolytes, the formation of doped iron coatings on the cathode is determined by the specific crystallization conditions in the presence of the organic component, by the electrolyte acidity, by the hydrodynamic convection conditions, and by other factors that influence the cathode polarization.

For the deposits obtained at characteristic modes of electrolysis, it is efficient to consider the influence of the chemical composition on the properties of the deposits and the peculiarities of their formation. As the current density increases and the electrolyte acidity decreases, the carbon content in the coatings grows from 0.3 to 0.9% (see Fig. 8). The pattern of carbon distribution in the deposit can be explained by the local

increase in the adsorption of the organic component, its decomposition, and overgrowing. This may be judged by the state of the fibers, grains, and layers with a more perfect metal structure and their fringe regions, which are revealed in the course of the sample microsection treatment with solution–indicators (Figs. 5, 6).

At low acidity and high current density, the formation of layers with a less pronounced metal structure is probably due to a decrease in the metal ion concentrations, consolidation of the -organic substance layer, and insufficiently intense hydrodynamic convection near the cathode surface. The mentioned factors increase the cathode polarization and contribute to an increase in the number of crystal nuclei and to a decrease in the dimensions of the crystal blocks of iron deposits.

According to the known theories of crystallization [8–10, 18, 19], formation of layered electrodeposited coatings in chloride, sulfate, and other electrolytes is due to the inclusion of hydroxides of hydrate–formation pH, especially in the presence of trivalent iron (Fe^{3+}, the hydrate–formation pH is ≈ 3). In MSC electrolytes, in the absence of absolute valence metal ions (Fe^{3+}, etc.), formation of layered coatings at pH < 7–8 is explained by carbon inclusion, and, at pH > 7–8 in the near-cathode layer, it is explained by hydroxides of iron, nickel, and manganese.

The interaction of substances in the near-cathode layer at electrocrystallization stages in a multicomponent electrolyte is a complex process depending on many factors. One of them is the presence of a carbon-containing component in the electrolyte. Therefore, it is necessary to consider the possible conditions of carbon inclusion in the coatings for improvement of their properties.

According to the research data, the energy of breaking bonds with hydrogen is $E = 10^{-2} \times 457$ kJ/mol for CH_2–H, $E = 10^{-2} \times 430$ kJ/mol for CH–H, and $E = 10^{-2} \times 338$ kJ/mol for C–H.

At the cathode polarization and achievement of certain energy levels of the electric field influence on ions (according to one of the probable schemes), carbon can form a stable bond with iron atoms situated in the deposit crystal lattice. According to another scheme, ions of iron methyl sulfate adsorbed on the forming deposit due to breaking of bonds (CH_n–H) in the methyl group according to the scheme $CH_3 \longrightarrow CH_2 \longrightarrow CH \longrightarrow C$ can be decomposed up to the state Fe–C, which is characterized by a less stable bond, and, in this form, they can be included in the deposit. In this case, the carbon atom can occupy the position of a substitutional or interstitial atom in the crystal lattice and can form compounds of the $Fe_{(n)}$–C type with iron and of the $Me_{(n)}$–C type, which are similar to the cementite or base components in the doped steels described earlier, with other metals.

Hydrogen ions, which become free due to bond breaking, can form gaseous hydrogen (H_2) and intensify gas–hydrodynamic convection of the electrolyte.

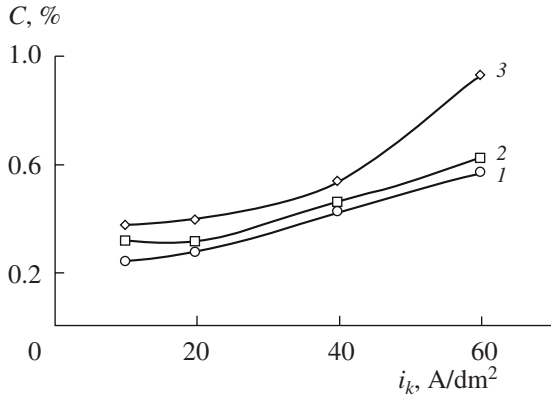

Fig. 8. Carbon content in the coatings obtained in the MSC 3 electrolyte.

Hydrogen in the ionic form will contribute to acidifying of the near-cathode layer, to pH stabilization, and to a decrease in the probability of formation of hydroxides and their inclusion in the deposit.

Thus, the quantity of hydroxide compounds getting into the deposit will depend on the considered factors, the electrolyte acidity, and the current density.

The content of doping elements (up to 0.9% carbon, 2–6% nickel, and 2–4% manganese) should be estimated as an additional energy factor that positively influences the quality and structure of the coatings.

In addition to the mentioned factors, it is efficient to consider the probable formation of a crystalline structure of doped iron coatings at the nanolevel.

The increase of the microhardness with lowering of the temperature and the acidity of the electrolyte (see Fig. 2) is probably due to the presence of doping elements of nickel (r_a = 1.24 Å) and manganese (r_a = 1.31 Å) in the metal base of the coatings. At small differences of the parameters of the ionic form and the atomic radii, these elements can form a particular crystalline structure with iron atoms (r_a = 1.28 Å) being situated in this structure as substitutional or interstitial atoms. A certain role in the formation of the hardening structures is played by carbon atoms too. Taking into account the mean distances between the iron atoms forming the crystal lattice, the highest equilibrium state of the crystal along any axis will be approximately determined by the ratio of the number of atoms of nickel and manganese (mutually compensating for distortions of the parameters of the elementary crystal lattices) being 4 : 3. A material with this crystal structure can be characterized by a higher equilibrium energy state and, therefore, a higher hardness than, for example, hydrogen-containing strained crystal formations of electrodeposited iron.

A content of doping elements of 2–6% and of carbon up to 0.5–1% in iron electrodeposited coatings improves their properties and can contribute to the formation of hardening structures at their heat or laser treatment.

The research analysis has shown that there is a certain interrelation between the principal characteristics of the structure, the parameters of the fine structure, the hardness, and the chemical composition; taking into account this interrelation, one can predict the technological modes for obtaining of materials with the required properties.

The obtained results of the study of the coating properties allow making conclusions concerning sphere of their application in industry. Thus, technological modes for obtaining of soft iron coatings with a fibrous structure can be recommended for recovery and hardening of surfaces of fixed joint pieces. Hard coatings with granular and layered structures and a high carbon content can be applied for recovery and hardening of surfaces of pieces of fixed and movable joints operating under conditions of friction, where high wear resistance is required.

CONCLUSIONS

1. A composition of the MSC 3 electrolyte for obtaining doped iron coatings containing nickel, manganese, and carbon is proposed.

2. It is found that, in the MSC 3 electrolyte, by varying the electrolysis conditions within pH = 0.8–1.6, T = 298–333 K, and a current density of 2–8 kA/m^2, one can obtain coatings with a thickness up to 2–3 mm and a microhardness of 4.5–7.2 GPa. The hardness of the coatings in the range of 2–8 kA/m^2 is provided by the stabilization of the temperature and the acidity of the electrolyte.

3. It is revealed that, by varying the electrolysis modes, it is possible to obtain doped iron coatings containing up to 0.9% carbon, 2–6% nickel, and 2–4% manganese, which are characterized by fibrous–columnar, granular, and layered structures.

4. Some conditions of the formation of various structures of doped iron coatings are characterized. It is shown that the increase in hardness within 4.5–7.2 GPa is due to the decrease in the mosaic block dimensions from D = 1380–1160 Å to D = 120–270 Å and due to the chemical composition variation. Probable schemes of carbon inclusion in iron coatings and the appearance of crystal formations based on intermetallic iron–nickel–manganese and metal–carbon compounds of the cementite type in iron–carbon alloys are considered.

REFERENCES

1. Pleshka, E.D., Study and Development of Technology for Recovery of Motor–And–Tractor Pieces by Iron–Plating in Methyl Sulfate Chloride Electrolyte, *Extended Abstract of Cand. Sci. (Eng.) Dissertation*, Chisinau: Agric. Inst., 1979.
2. Pleshka, E.D., Efficiency of Piece Recovery in the Electrolyte of Increased Stability, in *Progressivnye sposoby vosstanovleniya iznoshennykh detalei mashin* (Advanced Methods of Recovery of Worn-Out Machine Pieces), Chisinau: Agric. Inst., 1983.
3. *Rekomendatsii po vypolneniyu tekhnologicheskogo protsessa vosstanovleniya detalei tipa "os'", "val" elektricheskim zhelezneniem* (Recommendations on Realization of Technological Process for Recovery of Pieces of the "Axis" and "Axle" Types by Electric Iron Plating), Moscow: GOSNITI, 1985.
4. Sidel'nikova, S.P., Study of the Process of Electrochemical Deposition of Iron from Methyl Sulfate Electrolytes, *Extended Abstract of Cand. Sci. (Chem.) Dissertation*, Chisinau, 1974.
5. Petrov, Yu.N. and Sidel'nikov, V.K., Study of Wear Resistance of Electrolytic Alloys of Iron and Phosphorus, *Trudy Kishinevskogo SKhI* (Proceedings of Chisinau Agric. Inst.), vol. 87, pp. 60–67.
6. Gol'dshtein, M.I., Litvinov, V.S., and Bronfin, B.M., *Metallofizika vysokoprochnykh splavov* (Physics of Metals of High-Strength Alloys), Moscow: Metallurgiya, 1986.
7. Rotinyan, A.L., Tikhonov, K.I., and Shoshina, I.A., *Teoreticheskaya elektrokhimiya* (Theoretical Electrochemistry), Leningrad: Khimiya, 1981.
8. Fiser, H., *Elektrolitische Abscheidung und Elekrokristallisation von Metallen*, Berlin: Springer, 1954.
9. Antropov, L.I., *Teoreticheskaya elektrokhimiya* (Theoretical Electrochemistry), Moscow: Vysshaya Shkola, 1984.
10. Skorchelleti, V.V., *Teoreticheskaya elektrokhimiya* (Theoretical Electrochemistry), Leningrad: Khimiya, 1970.
11. Kotik, F.I., *Uskorennyi kontrol' elektrolitov, rastvorov i rasplavov. Spravochnik* (Accelerated Control of Electrolytes, Solutions, and Melts. Handbook), Moscow: Mashinostroenie, 1978.
12. Petrov, Yu.N. et al., To the Problem of Variation of Electrolytic Iron Potential Depending on Electrolysis Conditions, *Trudy Kishinevskogo SKhI* (Proceedings of Chisinau Agric. Inst.), 1869, vol. 54, pp. 11–14.
13. Gin'e, A. *Rentgenografiya kristallov* (X-Ray Diffraction of Crystals), Translation from French, Moscow: Gosizdat Fiz.–Mat. Liter., 1961.
14. Rachinger, W.A., A Correction for the α_1 α_2 Doublet in the Measurement of Widths of X-ray Diffraction Lines, *J. Sci. Instrum.*, 1948, vol. 25, no. 7, pp. 254–255.
15. Gorelik, S.S. et al., *Rentgenograficheskii i elektrograficheskii analiz* (X-Ray and Electron Diffraction Analysis), Moscow: Metallurgiya, 1970.
16. Stepin, V.V., Kurbanova, V.I., and Fedorova, N.D., *Analiz chernykh metallov i splavov* (Analysis of Ferrous Metals and Alloys), Moscow: Mashinostroenie, 1980.
17. Antropov, L.I., *Teoreticheskaya elektrokhimiya* (Theoretical Electrochemistry), Moscow: Vysshaya Shkola, 1984.
18. Loshkarev, Yu.M., Cathodic Process in Electrolysis of Manganese Chloride Solutions, in *Gidrometallurgiya khloridov* (Hydrometallurgy of Chlorides), Kiev, 1964.
19. Loshkarev, Yu.M. and D'yachenko, T.F., *Teoriya i praktika blestyashchikh pokrytii* (Theory and Practice of Lustrous Coatings), Vilnyus, 1963.
20. Vagramyan, A.T. and Solov'eva, Z.A., *Metody issledovaniya elektroosazhdeniya metallov* (Methods of Study of Metal Electrodeposition), Moscow: Akad. Nauk SSSR, 1960.

ISSN 1068-3755, Surface Engineering and Applied Electrochemistry, 2008, Vol. 44, No. 4, pp. 271–280. © Allerton Press, Inc., 2008.
Original Russian Text © Yu.K. Stishkov, A.V. Samusenko, 2008, published in Elektronnaya Obrabotka Materialov, 2008, No. 4, pp. 25–37.

ELECTRICAL PROCESSES IN ENGINEERING AND CHEMISTRY

Computer Simulation of Corona Discharge in an Inert Gas

Yu. K. Stishkov and A. V. Samusenko

St. Petersburg State University, ul. Ul'yanovskaya 3, St. Petersburg, Petrodvorets, 198504 Russia
E-mail: stishkov@paloma.spbu.ru

Received January 16, 2008

Abstract—In this document, computation of the corona discharge in a "cylinder–cylinder" electrode system is described. The Fokker–Planck equation is used to describe the kinetics of the electrons. The basic features of the physical process were observed in the solution. It shows that the stationary mode is possible only when the voltage is larger than a definite threshold value. One can discern two character areas between the electrodes. The internal area where the ionization is active and the current is carried both by electrons and ions has radius of 100–200 micrometers. The rest of the accommodation constitutes the drift area. The solution enables one to compare the illuminating zone and the zone of electrons multiplication. It revealed some features of rare gas discharge that preclude from directly applying the results of this work to discharge in air. Above all, it is a small value of negative charge density, which is caused by the electron conduction character in the external area. Nevertheless the solution of this model problem displays the wide possibilities of the method.

DOI: 10.3103/S1068375508040042

The solution of the problem on corona discharge in a filament–cylinder electrode system is considered in this work. The kinetic equation for electrons is solved in the Fokker–Planck approximation.

CORONA DISCHARGE

Corona discharge develops in gases at pressures in the neighborhood of the atmospheric one in sharply nonuniform electric fields. It is the cause of waste in electric mains and of air isolation infringement in various high-voltage devices. Because of this, the calculation of corona discharge development processes is an important electrotechnical problem.

A filament in a cylinder (Fig. 1) is an example of the configuration of electrodes with a sharply nonuniform electric field. Two specific regions are distinguished in corona discharge: the glow region with relatively high field intensity where the impact ionization can occur (the size of it is usually about a hundred micrometers) and the external zone where the field intensity is relatively low and ionization is almost completely absent. The charged particles generated in the corona glow region drift through this area to the counter electrode.

The discharge onset causes an abrupt current jump (up to three orders) at the negligible growth of the voltage (Fig. 2). The current jump is attended with the appearance of a specific fluorescence near the electrode with a little radius of curvature (Fig. 3). This effect shows the threshold nature of the discharge initiation.

The fluorescence is caused by excited molecules emitting photons when returning into the principal state. The excitation is produced by electron impact; the fluores-

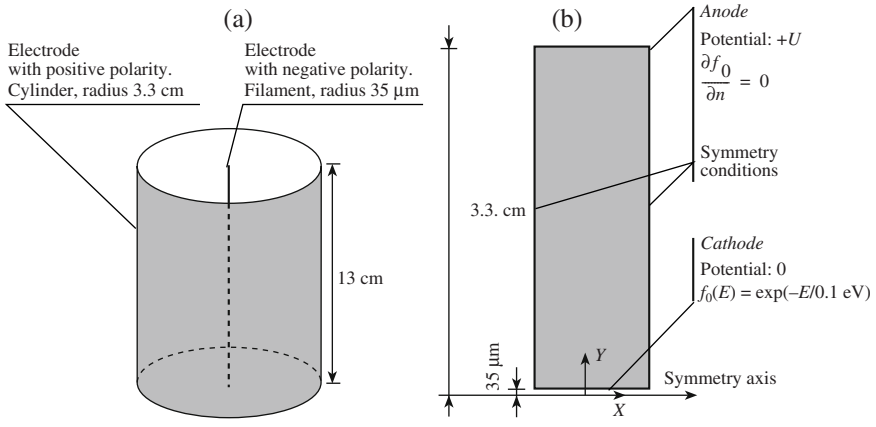

Fig. 1. (a) Configuration of "filament–cylinder" electrodes. their dimensions correspond to the installations in the high-voltage laboratory of the Radiophysics Research Institute of SPbSU; (b) The model in CFD-ACE.

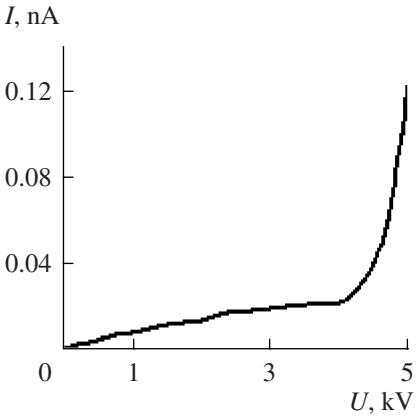

Fig. 2. Typical current–voltage characteristic for air. The current jump to the right is the corona discharge ignition.

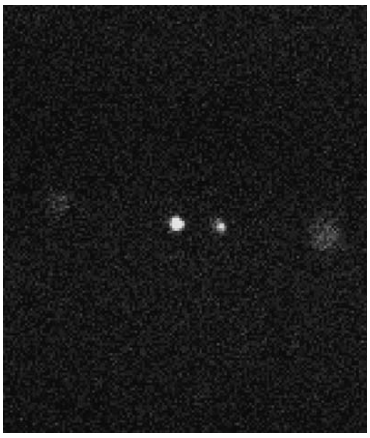

Fig. 3. Fluorescence centers of corona discharge on the conducting filament.

cence is indicative of a great concentration of electrons in the corona glow region and high electron temperature permitting overcoming the ionization and agitation reaction thresholds, which are rather high (about 10 eV).

Review of Methods of Corona Discharge Simulation

Up to now, the universally recognized methods of corona discharge simulation include the calculation of the processes mainly in the corona external zone in the air where ionization practically doesn't occur. For instance, the Daich–Popkov method [1] is widely used. This method permits one to accurately calculate the space charge and the current through the system, but, to realize the method, it is necessary to comply with two conditions: there occurs the unipolar ionic conduction in the external zone, and the threshold voltage value and the field intensity near the corona electrode are known from the experiment. The procedure permitting one to compute the processes occurring in the corona glow region is presented in this work.

The behavior of electrons in the fields with high intensity was calculated at the simulation of single electron avalanches. The Fokker–Planck approximation, the Monte-Carlo method, and other approaches were used here. However, a single avalanche is a nonindependent phenomenon. The corona discharge computation requires accounting for the conditions leading to the independent nature of the process. It is necessary to allow for the dynamics of the electrons and ions and the electric field variation.

It should also be noted that, in the majority of the works, the ionization processes were taken into account with the help of the semiempirical formula describing the growth of the electron flow:

$$j_e(x) = e^{\alpha x}.$$

Here, α is the effective coefficient of the impact collision ionization, and x is the coordinate along the line of the electric field force. In this work, there are prescribed the characteristics of the main reactions influencing the discharge process, thus allowing one to realize in full measure the peculiarities of the discharge in this gas. In addition, there arises the possibility to analyze the effect of different microprocesses with the participation of ions and electrons in the effect on the temperature, concentration, and flows of the charged particles.

Dynamics of the electrons in the discharge

When calculating the corona discharge in the air, one should take into consideration the complex chemical composition of air, as well as a great number of various reactions. In particular, the reaction of electron trapping plays a large role here. This being so, considering the novelty of the approach, there has been developed a calculating board for argon, an inert gas where there is no trapping and the number of the required reactions is minimum. The central problem with the calculation is the dynamics of the electrons. Let's consider more thoroughly the processes with their participation.

Collisions of an electron with the gas neutral molecules, as well as recombination, play a significant part at low concentrations of electrons in corona discharge. The collisions of electrons can be divided into bumping and nonbumping ones. At the bumping collision, the total kinetic energy before and after the impact is conserved; there can occur only some redistribution of kinetic energy.

The electron is light as compared with all the other particles present in the system. Colliding with a heavy particle, a light one can lose a small part of its kinetic energy, thus the estimation [2] is valid:

$$\frac{\Delta E}{E} < \frac{2m_e}{M_{atom}}.$$

The exact value of the energy variation depends on the angle of the particle deflection after the impact. For argon, the energy portion the electron loses after one bumping collision can't be more than 5×10^{-5}. Thus, the electron accelerating in the field accumulates

energy even when undergoing numerous bumping collisions. As a result, there arises the effect of the high temperature of the electrons in comparison with the temperature of all the other kinds of particles in the system. Thanks to this, a large number of electrons can overcome the thresholds of molecule ionization. Thus, in the corona glow region, at the gas temperature of 300 K (0.039 eV), the electron temperature is about 5 eV. Nonbumping collisions are attended with the transition of the kinetic energy into other energy kinds. Collisions with excitement when an atom or molecule takes the electron kinetic energy transiting into another state with larger potential energy is the first type of such processes. In a short time (about 10^{-10} sec), the atom returns into the principal state irradiating a photon. Ionization is another event caused by the interaction of an electron with neutral atoms. The electron loses kinetic energy, and the atom turns into a pair of charged particles: an electron and ion. Recombination is also a nonbumping collision: an electron meets with a positive ion and ceases its life. There exist several mechanisms of recombination; however, our purpose is to solve this problem in order to build the simplest model of the discharge. Consequently, only one mechanism is present in the calculation, namely, photorecombination when an electron with an ion forms a neutral atom and the energy excess is irradiated as a photon.

The free path is a suitable characteristic to estimate the reaction probability. This is the average distance that a particle goes with the given energy E between the acts of single reactions. For example, at the bumping collision of an electron with molecules whose concentration is n and the reaction cut set is σ, the path is given by formula [2]:

$$l = \frac{1}{n\sigma(E)}. \tag{1}$$

The calculation for gas at a temperature of 300 K and at atmospheric pressure are presented; furthermore, the concentration n under these conditions is 2.45×10^{25} l/m^3. Section-electron energy experimental relationships are taken from the JILA data base composed at the university [3].

Let us consider the energy range 5–20 eV, where the thresholds of ionization and excitation of argon are. The path with respect to the bumping collision is 0.4–1.0 μm for argon. The path with respect to excitation (for the most intensive reaction) is 10–40 μm and with respect to ionization is over 20 μm. The path with respect to the bumping collision is relatively short; therefore, there occur several tens of bumping collisions between nonbumping ones and the motion of the electron becomes chaotic and the distribution of the velocities is "blurred". On the other hand, the power consumption at several tens of bumping collisions is small, whereas, at nonbumping collision, the electron gives up nearly all its energy. That is, the electron spectrum is determined not by bumping collisions but by excitation and ionization. Electrons will be distributed with respect to energies not according to the Boltzman law. Usually, it is necessary to calculate the kinetic equation for electrons in order to solve such a problem; however, the randomicity of the electrons allows us to apply the Fokker–Planck approximation.

The Fokker–Planck approximation for the kinetic equation

Strictly speaking, analyzing the motions of many electrons in the electric field, we should look for a function of the electron distribution with respect to the velocities at the given point:

$$f(\vec{r},\ \vec{V},\ t) = f(r_x, r_y, r_x, V_x, V_y, V_x, t).$$

It is evident that such an approach is rather complicated, as now it is necessary to find the function of seven variables. The situation becomes simpler when the characteristic scales of time and distance are such that the distribution with respect to the velocities becomes almost isotropic. In other words, the distribution function depends only on |V|. Physically, it is provided by bumping collisions with heavy particles; that is, we suppose the electron to experience a sufficient number of collisions so that the different directions of the electron velocities become equiprobable.

True enough, in such a case, the electric current is impossible, as electrons upon the average move nowhere. Thus, the first correction for anisotropy is taken into consideration. Namely, if the drift direction corresponds to the angle $\theta = 0$ in spherical coordinates (in the velocity space), we seek the function f in the following form:

$$f(\vec{r},\ |V|, \theta, \varphi, t) = f_0(\vec{r},\ |V|) + f_1(\vec{r},\ |V|)\cos\theta.$$

where $f_1 \ll f_0$. If the current direction is a fortiori unknown, f_1 becomes a vector quantity:

$$f(\vec{r},\ |V|, \theta, \varphi, t) = f_0(\vec{r},\ |V|) + f_1(\vec{r},\ |V|)\vec{n}.$$

Here, n is the unit vector in the velocity space.

At this level of simplification, the dynamics of the electrons are described by the Fokker–Planck equation with allowance made for the potential φ:

$$\begin{cases} V\dfrac{\partial f_0}{\partial t} - \nabla\left[\chi\left(\nabla f_0 + \nabla\varphi\dfrac{\partial f_0}{\partial E}\right)\right] \\ -\dfrac{\partial}{\partial E}\left[\chi\nabla\varphi\left(\nabla\varphi\dfrac{\partial f_0}{\partial E} + \nabla f_0\right)\right] = VS; \\ \vec{f}_1 = -\dfrac{V}{\nu}\nabla f_0 - (\nabla\varphi)\dfrac{V}{\nu}\dfrac{\partial f_0}{\partial E}; \\ \chi = \dfrac{V^3}{3\nu}; \\ E = \dfrac{m_e V^2}{2e}. \end{cases} \tag{2}$$

Here, ν is the frequency of bumping collisions, and E is the kinetic energy. Equations (2) ρ are written for the case when the distribution function argument is not |V|, but the kinetic energy in eV is $E = m_e V^2/2e$. Obviously, it is only a matter of convenience not influencing the equation meaning.

The inapplicability of the Boltsman approximation

The concrete definition of the distribution of electrons with respect to energies is a subsequent level of the kinetic equation simplification. At active exchange of impulses at bumping collisions among many particles, there is established the Boltsman exponential distribution:

$$f(E) = \frac{1}{kT}\exp\left[-\frac{E}{kT}\right]. \quad (3)$$

However, as noted above, at the bumping collision with the gas particle, the portion of energy that the electron can give up is approximately 10^{-4}; that is, in order for such a distribution to be established, about 10 thousand collisions are necessary. However, much earlier (after tens of bumping collisions), there occurs a nonbumping collision when the electron gives up a significant part of its energy.

Electron–electron bumping collisions are also low-probable as the gas ionization level is very small (10^{-11}). Such collisions are less probable than nonbumping collisions with neutral particles of the gas.

Thus, the electron energy balance is established mainly through the nonbumping collisions, and the application of the Boltsman approximation is ungrounded. The solution shows that the distribution of electrons with respect to their energies differs significantly from the exponential distribution (3).

Set of equations

The possibility of the numerical solution of the Fokker–Planck equation (2) caused the choice of the CFD-ACE program package to calculate this problem. We describe other equations solved jointly.

The program requires taking account of the continuous medium equations. It wasn't necessary for this very problem, as the characteristic times of the solution are small enough. Also, really, the solution for the field of velocities gave the machine zero, and the gas pressure didn't change. Nevertheless, here are these equations:

$$\begin{cases} \dfrac{\partial}{\partial t}(\rho_{zhe}\vec{v}) + (\nabla\rho_{zhe}\vec{v})\vec{v} = -\nabla p + (\nabla\mu\nabla)\vec{v} + \vec{S}_{\vec{M}}; \\ \dfrac{\partial\rho_{zhe}}{\partial t} + \nabla\rho_{zhe}\vec{v} = 0; \\ \rho_{zhe} = f(P). \end{cases} \quad (4)$$

The gas density ρ_{zhe}, the pressure P, and the field of velocities v are the sought-for functions.

The calculation of the electric field is carried out in the electrostatic approximation; i.e., it is supposed that the field is described by the Poisson equation:

$$\nabla\varepsilon\varepsilon_0\nabla\varphi = \rho. \quad (5)$$

The electric potential φ is the sought-for function.

In solving equation (5), the data of other modules are used: the charge density ρ is computed on the basis of concentrations of ions and electrons:

$$\rho = \sum_i q_i c_i + en_e.$$

The gas is assumed to be multicomponent, and consisting of particles with different masses and charges. As all particles, except for electrons, are heavy enough, they actively exchange impulse and energy with each other, and their temperature is assumed equal to the medium temperature T and the distribution with respect to energies is assumed to be the Boltsman one.

The change of the concentration of the components Y_k at every point is described by a transport equation incorporating the ruin and generation of particles in various reactions and is added by formulas for the speeds of reactions:

$$\begin{cases} \dfrac{\partial}{\partial t}(\rho_{zhe}Y_k) + \nabla(\rho_{zhe}(\mu_k\nabla\varphi)Y_k) = \nabla(\Gamma_k\nabla(\rho_{zhe}Y_k)) \\ + M_k\sum_j \nu_{kj}\omega_j; \\ \omega_j = k_j\prod_i\left(\dfrac{\rho_{zhe}Y_i}{M_i}\right)^{\nu_{ij}}; \\ k_j = A_jT^{n_j}\left(\dfrac{p}{P_{atm}}\right)^{m_j}e^{-E_a/RT} \text{ (Arrenius form) or} \\ k_j = \int\sqrt{E}\sigma(E)f_E(E)dE \text{ (the reaction cross section)} \end{cases} \quad (6)$$

Here, M_i is the mass of one molecule of the ith component, μ_i is the mobility, Γ_i is the diffusion coefficient possibly depending on the medium temperature, and ν_{ij} are the stoichiometric coefficients.

The concentrations of the components Y_k are the sought-for functions.

The conversions are incorporated by the introduction of the functions ω_i (the intensity of the reaction). Here, the index i is the reaction number. The intensity ω_i is the number of reaction acts in the volume unit for the time unit. The intensity depends on the concentration of the participating components, as well as on various parameters incorporated in the reaction rate coef-

ficient k_j, where j is the reaction number. This important parameter can be given in the so-called Arrenius form or by the table of the reaction cross section; both variants are presented in set (6).

The Arrenius form is simpler and requires less experimental data on the reaction, but it has one very important drawback: the reaction rate depends only on the temperature, i.e., on the average energy of the components, and the distribution of the components with respect to the energies is not taken into consideration. Such an approach is justified when the particles have the Boltsman distribution with respect to energies. However, the distribution of electrons carrying the bulk of the collision energy can differ greatly from the Boltsman one, so, by prescribing the cross section, we make allowance for the possibility of different distributions.

It should be emphasized that, though in formulas for the reaction intensity in (6) the electrons are accounted for along with other particles, the transfer equation (the first equation of set (6)) is not applied to the electrons; their dynamics are calculated with the Fokker–Planck equation.

The data of other modules are used in the set of equations (6): in the reactions with participation of electrons, the electron concentration n_e, as well as the electron distribution with respect to the energies $F_E(E)$, is computed from the function of the electron distribution f.

The dynamics of the electrons and the distribution with respect to the energies is described by the Fokker–Planck equation (2).

The sought-for functions f_0 and f_1 are the functions of the electron distribution with respect to space and energy and the first correction to it.

In equation (2), the data of other modules are used: the frequency of the bumping collisions ν is computed on the basis of the function of the electron distribution with respect to the energies and the concentration of heavy particles, for instance, when allowing for collisions only with the particles of component no. 1:

$$\nu(E) = \sqrt{\frac{2e}{m_e}}\sqrt{E}\sigma_{\text{el}}(E)\frac{\rho_{\text{zhe}}Y_1}{M_1}. \qquad (7)$$

In equation (2), there also appears the electric potential φ calculated by the Poisson equation (5).

The function of the distribution f_0 gives information on the concentration of the electrons:

$$n_e = \int_0^\infty f_0(E)dE. \qquad (8)$$

The first correction for the anisotropy of the distribution with respect to the velocities allows one to compute the electron current density:

$$\vec{j}_e = q_e\frac{8\pi}{3}\int_0^\infty \vec{f}_1(E)\sqrt{\frac{E}{m_e}}dE. \qquad (9)$$

As is seen from set (2), the solution of the kinetic equation in the Fokker–Planck approximation doesn't require the prescription of the electron mobility and the diffusion coefficient. Such coefficients don't even appear in the equation, as it takes into account that electrons with different energy have different drift and heat velocities owing to the strong dependence of the reaction cross section on the electron energy. The only coefficient χ characterizing the diffusion of electrons in the phase space of the coordinates and velocities is calculated from the data on the bumping collision reaction cross section. The frequency of the collisions is given by formula (7).

However, the average drift velocity can be calculated from the solution, as the ratio of the electron current to the electron concentration given by formulas (8) and (9) is the following:

$$\vec{V}_d = \frac{\vec{j}_e}{n_e e}.$$

The mobility is computed as the ratio of the drift velocity to the electric intensity:

$$\mu_e = \frac{V_d}{|\nabla\varphi|}. \qquad (10)$$

Hence, the mobility can substantially depend on the coordinate.

It should be noted that CFD-ACE, in addition to the basic unknown functions directly obtained when solving the set of equations, introduces a lot of derivatives into the solution file. These are the reaction intensities, flows of electrons and gas components, coefficients of diffusion and mobility, the space charge density, and many others; this being so, there is no necessity to perform calculations with formulas (8)–(10) on one's own.

Conditions of the problem

We are coming to the description of the model used to solve this problem. The following properties and parameters are prescribed for the volume:

For the continuous medium equations, 1.4 kg/m^3 is the argon density under standard conditions, the is pressure 101.3 kPa, and the temperature is 300 K; the viscosity (dynamic) is 1.8×10^{-5} kg/m s. Two models with different sets of chemical reactions are considered. The first model is a simplified one containing the minimum number of processes necessary for the occurrence of a

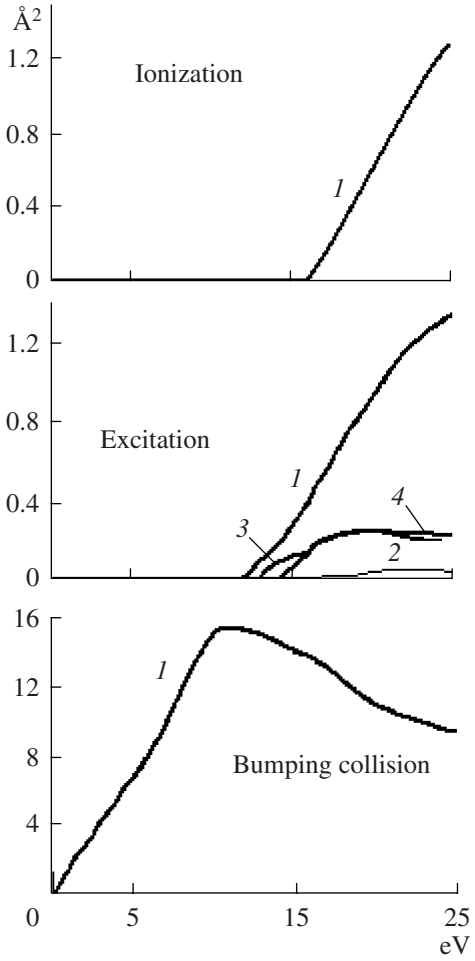

Fig. 4. The reaction cross section versus the collision energy experimental characteristics used when solving the problem. The JILA database is the source. *1* – 11.5; *2* – 13.15; *3* – 13.10; *4* – 14.1 eV.

discharge, namely, bumping collision, ionization, secondary surface emission, and recombination. The following formulas describe the bumping collision and ionization:

$$e + Ar \longrightarrow e + Ar \text{ Bumping collision}$$

$$e + Ar \longrightarrow e + Ar^{+} \text{ Ionization}$$

Four reactions of excitation (with the levels 11.5 eV, 13.1 eV, 13.15 eV, and 14.1 eV) are also considered in the complicated model. The formula describing such reactions is

$$Ar + e \longrightarrow Ar^{*} + e.$$

One of the mentioned levels (11.5 eV) is metastable; its life time is about 1.3 s [2]. This point is important when modeling the discharge, as an excited atom has less ionization potential than an atom in the unexcited state. Long-living excited atoms most likely meet an electron and become ionized. Nevertheless, as the model problem was formulated, it was decided not to examine such a process, which undoubtedly makes the solution analysis more complicated. All four levels are assumed not to be metastable; the excited atom of such levels returns to the principal state in the time 10^{-8} to 10^{-7} s while emitting a photon:

$$Ar^{*} \longrightarrow Ar + h\nu.$$

There is almost no chance for the excited atom to collide with an electron during such a short time, so a simplified scheme of the process description is used. Both reactions (excitation and deenergizing) are described by one formula:

$$e + Ar \longrightarrow e + Ar + h\nu,$$

with the excited atoms being not described as single components, and the future emission of a photon causing the loss of the respective energy by the gas is accounted immediately after the collision.

The reaction cross section versus the collision energy characteristics is given for the excitation, ionization and bumping collisions (Fig. 4). The experimental curves are taken from the database created at the University of Colorado [3].

There exist several important mechanisms of recombination in argon, and yet, for the sake of simplicity, only photorecombination (the energy excess is carried away by the photon) is preassigned in this problem. The process occurs in the following way:

$$Ar^{+} + e \longrightarrow Ar + h\nu.$$

The reaction is specified in the Arrenius form. Namely, it is assumed that the reaction rate ω depends on the concentration of electrons n_e and ions n^{+} in the following way:

$$\omega = cn_e n^{+}.$$

Here, the coefficient c is prescribed as 10^{-6} m^3/s.

For ion Ar^{+}, the mobility is preassigned as 1.5×10^{-4} m/(V s). The diffusion coefficient for ions is calculated from the Einstein relation:

$$\frac{D}{\mu} = \frac{kT}{q_i}.$$

Here, q_i is the electric charge of the ion.

Alongside the time and space variables, there is the energy variable for electrons. It acts as an equivalent axis in the space where the finite-element model is being built. Here, the calculation is carried out in the finite interval from 0 eV to 40 eV with even separation into 140 elements. At the model boundaries with respect to the energy, the boundary conditions are as follows. 0 eV: $f_0(0 \text{ eV}) = 1$ (the finite value of the distribution function at zero energy); 40 eV: $f_0(40 \text{ eV}) = 0$ (becoming zero at the boundary; it is assumed that such quick electrons hardly appear at all). The package per-

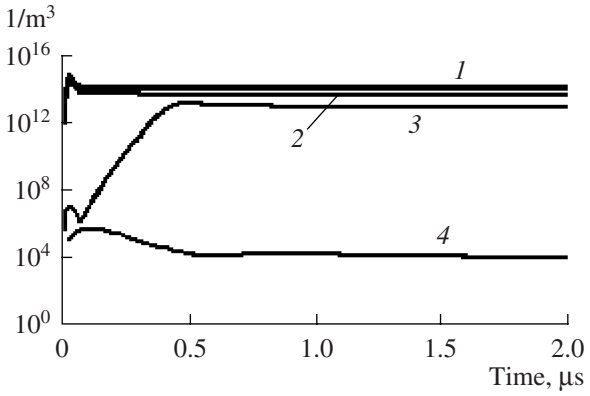

Fig. 5. The electron concentration versus the time characteristic at the distance of 1 mm from the cathode at different voltages. *U*, kV: 1 – 4; *2* – 3; *3* – 2; *4* – 0.5.

forms the normalization of the functions f_0 and the conditions with respect to it itself in the course of solving the problem.

The base boundary conditions are presented in Fig. 1. Introducing the conditions of symmetry at the model lateral boundaries allows one to solve the problem for electrodes with infinite height, and all values in the solution depend only on the radial coordinate.

The following boundary conditions are given at the cathode.

* The wall is impenetrable to gas and the trapping condition ($v = 0$).

* The surface reaction. Secondary emission:

$$Ar^+ \longrightarrow Ar + \gamma e.$$

* The value 0.1 is prescribed for the secondary emission coefficient γ. The meaning of the condition is the following: reaching the cathode, the ion Ar^+ becomes neutral knocking out an electron with probability of 0.1.

* The electron temperature at the cathode is 0.1 eV.

* Zero potential is prescribed.

* The condition on the distribution function: $f_0(E) = \exp[-E/0.1.\ \text{eV}]$ (The Boltsman distribution of the outgoing electrons with the average energy much less than the thresholds for the reactions of the bumping collision).

The following boundary conditions are given at the anode.

* The wall impenetrable to gas, and the trapping condition ($v = 0$).

* Zero flows for all chemical components except electrons.

* A positive electric potential *U*.

* The condition on the distribution function $\partial f/\partial n = 0$ (the normal derivative is zero).

The following initial conditions are specified.

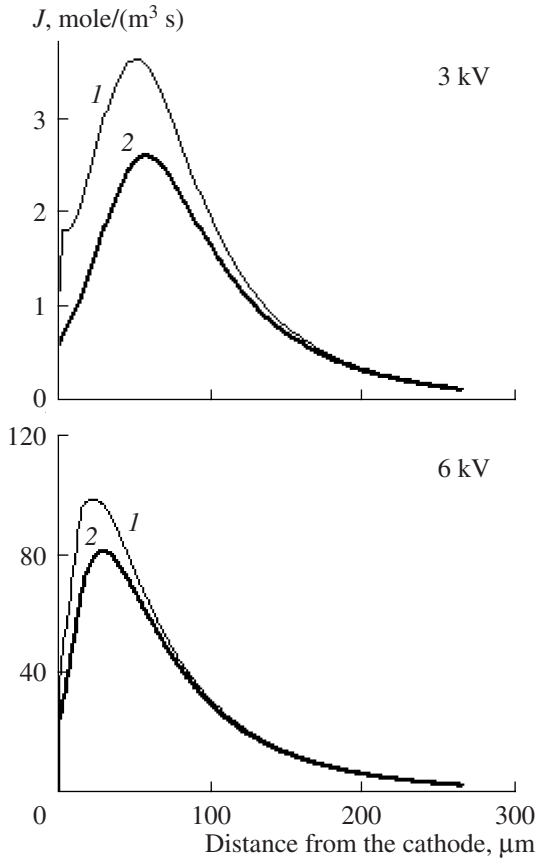

Fig. 6. Intensity of ionization and recombination at different voltages. *1* – Ionization; *2* – Recombination.

* The temperature is 300 K.

* The gas velocity is zero.

* Only neutral argon is presented from the chemical components.

* The electron concentration is 10^6 1/m^3.

* The function of the electron distribution with respect to the energies is the Boltsman one at every point with the average energy 0.1 eV.

The problem on the occurring of discharge at the instant switching on of the voltage at the moment $t = 0$ is being solved.

Analysis of the calculation results

Consider the main results of the modeling. In Fig. 5, it is shown how the electron concentration changes at different voltages. At voltages higher than 2 kV, it exponentially grows and then becomes stable. At less voltage, the concentration exponentially drops till the zero level. Thus, 2 kV is the discharge ignition threshold.

Figure 6 presents the intensity of the ionization and the recombination in the corona glow region at voltages

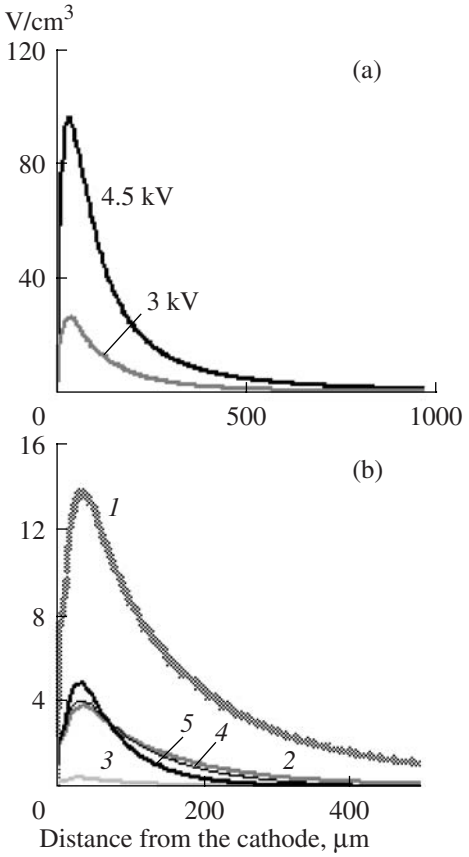

Fig. 7. (a)—Emitted intensity under steady conditions at different voltages; (b)—emitted intensity with respect to reactions (4 excitation reactions and recombination) under steady conditions at the voltage 3 kV. *U*, eV: *1* – 11.5; *2* – 13.10; *3* – 13.15; *4* – 14.1; 5 – recombination.

of 3 kV and 6 kV. The ionization exceeds recombination only in a small (100–200 μm from the cathode) area. It is called the discharge glow region; multiplication of electrons occurs here. Farther from the cathode μs, beyond the corona glow region, the ionization and recombination are compensated for; i.e., multiplication is absent.

In the experiment, the corona discharge is observed by the luminescence pattern, so it is important that the numerical solution permits us to obtain the intensity distribution of the reactions in the course of which the photons are generated. Knowing the photon energy for every reaction, we get a chance to study the emission of the radiant energy in different regions of the model. As the graph in Fig. 7 shows, the main part of the photonic energy is emitted in the course of the excitation reaction with the least threshold.

The solution shows that the luminescence area width exceeds the ionization area width. We assume that the typical dimension of the region where this quantity is concentrated is the radius of the zone where the quantity value may amount to more than 10% of the maximum. At the voltage 3 kV, the typical dimension of the region for the ionization intensity measures 190 μm, and the typical dimension of the region for light emission power measures 350 μm.

In an electric field, negative and positive charges move in different directions, and there occurs the so called separation of charges. There appear regions with positive (at the cathode) and negative (at the anode) space charge (Fig. 8). The mobility of the electrons forming the negative charge is much less than the mobility of the ions, thus the absolute magnitude of the negative density is far less than the magnitude of the positive density.

The presence of the space charge causes the disturbance of the electric field distribution, thus reducing the intensity near the cathode (Fig. 9).

The electric current density under steady conditions reduces in reverse proportion to the distance from the

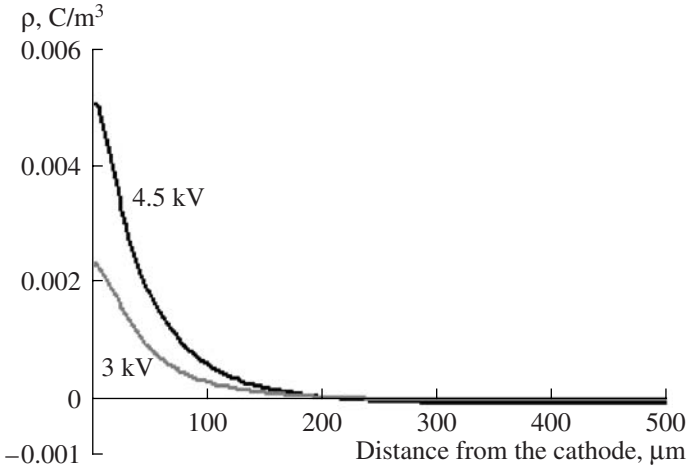

Fig. 8. Electric charge density at different voltages.

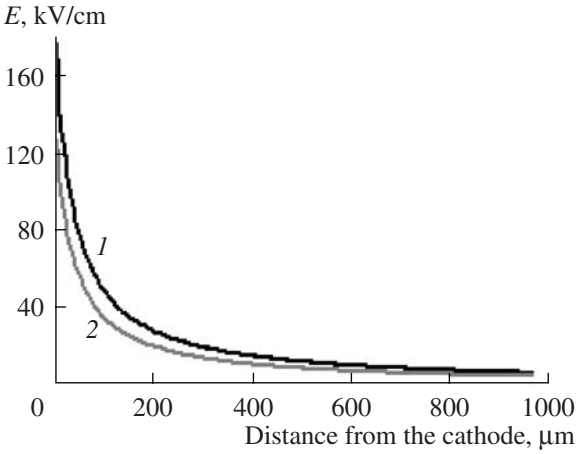

Fig. 9. Electric intensity at zero time and under steady conditions disturbed by the space charge. *1* – Without charge. *2* – Steady conditions.

problem symmetry axis r, so it is more convenient to speak of the total current through a conventional cylindrical surface whose axis coincides with the symmetry axis. As we consider the problem on cylindrical electrodes at infinite height, we should speak of the current per unit of height $I(r)$ of the system. Since all the quantities in the problem depend only on the radial coordinate r, the current per unit of length is connected with the current density $j(r)$ by a simple relation:

$$I(r) = 2\pi r j(r).$$

Under steady conditions, the current through the cylindrical surface I doesn't depend on the radial coordinate.

The current per unit of length I versus the radial coordinate characteristic is shown in Fig. 10. At a small distance from the cathode, in the discharge glow region, the current is transported mainly by ions, and, farther on beyond the region boundaries, it transforms into an electron current with the sum of the electron and ion currents being constant, as it must under steady conditions. The total current grows rapidly with the intensity increase, and the corona region where there occurs the multiplication of electrons enlarges.

As in the problem, there is carried out the calculation of the function of the electron distribution (FED) with respect to the energies, and we have a chance to derive the spectrum of the electrons at any point of the space. The FED at different distances from the cathode is presented in Fig. 11. Although the temperature of the electrons isn't more than 6 eV, there are a lot of electrons with energy exceeding the ionization potential 15.8 eV in the discharge glow region. In the external region of the corona, there are no such electrons. Here, the energy balance is maintained by nonbumping collisions with excitation; thus, the distribution is cut at

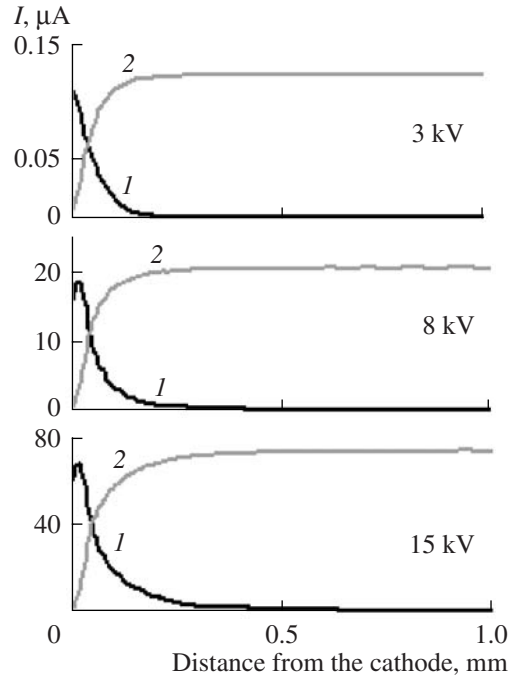

Fig. 10. Current through the cylindrical surface of radius r coaxial with the axis of symmetry of the problem for 1 cm of the system height. *1* – ions; *2* - electrons.

energies of 11–14 eV corresponding to the thresholds of these reactions. It is seen that, with moving away from the cathode, there diminishes the distribution "tail" permitting the ionization processes to proceed.

This effect shows that the concurrence of excitation and ionization plays a crucial role in the discharge processes; it is precisely excitation that doesn't allow the electron to accumulate energy for ionization in the external region of the discharge.

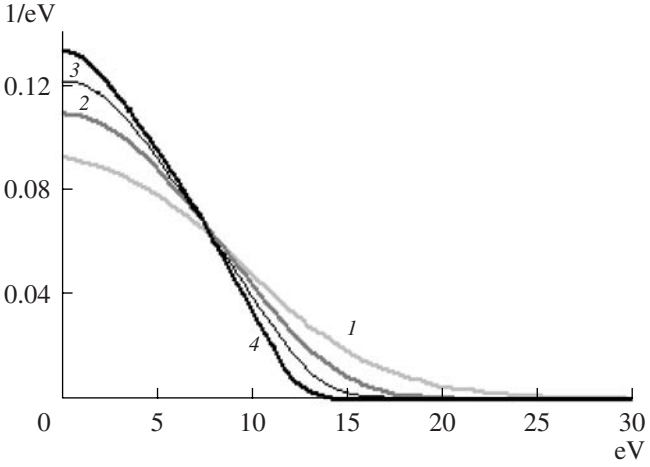

Fig. 11. Electron spectrum at different distances from the cathode. *1* – 10; *2* – 100; *3* – 300; *4* –1000.

CONCLUSIONS

In this work, it has been possible to build a corona discharge model exhibiting the principal features of the process.

The solution shows that steady conditions are possible at voltages exceeding some threshold value. This value corresponds to the condition of the self-maintained discharge origin. Then, two typical regions are observed in the interelectrode space. One is the discharge glow region where active multiplication of electrons occurs and the current is transported both by ions and electrons. This region's radius is 100–200 μm. The rest of the space forms a much larger zone of drift. Here, the current is transported only by electrons, ionization diminishes rapidly with the cathode moving away, and it is completely compensated for by recombination. The solution allows one to compare the luminescence zone with the zone of electron multiplication and to show that the first one is larger.

Thus, in this work, we managed to simulate the processes occurring in a discharge glow region. In this problem, the intensity of the ionization and the excitation is determined on the basis of the function of the electron distribution with respect to the energy, the spectrum of electrons. As the solution demonstrates, the distribution in the glow region differs greatly from the Boltsman distribution; the profile is considerably changing with moving away from the cathode. It directly influences the probability of ionization and excitation. Thus, when simulating the processes in the discharge glow region, it is impossible to avoid the calculation of the electron spectrum.

The solution has also disclosed the peculiarities of the discharge in an inert gas, which don't permit one to apply the results directly to the discharge in the air. First of all, this is the small magnitude of the charge negative density caused by the fact that the current in the drift zone is transported by electrons whose mobility is big in comparison with the mobility of ions. As is known, in the air, in the drift zone, the current is transported by negative ions not appearing in inert gases; thus, the role of the negative space charge in the air becomes crucial. Nevertheless, the solution of this model problem shows the wide capabilities of the method. We can expect some progress in the solution of the more complicated problem—the calculation of the processes in the air discharge glow region.

REFERENCES

1. Buyanov, A.V., Elagin, I.A., Pavleino, V.F., Stishkov, Yu.K., and Statuya, A.A., Modeling of Corona Discharge by Daich-Popkov method in ANSYS medium, *Sbornik dokladov VI mezhdunarodnoi nauchnoi konferentsii po sovremennym problemam elektrofiziki i electrodinamiki zhidkostei* (Proc. VI Int. Conf. on Modern Problems of Electrophysics and Electrodynamics of Liquids), St. Petersburg, 2003, pp. 37-41.
2. Raizer, Yu.P., *Fizika gasovogo razryada* (Physics of Gas Discharge), Moscow: Nauka, 1992.
3. Materials to the program package CFD-ACE, ESI-CFD group, 1994-2004.

ISSN 1068-3755, Surface Engineering and Applied Electrochemistry, 2008, Vol. 44, No. 4, pp. 281–284. © Allerton Press, Inc., 2008.
Original Russian Text © L.A. Kuz'micheva, Yu.V. Titova, A.I. Maksimov, 2008, published in Elektronnaya Obrabotka Materialov, 2008, No. 4, pp. 38–41.

ELECTRICAL PROCESSES IN ENGINEERING AND CHEMISTRY

Investigation of the Opportunity for Increasing the Yield of Hydrogen Peroxide in Plasma–Solution Systems

L. A. Kuz'micheva, Yu. V. Titova, and A. I. Maksimov

Institute of Solution Chemistry, Russian Academy of Sciences, ul. Akademicheskaya 1, Ivanovo, 153045 Russia
E-mail: jvt@isc-ras.ru

Received December 24, 2007

Abstract—The influence of the addition of alcohol (ethanol and propanol-2) to an electrolyte solution on hydrogen peroxide formation under the action of glow and gliding discharges of atmospheric pressure was studied. The addition of alcohol up to 0.1 mol/l was found to increase the yield of H_2O_2 significantly.

DOI: 10.3103/S1068375508040054

INTRODUCTION

Plasma–solution systems are very promising with respect to the development of effective methods of purification and sterilization of water, aqueous solutions, and products [1]. The mechanisms of such processes may be sufficiently complex, but, as a rule, they include reactions of OH radicals, which are generated in the solution under the action of plasma, and the product of their dimerization—hydrogen peroxide. H_2O_2 is a relatively stable secondary oxidizing agent formed at the gas discharge treatment of the aqueous solutions of electrolytes.

Convenient for practical applications are discharges with an electrolyte cathode using sources of direct or industrial frequency voltage with a relatively low voltage on the order of one or several kilovolts. Glowing and sliding glowing discharges with the electrolyte electrodes related to them, as well as such discharges generated within the volume of the solution, act as the diaphragm and end ones [1, 2]. The chemical processes initiated by the action of glowing discharge in a solution may proceed under the action of OH radicals in a small area of the direct effect of the discharge on the solution only (in the cathode spot); in the rest of the solution volume, the reactions proceed with the participation of hydrogen peroxide [1], and, hence, the increase in the yield of H_2O_2 has a practical value. Formation of hydrogen peroxide under the action of glowing discharge was sufficiently studied in detail by us earlier [1, 3, 4]. The action of gliding discharge on a solution of electrolytes was investigated in [5–7]. It was shown in them that this discharge type is more effective than the glowing one with respect to initiation of oxidation processes.

The yield of H_2O_2 in a plasma–solution system obviously depends on both the discharge characteristics and the chemical composition and concentration of the electrolyte solution [1, 2]. Some alcohols are known to be effective traps for OH radicals and are used in investigations of the processes of hydroxyl radicals and hydrogen peroxide formation in plasma–solution systems [8, 9]. However, our experiments have shown that small additions of these substances to the electrolyte solution affected by the action of the gas discharge are capable of increasing the yield of H_2O_2 by several times.

The object of the work is to study the influence of the additions of alcohols (ethanol and propanol-2) on the accumulation of hydrogen peroxide under the action of glowing and sliding discharges.

EXPERIMENTAL

Schemes of the experimental installations are given and described in [7]. The glowing discharge was in the air between the metal anode with an edge being in the gas phase and the solution surface. The value of the discharge gap was 4 mm. The sliding discharge was generated between the anode of variable curvature and the electrolyte surface. An air stream moved above the solution surface in the direction of increasing the discharge gap. The interelectrode distance was 4–8 mm. A more detailed description of the two types of discharges is given in [3, 5–7].

The accumulation of hydrogen peroxide was defined by the method of iodometric titrations with ammonium molybdate as a selective catalyst using the standard procedure [10]. As the process solutions, distilled water and 0.01 M solutions of Na_2SO_4 with additions of ethanol and propanol-2 up to a concentration of 0.05 to 1 mol/l were used. The volume of the process solution was 100 ml; the discharge current was 10 mA. The solutions of electrolytes were mixed during the whole process of the plasma treatment. During the experiments, the pH and electroconductivity of the solutions were controlled as well.

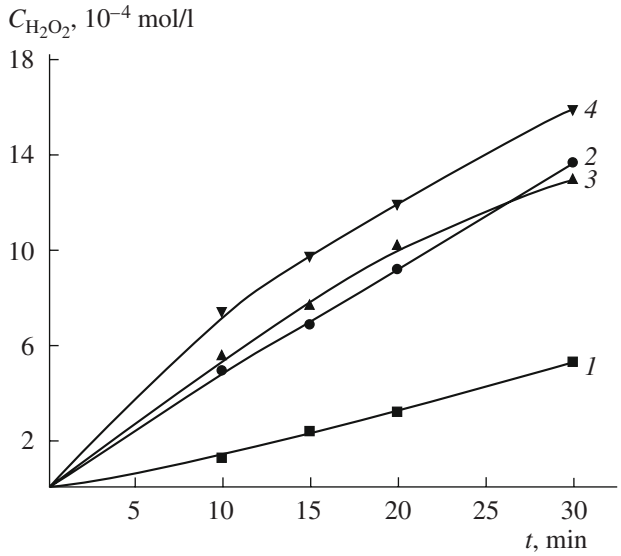

Fig. 1. Accumulation of hydrogen peroxide under the action of glowing discharge: (*1*)—in a 0.01M solution of Na_2SO_4; (*2*)—in a 0.01M solution of Na_2SO_4 with the addition of ethanol to a concentration of 0.1M; (*3*)—in a 0.01 M solution of Na_2SO_4 with the addition of propanol-2 to a concentration of 0.1M; (*4*)—in a 0.01M solution of Na_2SO_4 with the addition of propanol-2 to a concentration of 0.05M.

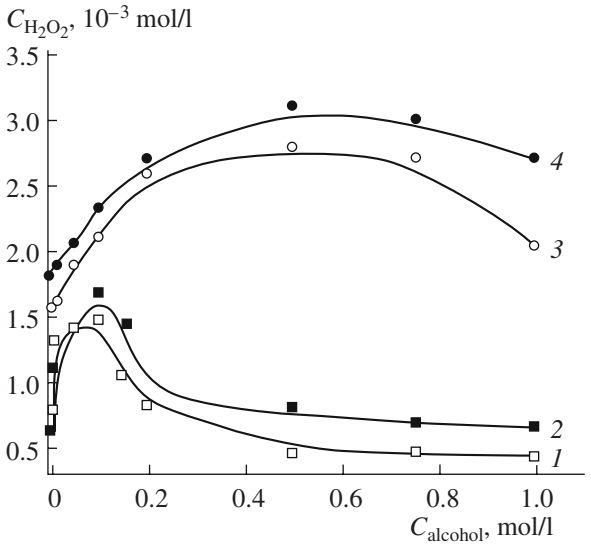

Fig. 2. Accumulation of H_2O_2 in water under the action of glowing (*1*, *2*) and gliding (*3*, *4*) discharges vs. the concentration of ethanol (*2*, *4*) and propanol-2 (*1*, *3*) in the solution. The solution volume is 100 ml, the discharge current is 10 mA, and the treatment time is 30 min.

RESULTS AND DISCUSSION

Since alcohols are sufficiently effective traps of OH radicals, one might expect that with increasing the concentration of alcohols in the electrolyte solution the yield of H_2O_2 as a product of $OH^{\bullet}$ dimerization should decrease. However, experimental data show that the yield of hydrogen peroxide at small additions of alcohols increases in comparison with the solution (Fig. 1). Thus, adding ethanol to the 0.01M Na_2SO_4 solution up to a concentration of 0.1 mol/l at 30-minute treatment causes an increase of the yield of H_2O_2 from 5.2×10^{-4} up to 1.4×10^{-3} mol/l, and adding propanol-2 up to a concentration of 0.05 mol/l increases the yield of hydrogen peroxide up to 1.6×10^{-3} mol/l (Fig. 1).

Current output of hydrogen peroxide in a 0.01 M solution of Na_2SO_4 with addition of alcohols under the action of glowing discharge at a current of 10 mA

Concentration of alcohol, mol/l	Yield of H_2O_2, mol/F	
	Ethanol	Propanol-2
0	0.28	0.28
0.01	0.48	0.45
0.05	–	1.1
0.1	0.61	0.77
0.3	0.30	–
0.5	0.23	0.15

From the initial section of the kinetic curves, the current outputs of H_2O_2 in the solutions of sodium sulfate under the action of the glowing discharge as the number of formed molecules of hydrogen peroxide counting upon one falling single-charged ion (or the amount of H_2O_2 substance formed in the solution while passing one faraday of electricity through it) was calculated. The calculation was carried out according to the formula

$$f = R_0 V N_A / (N_A I / F),$$

where R_0 is the rate of hydrogen peroxide generation during the initial moment of time, mol/(l s); V is the volume of the treated solution, l; N_A is the Avogadro constant, 6.02×10^{23} mol^{-1}; I is the current strength, A; and F is the Faraday constant, 9.46×10^4 mol/charge (or mol/F). Results of the calculations obtained are presented in the table.

The dependence of the H_2O_2 concentration obtained in the solution as a result of the 30-minute plasma treatment with glowing and sliding discharge on the concentration of alcohols is presented in Fig. 2. The passage through a maximum of the curves indicates that the alcohols participate not only in the processes of hydrogen peroxide formation but also in the processes of H_2O_2 consumption. Moreover, with increasing the temperature of the solution, the rate of the inverse process increases. Thus, the rate of hydrogen peroxide consumption increases with both increasing the concentration of alcohol and increasing the average temperature of the solution. Then, the maximum position on the curve will depend on how quickly the solution heats up.

In the case of the sliding discharge, under otherwise equal conditions, the heating of the solution is much less than in the case of the glowing discharge (since the area of the cathode spot is not localized). Hence, under the action of the sliding discharge, the size of the maximum and its position moves to the side of the higher concentrations of alcohol.

The action of the glowing discharge on the solution leads to reducing the pH of the electrolyte solutions [1]. However, in the case of using the electrolyte solution–alcohol mixtures, acidification of the solution as a result of the plasma treatment either proceeded to a much smaller degree or was not observed at all (Fig. 3). In our opinion, the following explanation can be given for this fact. It is shown in work [11] that, under the action of glowing discharge on the electrolyte solution in the liquid phase, the accumulation of nitric acid takes place, which causes increasing acidity in the system. One may expect that, in the presence of alcohol in the electrolyte solution, its interaction with HNO_3 occurs [12]:

$$C_2H_5–OH + HNO_3 \longrightarrow C_2H_5–O–NO_2 + H_2O$$

or

$$CH_3CH(OH)CH_3 + HNO_3 \longrightarrow CH_3CH(O–NO_2)CH_3 + H_2O.$$

The consumption of the acid in these reactions leads to that the final pH value of the solution appears to be higher than when using the electrolyte without adding alcohols.

The difference in the pH values observed during the experiments most likely is connected with the fact that the yield of nitrogen oxides formation in the gas phase (and, consequently, of nitric acid in the solution) is bound with the character of the discharge. While the sliding discharge is occurring, the area of the contact of the plasma zone with the solution is much more and so the yield of nitric acid is higher resulting in the lower pH values of the solution.

Increasing the yield of hydrogen peroxide in the considered plasma–solution system, in our opinion, is caused by the chemical reactions with participation of the alcohols initiated by the action of the glowing discharge. The action of the glowing discharge on the solution of ethyl alcohol at reduced pressure has been investigated in the work of Almubarak and Wood [13]. The main products of the interaction were acetaldehyde, hydrogen peroxide, and 2,3-butanediol. The authors suggest a number of basic reactions proceeding in the solution, and additional channels (besides dimerization of OH radicals) of hydrogen peroxide formation are shown. One of them is connected with intermediate formation of an organic peroxide radical ($CH_3CHOH\cdot$), the second includes a peroxyl radical ($HO_2\cdot$) as an intermediate product. Since glowing and sliding discharges are similar in nature, it is possible to assume that the action of the latter on the solutions with adding alcohols leads to qualitatively similar results.

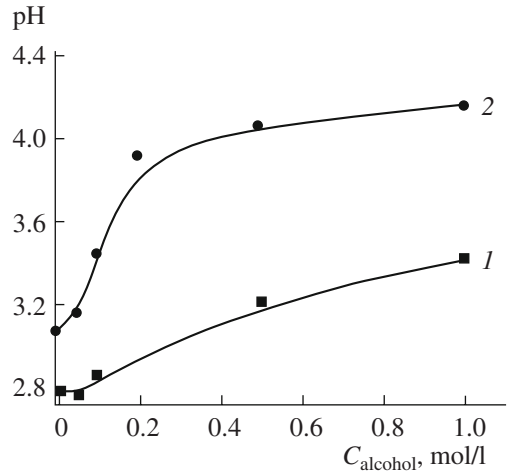

Fig. 3. Influence of the alcohol concentration on the pH value of the solution after the 30-minute treatment with glowing (*1*) and gliding (*2*) discharges. Water, the solution volume is 100 ml, and the discharge current is 10 mA.

It should be noted that replacement of the aqueous solution with the electrolyte solution–alcohol mixture influences the properties of the very discharge too. At the concentration of alcohol of more than 0.5 mol/l, the appearance of the discharge varies: the plasma zone is considerably narrowed, and the color of the discharge changes from violet to blue. The latter means that the chemical composition of the gas phase also changes as a result of transferring alcohol molecules and products of their oxidation from the solution.

REFERENCES

1. Zakharov, A.G., Maksimov, A.I., and Titova, Yu.V., Physicochemical Properties of Plasma–Solution Systems and Possibilities of Their Technological Applications, *Usp. Khim.*, 2007, vol. 76, no. 3, pp. 260–278.
2. Maximov, A.I., Physics, Chemistry and Applications of the AC Diaphragm Discharge and Related Discharges in Electrolyte Solutions, *Contrib. Plasma Phys.*, 2007, vol. 46, nos. 1–2, pp. 1–8.
3. Kuz'micheva, L.A., Titova, Yu.V., and Maksimov, A.I., Formation of Hydrogen Peroxide Under the Action of Atmospheric Pressure Glow Discharge upon Aqueous Solutions of Electrolytes, *Elektron. Obrab. Mater.*, 2004, no. 4, pp. 57–61.
4. Maximov, A.I., Kuzmicheva, L.A., Khlustova, A.V., et al., Transfer of Solution Components to a Plasma Zone in Chemical Reactions Initiated by a Glow Discharge in Electrolyte Solutions, *Mendeleev Commun.*, 2007, no. 17, pp. 1–3.
5. Janca, J., Kuzmin, S., Maximov, A., et.al., Investigation of the Chemical Action of the Gliding and "Point" Arcs Between the Metallic Electrode and Aqueous Solution, *Plasma Chem. Plasma Process.*, 1999, vol. 19, no. 1, pp. 53–67.
6. Maximov, A.I. and Titova, J.V., The Investigation of Chemical Action of Gliding and Glow Discharges

Between Metallic Electrode and Aqueous Solution, *Elektron. Obrab. Mater.*, 2002, no. 1, pp. 64–68.

7. Kuz'micheva, L.A., Titova, Yu.V., and Maksimov, A.I., Investigation of Atmospheric-Pressure Gliding Discharge Action on an Electrolyte Solution, *Elektron. Obrab. Mater.*, 2008, no. 2, pp. 35–38 [*Surf. Eng. Appl. Electrochem.* (Engl. Transl.), 2008, no. 2, pp. 106–109].
8. Polyakov, O.V., Badalyan, A.M., and Bakhturova, L.F., Investigation of the Structure of a Solution Primary Reaction Zone in Conditions of Anode Microdischarges Influence, *Chemistry for Sustainable Development*, 2001, vol. 9, no. 9, pp. 749–757.
9. Joshi, A.A., et al., *J. Hazard. Mater.*, 1995, vol. 41, p. 3.
10. Skoog, D. and West, D., *Osnovy Analiticheskoi Khimii* (Fundamentals of Analytical Chemistry), Moscow: Mir, 1979, vol. 1.
11. Kuz'micheva, L.A., Titova, Yu.V., and Maksimov, A.I., Influence of gas-phase processes initiated by a glow discharge on the properties of electrolyte solutions, *Elektron. Obrab. Mater.*, 2006, no. 3, pp. 148–152 [*Surf. Eng. Appl. Electrochem.* (Engl. Transl.), 2006, no. 3, pp. 58–63].
12. Terney, A., *Sovremennaya Organicheskaya Khimiya* (Modern Organic Chemistry), Moscow: Mir, 1981, vol. 1.
13. Almubarak, M.A. and Wood, A., Chemical Action of Glow–Discharge Electrolysis on Ethanol in Aqueous Solution, *J. Electrochem. Soc.*, 1977, vol. 124, no. 9, pp. 1356–1361.

ISSN 1068-3755, Surface Engineering and Applied Electrochemistry, 2008, Vol. 44, No. 4, pp. 285–287. © Allerton Press, Inc., 2008.
Original Russian Text © M.K. Bologa, I.V. Kozhevnikov, 2008, published in Elektronnaya Obrabotka Materialov, 2008, No. 4, pp. 42–44.

ELECTRICAL PROCESSES IN ENGINEERING AND CHEMISTRY

Electrohydrodynamic Pump Characteristics at Different Parameters of the Interelectrode Space

M. K. Bologa and I. V. Kozhevnikov

Institute of Applied Physics, Academy of Sciences of Moldova,
ul. Academiei 5, Kishinev, MD-2028 Republic of Moldova

Received April 14, 2008

Abstract—The possibility to improve EHD-pump characteristics by partially limiting and using the backward (cellular) flows in the interelectrode space is shown. The optimal parameters of the flow-limiting diaphragm, the accumulator, and the interelectrode space are determined.

DOI: 10.3103/S1068375508040066

Research works on the study and improvement of electrohydrodynamic (EHD) pumps testify that their characteristics considerably depend on the dielectric liquid ionization processes on the electrodes and the EHD-flow structure in the interelectrode space (IES). Whatever the electrode geometry is, as a rule, in the IES, there arise backward (vortex) flows [1, 2], in which the major dissipation of the electric field energy occurs.

Backward flows can be partially suppressed by narrowing the canal; however, this is accompanied by the growth of wall friction in the IES and a decrease of the EHD-flow intensity. Thus, it is worthwhile to use vortex flows that are partially suppressed. To study the opportunity to use such an approach for the improvement of EHD-pump characteristics, it is employed using an installation consisting of a rectangular container filled with a working medium (kerosene) where an EHD pump is mounted (Fig. 1). Electrodes *1* and *2* are placed in coaxial dielectric casing *3*. The pump electrode accumulator *2* is made in the form of a plate with through holes; emitter *1* is a wire with a 1 mm diameter with varnish insulation with perforation. The electric field heterogeneity level at the perforation is better than in the case of a needle electrode, but the electric field threshold intensity at which there occurs the breakdown of the interelectrode space is higher. Dielectric plate *4* with a hole, in whose centre there is a perforation in the insulation, is mounted immediately adjacent to the emitter. The space between the electrodes is varied with the help of dielectric bushes *5*. The electrodes are located using grips *6* and *7*. The pump outlet branch pipe is connected with piezometer *8* with drain *9* to measure the flow rate. The head produced by the pump is determined at the zero flow rate, thus permitting one to obtain reliable data on the effect of various factors on the EHD-pump work.

The relationships between the head characteristics of the pump under investigation and the voltage at different geometries of the emitter are presented in Fig. 2.

In the case of an emitter plate with a through hole on whose edges there occurs the ionization of the dielectric liquid, the head characteristics (curve *1*) are considerably worse due to the concentration of the electric intensity being lower than at the perforation and needle, thus reducing the extent of the working medium ionization. It should be noted that the unsteadiness of the electrohydrodynamic flow is caused by the nonuniformity of the liquid charging on the long edge of the hole. This being so, a wire in varnish insulation with a perforation is used as the

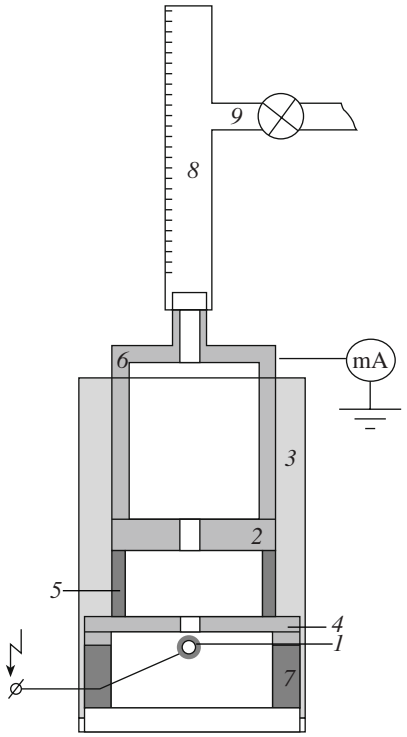

Fig. 1. The electrohydrodynamic pump diagram.

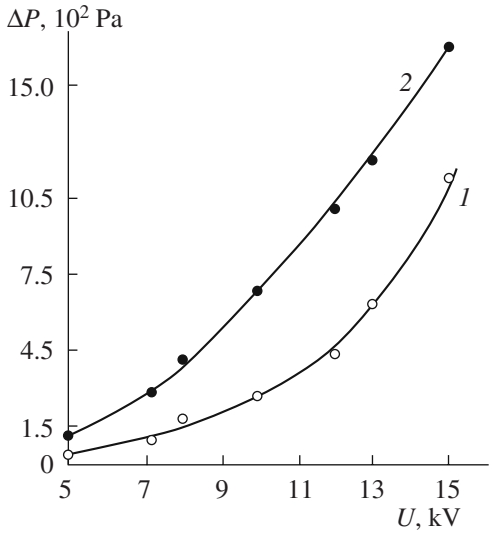

Fig. 2. The head versus the potential difference characteristic. Emitter: *1*—flat plate; *2*—wire with perforation.

emitter. The pump characteristics are greatly influenced by the thickness h of the dielectric plate placed immediately adjacent to the emitter (Fig. 3). As h is increased, with the interelectrode space l being constant, the thickness of the liquid layer between the dielectric plate and the accumulator reduces thus causing the redistribution of the electric field and growth of the interelectrode space wall friction. It results in the worsening of the head characteristics (curves *1–3*, Fig. 3). Variation of h of less 1 mm doesn't affect the pump parameters, but decreasing the diameter d_1 of the hole in the dielectric plate somewhat raises the head (curves *1* and *2*, Fig. 4). The dielectric plate with a hole plays the part of a diaphragm limiting the backward flows, which cause the sucking in effect at the perforation area on the wire. The interelectrode space l also influences the pump characteristic (Fig. 5) by improving it with l being reduced at the constant potential difference between the electrodes (curves *1–3*, Fig. 5) at the expense of the electric intensity E growth.[1]

The same relationship is observed with the increase of l at constant E (Fig. 6) due to the reduction of the interelectrode space wall friction. The head produced by the pump considerably depends on the diameter d_2 of the hole in the accumulator. The relationships between the head and the potential difference between electrodes at various d_2 are presented in Fig. 7 (curves *1–3*).

The optimal results are obtained in the case when $d_2 = 2$ mm. The accumulator hole diameter reducing the electric intensity increases at the expense of the diminution of the distance between the perforation and the hole edge and the unsteadiness of the electrohydrodynamic flow typical for the needle–ring system.

The replacement of the accumulator (the plate with a hole by a metallic net) also causes the improvement of the head (curves *2–4*). The use of the net (at some drop of the head, curves *1, 4*) simplifies the pump design. The IES optimal parameters (h, l, d_1, and d_2) are established. The maximum static head of 5025 mm (625 mm of kerosene in a column) is obtained, and it isn't the limiting value.

Thus, using the flow limiting diaphragm and backward (cellular) flows in the interelectrode space liquid free layer, it is possible to substantially improve the characteristics of the electrohydrodynamic pump with the wire–plate electrode system.

[1] Grosu, F.P., Bologa, M.K. *Elektronnaya Obrabotka Materialov*, 2008, no. 4 (252), pp. 42–44.

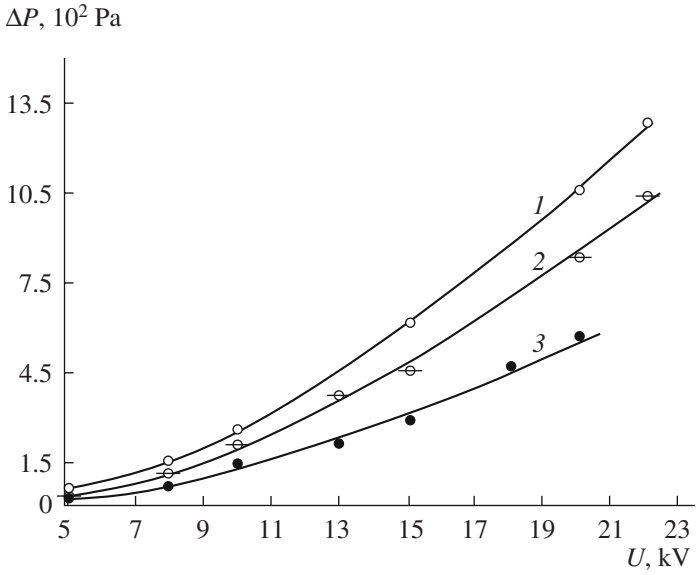

Fig. 3. The head versus the potential difference characteristic at different thicknesses of the dielectric plate, h (mm): *1*—1.0; *2*—2.0; *3*—3.0.

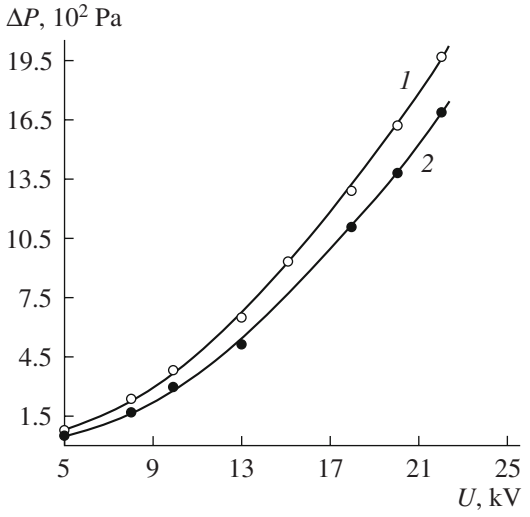

Fig. 4. The head versus the potential difference characteristic at different diameters of the hole in the dielectric plate, d_1 (mm): *1*—1.5; *2*—2.0.

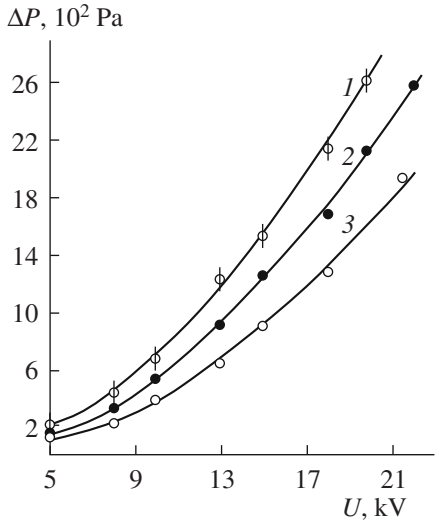

Fig. 5. The head versus the potential difference characteristic at different distances between the electrodes, l (mm): *1*—1.2; *2*—2.0; *3*—3.0.

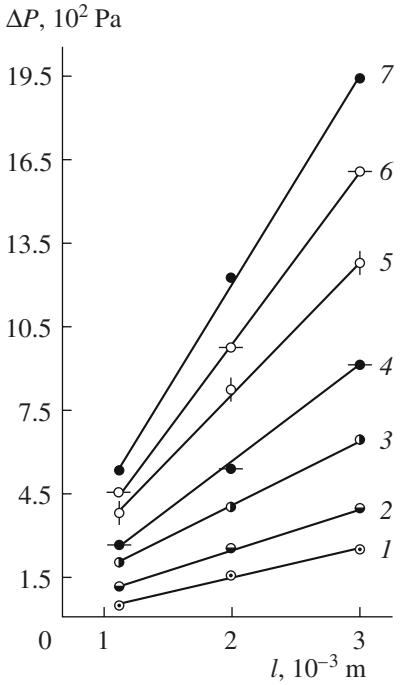

Fig. 6. The head versus the distance between the electrodes characteristic at different electric intensities, E (kV/mm): *1*—2.7; *2*—3.33; *3*—4.33; *4*—5.0; *5*—6.0; *6*—6.67; *7*—7.33.

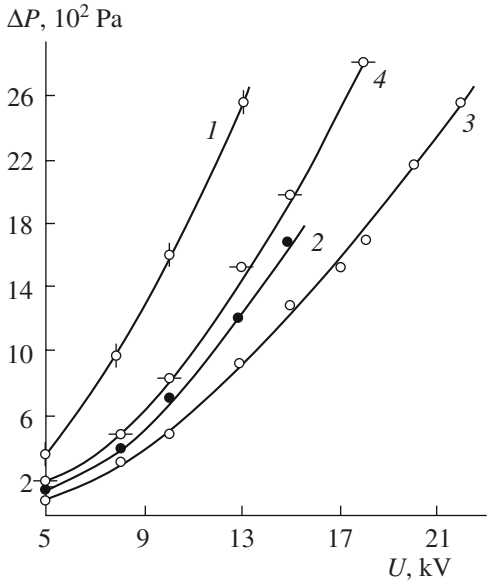

Fig. 7. The head versus the potential difference characteristic at different diameters of the hole in the accumulator, d_2 (mm): *1*—1.0; *2*—2.0; *3*—3.0; *4*—accumulator net (1 × 1 mm).

REFERENCES

1. Bologa, M.K., Grosu, F.P. and Kozhuhar', I.A., *Electrokonvektsiya i teploobmen* (Electroconvection and Heat Exchange), Kishinev: Shtiintsa, 1977.

2. Stishkov, Yu.K. and Ostapenko, A.A., *Elektrogidrodinamicheskie techeniya v zhidkikh dielektrikakh* (Electrohydrodynamic Flows in Liquid Dielectrics), Leningrad, 1989.

ISSN 1068-3755, Surface Engineering and Applied Electrochemistry, 2008, Vol. 44, No. 4, pp. 288–292. © Allerton Press, Inc., 2008.
Original Russian Text © N.V. Polishchuk, M.S. Panchenko, I.M. Panchenko, 2008, published in Elektronnaya Obrabotka Materialov, 2008, No. 4, pp. 45–50.

ELECTRICAL PROCESSES IN ENGINEERING AND CHEMISTRY

Influence of the Radii of Quartz Capillaries on the Rising Height of Water in an Electric Field

N. V. Polishchuk, M. S. Panchenko, and I. M. Panchenko*

Rovno State Humanitarian University, ul. Ostafova 31, Rovno, 33000 Ukraine

** The European University of Finance, Information Systems, Management, and Business, ul. Kievskaya 64B, Rovno, 33028 Ukraine*

Received February 7, 2008

Abstract—In quartz macrocapillaries of various radii, discharge fields of identical intensity result in an additional rise of water in different ways. This is caused by different changes in the properties of the liquid and solid phases, as well as the strong influence of the fields.

DOI: 10.3103/S1068375508040078

Practically all natural bodies and, in most cases, bodies of artificial origin are penetrated by a network of macro- and micropores, which are transport channels for water in the processes of moistening and drying, as well as places for liquid in equilibrium conditions. For natural and industrial use of such bodies, the rise in the height of the water often has a crucial importance, since the vital functions of plants and animals, as well as the physical, chemical, and technological properties of bodies of abiocoen, are defined by molecular interactions of the solid phase of the bodies with the surrounding liquid and the vapor–air media kept in macro- and microcapillaries.

External electric fields (EFs), which are always present both in nature and in the conditions of various manufacturing processes, effect the molecular interactions between the solid, liquid, and vapor phases, since these interactions have an electromagnetic nature. The thermodynamic equilibrium between the phases at equality of the pressure and temperatures is always broken if they have various electrochemical potentials. Particularly, a significant infringement can occur if a moist body is affected by an external nonuniform electric field (NUEF), which breaks the uniform distribution of free and polarization charges. In this case, the arising ponderomotive forces actuate the loose phase, i.e., water. Tonks in 1935 and Frenkel in 1936 already showed that there is a hump on the liquid surface in EF, and, at increasing the voltage between the electrodes, it is extended in a cone and droplets of the liquid are emitted from its top; i.e., there is a breaking of the liquid surface [1].

It is known that separate cylindrical capillaries obtained artificially (N.V. Churaev et al., the Institute of Physical Chemistry, Russian Academy of Sciences) are an elementary model of macropores of real capillary–porous bodies. In these bodies, the macropores are the large reservoirs wherefrom the microcapillaries soak up water and deliver it to significant height (soils, grounds, plants, etc.). However, in the microcapillaries, the water motion occurs slowly (its speed is in direct proportion to the square of the capillary radius and is in inverse proportion to the length of the liquid column). In the macrocapillaries, the liquid motion occurs quickly, but the rise height is small owing to the counteraction of the gravity. The consequence of its action can be reduced at the expense of the ponderomotive forces of NUEF, which is confirmed in [2].

It follows from the theoretical backgrounds [2] that the rise height of the liquid h_e in the macrocapillary ($r_0 > 1 \times 10^{-7}$ m) in the conditions of NUEF counteracting gravity should be equal to

$$h_e = \frac{2\sigma_{12}\cos\theta}{r_0((\rho_1 - \rho_2)g - f_x)}, \quad (1)$$

where σ_{12} is the surface tension on the boundary with the moist air, θ is the limiting wetting angle, r_0 is the capillary radius, ρ_1 is the density of water, ρ_2 is the density of the vapor–air medium, g is the acceleration of gravity, and f_x is the volume density of the ponderomotive forces.

If we assume that the dielectric permeability of water is proportional to its density, the classical expression for the f_x value appears as follows [3]:

$$f_x = \rho_e E + 0.5\varepsilon_0(\varepsilon_1 - 1)\nabla E^2, \quad (2)$$

where ε_0 is the electric constant, ε_1 is the dielectric permeability of water, E is the EF intensity, and ρ_e is the density of the free electrical charges. Using Jurin's formula for the rise height h_0 of the water in the capillary in the absence of EF

$$h_0 = \frac{2\sigma_{12}\cos\theta}{r_0(\rho_1 - \rho_2)g} \quad (3)$$

and inputting the value of the relative rise height h_e/h_0 of the liquid in NUEF, we obtain

$$\frac{h_e}{h_0} = \frac{1}{1 - \dfrac{(0.5\varepsilon_0(\varepsilon_1 - 1)\nabla E^2 + \rho_e E)}{(\rho_1 - \rho_2)g}}. \quad (4)$$

It follows from the expression (4) that the relative rise height of the liquid in the macrocapillary should not depend on its radius. Experimental data [2] contradict this statement. In Fig. 1 in [2], the dependence of h_e/h_0 from r_0 is precisely traced, since the dependence curves $h_e/h_0(E)$ at different r_0 of the capillary tubes (CTs) are located in various manners.

As follows from the figure (the $h_e/h_0(r_0)_{E = \text{const}}$ [2] curve), the maximum value of h_e/h_0 at the fixed E value is observed at $r_0 = 1.9$ mm, i.e., at $a_k/2$, where a_k is the capillary constant of water [4]. The quartz CTs while soaking water settled down vertically between the metal electrodes: a plate was in the water, and an edge was above the CT mouth in the air. At r_0, which is either more or less than 1.9 mm, impetuous dropping branches of the $h_e/h_0(r_0)_{E = \text{const}}$ curve are observed. It is connected with the fact that, when decreasing r_0, to initiate and propagate the spark discharge (SD) (the value of E is chosen such that the SD occurs in the CT with $r_0 = 1.9$ mm), it is necessary to sharply increase the intensity E of the EF, since the volume of the ionization zone is reduced in inverse proportion to the cube of the radius. At $r_0 < 1.9$ mm, the initiation and transformation of the corona discharge (CD) into the SD in the narrow CTs are carried out at much greater E than in the CTs with greater r_0. If $r_0 \ll 1.9$ mm, the CD can not arise at all. In such CTs, the possibility of initiation of the SD also essentially decreases even at $E \gg 16 \times 10^6$ W/m. According to [5], the breakdown voltage in the concrete samples of 1 cm thickness $U_{br} = 66–54lgr_0$ (U_{br} is in kV, r_0 is in microns).

It is consistent with the avalanche stream theory of gases breakdown. The experimental data obtained by Raether in the Wilson chamber show that the maximum radius of an electronic avalanche during the moment of streamer formation at breakdown of the air gap of 1 cm is within the limits of 0.07–0.13 mm [6].

In the CTs with $r_0 > 1.9$ mm, reduction of the $h_e/h_0(r)_{E = \text{const}}$ values (in spite of the favorable conditions for the entering of the field lines into their volume and propagation of both the CD and the SD) is connected with the fact that the wider is the CT, the greater the liquid weight to be raised per each height unit. However, at the fixed values of E and ∇E^2, the same ponderomotive force effects this weight. Therefore, the greater the liquid weight in the tube, the smaller the height to which it rises in NUEF. In addition, in the wide CT in discharge NUEFs, especially at the SD, a deeper electrophysical treatment of the liquid and the tube substance is processed. In the case of initiation of the CD or the SD, the volume and film liquids that contact with the meniscus, as well as the surficial layers of the tube wall, are saturated with ions of the same polarity as the potential of the electrode wherefrom the discharge is propagated [7]. Reduction of the h_e/h_0 values is also caused by the radical change (electrophysical modification) in the physical and chemical properties of the water and the surficial layer of the solid phase and the adhesiveness of both the CT and water at the same time [8–12]. It testifies to changing the mechanism of the influence of the additional rise of the liquid at a significant intensity of the external discharge EF due to a change in the properties of the interacting phases in the wide CTs.

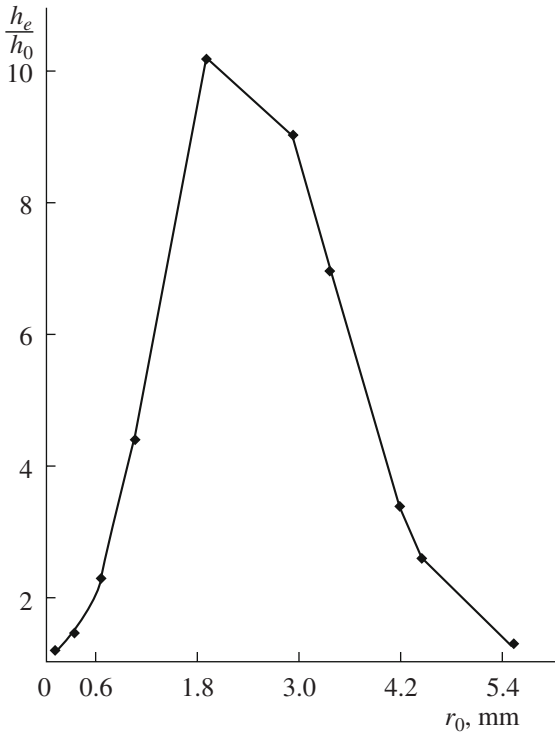

Dependence of the water relative rising height h_e/h_0 ($T = 293$ K) on the r_0 radii of the quartz CT at $E = 16 \times 10^6$ W/m of constant EF.

As a whole, for the given radii of the CTs (see the figure), the discharge fields are capable of significantly influencing the water rise. This occurs owing to the interaction of the three phases and the influence of external NUEFs on them, especially the discharge ones, which shift the moist heterogeneous system far from the initial equilibrium condition due to a significant change in the superficial and volume properties of its phases and, first of all, the liquid phase.

Such an electrohydrodynamical (EHD) Δh_e-effect (the difference in the heights of the liquid column in the field and out of the field) can be used to intensify the processes of water filtration and impregnation of the real porous bodies by liquid dielectrics, as well as to accelerate drainage of the moist bodies due to approaching the zone of water evaporation to the sur-

face of the porous body with subsequent dispersing of it and ejecting the charged droplets out the body borders without expenses of the phase transition heat.

In the area of the discharge, even low-current EFs with a large field intensity of the CD or the SD exist. In Young's formula, all the interphase superficial tensions change in a complicated manner [13–19], and, therefore, it is necessary to replace the values of σ_{12} and θ in the numerator of (1) with σ_{12}^e and θ_e. In work [19], the value of the Δh_e-effect in EF of a flat vertical condenser was calculated by the formula $\Delta h_e = \varepsilon_0(\varepsilon - 1)E^2/2\rho_1 g$, which does not consider the changes in the superficial tension and the limiting wetting angle and the other properties of the liquid in the discharge fields.

Due to the action of strong NUEFs, the nonuniform concentrations of the polarization and free charges occur along the length of the tube, predetermining the occurrence of internal NUEF additional to the external field, which is directed to the tube mouth too. It leads to pooling the cylindrical wetting film of macroscopic thickness in the same direction.

Under the influence of NUEF, water rises upwards [20, 21] up the walls of the wide vessel as in the CT of the large radius, which is explained by the complex joint action of the ponderomotive forces of NUEF, the free and bound charges on the surface of the interfacing liquid and gas, and the polarized dielectric wall of the vessel, as well as by the action of the superficial forces and the gravitation forces. As is well known, without a field, the rise height of the liquid near a vertical infinite plate that is wetted with a liquid is defined by the following formula [4]:

$$h = \sqrt{\frac{2\sigma_{12}}{\rho_1 g}(1 - \sin\theta)}. \tag{5}$$

It follows from formula (1) that, under the action of NUEF, in the denominator of (5), one needs to take the difference $\rho_1^e g - f_e$. Then,

$$h_e = \sqrt{\frac{2\sigma_{12}^e}{\rho_1^e g - f_e}(1 - \sin\theta_e)}. \tag{6}$$

Thus, actually, NUEF (especially the discharge ones) can substantially influence the rise height of the moistening liquid near the wall of the vessel. Due to the action of NUEF, the expression for the x^{th} coordinate of a point that is on the bent surface of a liquid [4] is the follwing:

$$x_e = \sqrt{\frac{\sigma_{12}^e}{\rho_1^e g - f_e}}\left\{\left[2\cos\left(45° - \frac{\theta_e}{2}\right) + \ln tg\frac{90° - \theta_e}{4}\right] - \left[2\cos\frac{\alpha}{2} + \ln tg\frac{\theta_e}{4}\right]\right\}, \tag{7}$$

where α_0 is the angle between the tangent at the given point of the bent surface of the liquid and the horizontal plane in it.

The y coordinate accordingly will be

$$y_e = \sqrt{\frac{2\sigma_{12}^e}{\rho_1^e g - f_e}(1 - \cos\theta_e)}. \tag{8}$$

Equations (7) and (8) are the ones of the liquid surface near an infinite plate and are presented in the parametrical form.

Thus, the presence of NUEF ($f_e \neq 0$), especially of large E and ∇E^2, can significantly change not only the height but also the form of the bent surface of the liquid near the vessel wall, and it causes pooling of the film above the meniscus, which leads to transferring the liquids by EF [21, 22]. Also, punching the meniscus along the axis of the wide CT with the corona wind (CW) assists it, since the corona wind puts on the pressure $\rho_1^e \overline{v}_{CW}^2/2$ [20], where $\overline{v}_{CW}$ is the average speed of the CD wind. The top of the deformed meniscus is known to correspond to $E_{\max}$ of EF [23]. At the same time, on the internal surface of the tube, there is a cylindrical film of macroscopic thickness of radius, naturally, less than r_0. Due to this, the Laplace force increases and the water column rises higher than in absence of the field. Owing to pooling of the cylindrical film, while increasing E and ∇E^2 of the discharge field, the CT section free from the liquid decreases, which also leads to the Δh_e effect. Counteraction of the processes that compete (the increased gravity, deformation of the meniscus, and the change in σ_{12}^e and other values) leads to fluctuating of the liquid column. It is also assisted by the pulse character of the CW and the SD.

With further increasing E—while approaching the meniscus to the CT mouth—and, consequently, ∇E^2, as well as the current density i, new effects occur, in particular, dispersing the wetting film and sound and thermal effects. The sound accompanying the SD assists the liquid rising according to the mechanism [24]; and the thermal influence dries up the wetting film and reduces the superficial tension that reduces the height of the liquid column.

At $E \approx 1 \times 10^7$ W/m, vapor–gas bubbles appear in the water column. This leads to a sharp reduction of the average density of the water–steam–air mix and consequently, according to (1), to the corresponding increase in h_e. In such a nonuniform dielectric, bound charges occur whose density is defined by the expression $\rho_b = \varepsilon_0 \vec{E}\,\nabla\varepsilon$. The similar charges on the bubbles cause their expansion, and the divided water columns are pushed out between them to the CT mouth.

At some critical value q_c of the charge on the water surface, the advantage of the electric force over the forces of the superficial tension and gravitation comes.

The stability of the liquid surface is broken; as a result, it appears visually as superfine droplets ejecting from the surface of the meniscus. They are grasped with the CW reflected from the liquid surface [25] and thrown away onto the walls of the CT in different (including quite considerable) distances from the liquid surface. New nonstationary processes increase in a greater measure; in particular, an increase in the frequency and amplitude of the fluctuations of the liquid column are observed, as well as ejecting droplets flows from the aqueous films on the walls of the CT.

As the meniscus moves to the capillary mouth, the CD transforms into the SD; consequently, the current density and the warming up of both the wetting film and the liquid of the basic column increases. It leads to the occurrence, on the one hand, of longitudinal and transverse ∇T and, on the other hand, to the intensification of the liquid motions caused by the jet stream. In the liquid column, due to water electrolysis and local volume boilings, comparatively large bubbles are formed, which significantly reduce the density of the vapor–liquid mixture and, consequently, according to (1), the height of the water column increases (ρ_1 decreases and, hence, the $(\rho_1 - \rho_2)$ difference does). The increase in the Δh_e effect is assisted also by the Evershed effect, which causes relative motion of the liquid and the bubbles and, consequently, overflowing of the liquid into the area of strong EF.

Increasing the water level in the CT under the influence of NUEF proves to be true according to the fact that, in [26], under the metal electrode with the polished hemispherical surface of d = 2.7 mm, the rise of the aqueous electrolyte in the wide vessel ($r_0 \longrightarrow \infty$) was also observed. At the same time, the electrolyte surface takes a conical form and the electric breakdown of the discharge gap is carried out between the electrolyte "edge" and the metal electrode.

Considering what was stated above and in [2], obviously, in the formula (1) for calculation of the rise height of water in the CT under the action of NUEF, it is necessary to use expression [27] instead of f_e in (2):

$$f_e = \sigma_e^e \nabla E - 0.5\varepsilon_0 E^2 \nabla \varepsilon_1 + 0.5\varepsilon_0 \nabla \left[E^2 \left(\frac{\partial \varepsilon_1}{\partial \rho_1^e} \right)_T \rho_1^e \right]$$

$$+ \frac{0.5\varepsilon_0(\varepsilon_2 E_2^2 - \varepsilon_1 E_1^2)}{h_s} + \rho_e E + \frac{\varepsilon_0 \varepsilon_1 z_i}{\varphi_0 h_e} \int \left(\frac{\iota}{\sigma_e} \right)^2 \left(\frac{\iota dr}{\sigma_e} \right)$$

$$\pm \frac{\Delta p}{\delta_e'} + \frac{\sigma_{12}^{e2}}{2\varepsilon_0 \varepsilon_1 h_s} + \frac{q^2 \cos^4 \theta_e}{16\pi^2 \varepsilon_0 \varepsilon_1 r_0^4 h_s} \qquad (9)$$

$$+ \frac{0.5\varepsilon_0 \varepsilon_1}{\delta_e'^3} \frac{l_e U^2}{\left(r_0 - \chi - \frac{\chi}{a'} \right) \ln \left(r_0 / \left(r_0 - \chi - \frac{\chi}{a'} \right) \right)^2}$$

$$- 0.5\varepsilon_0 E^2 \left(\frac{\partial \varepsilon_1}{\partial T} \right)_{\rho_1} \nabla T,$$

where the designations of the values and the physical meaning of the separate members are the same as in [27].

In (9), some members contain the values of the capillary radii; so, in the denominator of the expression (4) for the relative rise height of the water in the CT, the r_0 value and other specific parameters will be present that describe the change of the physical properties of the phases interacting in strong EF in the conditions of the proceeding of the discharge currents and the phenomena associated with them. However, a number of the parameters should be defined in the conditions of the specific experiments, since they are unknown now. As a consequence, expression (9) cannot be used directly to calculate the Δh_e effect yet; nevertheless, it qualitatively specifies the dependence of the relative rise height of the water in NUEF on the radii of the CT.

The information on the influence of the radii of the separate quartz CTs on the water rise in NUEF presented in the given work can be applicable to the description of the moisture exchange in real porous bodies in the conditions of the action of electric fields of various spatial configurations and various kinds of gas discharges.

REFERENCES

1. Frenkel', Ya.I., On the Tonks' Theory of Breaking a Liquid Surface by an Electrostatic Field in Vacuum, *Zh. Eksp. Teor. Fiz.*, 1936, vol. 6, no 4, pp. 347–350.
2. Polishchuk, N.V., Panchenko, I.M., Panchenko, M.S., and Karpovich, I.N., Effects of Action and Afteraction of Electric Fields on the Water Rise in Macrocapillaries, *Elektron. Obrab. Mater.*, 2002, no. 4, pp. 54–67.
3. Tamm, I.E., *Osnovy Teorii Elektrichestva* (Fundamentals of Electricity Theory), Moscow: Nauka, 1976.
4. Landau, L.D. and Lifshits, E.M., *Teoreticheskaya Fizika: Gidrodinamika* (Theoretical Physics: Hydrodynamics), Moscow: Nauka, 1986, vol. 6, 3rd ed.
5. Bernatskii, A.F., Tselebrovskii, Yu.V., and Chunchin, V.A., *Elektricheskie Svoistva Betona* (Electrical Properties of the Concrete), Vereshchagin, Yu.N., Ed., Moscow: Energiya, 1980.
6. Reter, G., *Elektronnye laviny i proboi v gazakh* (Electronic Avalanches and Breakdown in Gases), Komel'kov, B.C., Ed., Moscow: Mir, 1968.
7. Denisov, A.A. and Nagornyi, V.S., *Elektrogidro- i Elektrogazodinamicheskie Ustroistva Avtomatiki* (Electrohydrodynamical and Electrogasdynamical Devices of Automatics), Leningrad: Mashinostroenie, 1979.
8. Rogov, V.M. and Filipchuk, V.L., *Elektrokhimicheskaya Tekhnologiya Izmeneniya Svoistv Vody* (Electrochemical Technology of Changing the Water Properties), Lvov: Vysshaya Shkola, Izd. Lvov. Univ., 1989.
9. Bogomolova, L.D. and Zhachkin, V.A., Paramagnetic Centers in Ion-Implanted Inorganic Glasses, *Fiz. Khim. Stekla*, 1998, vol. 24, no. 1, pp. 3–30 [*Glass Phys. Chem.* (Engl.Transl.), 1998, vol. 24, no. 1, pp. 1–18].
10. Pukh, V.P., Baikova, L.G., Ivanov-Omskii, V.I., and Zvonareva, T.K., Influence of Ionic Bombardment on the

Strength of Glasses, *Fiz. Khim. Stekla*, 1998, vol. 24, no. 5, pp. 648–651 [*Glass Phys. Chem.* (Engl.Transl.), 1998, vol. 24, no. 5, pp. 460–462].

11. Grigor'ev, A.I., Shiryaeva, S.O., and Koromyslov, V.A., Considering the Effect of Electric Charge Relaxation in the Problem of Instability of the Charged Liquid Surface, *Elektron. Obrab. Mater.*, 1996, nos. 2–3, pp. 37–39.
12. Melcher, J.R. and Schwarz, W.J., Interfacial Relaxation Overstability in a Tangential Electric Field, *Phys. Fluids.*, 1968, vol. 11, no. 12, pp. 2604–2616.
13. Dubkova, V.I., Radtsevich, S.P., Komarevich, V.G., and Kotov, D.A., Influence of Ion-Beam Carbon-Fiber Surface Treatment on the Angle of Wetting by Epoxy Oligomers, *Inzh.–Fiz. Zh.*, 2005, vol. 78, no. 1, pp. 104–108 [*J. Eng. Phys. Thermophys.* (Engl. Transl.), 2005, vol. 78, no.1, pp. 519–523].
14. Koekin, V.K., The Method of Indication of the Water Activation Effect, *Elektron. Obrab. Mater.*, 1995, no. 1, pp. 74–75.
15. Ioffe, I.F., On the Influence of External Fields on the Thermodynamic Properties of Solutions and the Superficial Tension, *Zh. Eksp. Teor. Fiz.*, 1969, vol. 57, issue 2(8), pp. 529–533.
16. Brodskaya, E.N. and Rusanov, A.I., On the Influence of an Arbitrarily Directed Electric Field on the Superficial Tension of a Liquid, *Kolloidn. Zh.*, 1983, vol. 45, no. 4, pp. 636–643.
17. Nicolis, G. and Prigogine, I., Self-organization in Nonequilibrium System, New York: Wiley, 1977.
18. Shtainkhen, A. and Sanfel'd, A., Thermodynamic Stability of the Charged Surfaces, in *Sovremennaya Teoriya Kapillyarnosti: K 100-letiyu Teorii Kapillyarnosti Gibbsa* (Modern Calillarity Theory: To the 100-Year Anniversary of the Capillarity Theory of Gibbs), Ed. Rusanov, A.I. and. Gudrich, F.C., Leningrad: Khimiya, 1980, pp. 300–316.
19. Kopeikina, E.K., Influence of an Electric Field on the Superficial Tension of Nonpolar Liquids, *Elektron. Obrab. Mater.*, 1970, no. 4, pp. 57–59.
20. Yurchenko, N.F. and Zigmantas, G.P., Generation of Longitudinal Vortices in the Boundary Layer in the Presence of Body Forces, *Inzh.–Fiz. Zh.*, 1989, vol. 57, no. 3, pp. 392–398.
21. Kravtsov, A.A. and Rachev, L.A., Transmission of Low Conductivity Liquids with Forces of Electrostatic and Gravitation Fields, *Elektron. Obrab. Mater.*, 1978, no. 5, pp. 39–34.
22. Middendorf, W.H. and Brown, G.H., Liquid Dielectrics in an Electric Field, *Power Appar. System Part 3*, 1958, vol. 77, no. 3, pp. 795–799.
23. Mizdryakov, O.A., Intensity of an Electrostatic Field on the Surface of the Meniscus between Liquid and Gaseous Dielectrics in a Flat Condenser, *Elektron. Obrab. Mater.*, 1968, no. 6, pp. 38–40.
24. Kardashev, G.A., Sobolev, V.D., Churaev, N.V., and Shatalov, A.L., Influence of Fluctuations on the Liquid Level in a Capillary, *Kolloidn. Zh.*, 1976, vol. 38, no. 3, pp. 461–466.
25. Bologa, M.K. and Rudenko, V.M., On the Intensification of the Liquid Evaporation under the Action of an Electric Field, *Elektron. Obrab. Mater.*, 1975, no. 3, pp. 37–40.
26. Duradzhi, V.N., About the Electric Impulse Discharge between Metal and Electrolyte Electrodes, *Elektron. Obrab. Mater.*, 2001, no. 3, pp. 22–26.
27. Polishchuk, N.V., Panchenko, M.S. and Panchenko, I.M., On the Possibility that Atmospheric and Terrestrial Electricity Affect Water Filtration, *Elektron. Obrab. Mater.*, 2007, no. 1, pp. 57–62 [*Surf. Eng. Appl. Electrochem.* (Engl. Transl.), 2007, no. 1, p. 44–48].

ISSN 1068-3755, Surface Engineering and Applied Electrochemistry, 2008, Vol. 44, No. 4, pp. 293–296. © Allerton Press, Inc., 2008.
Original Russian Text © I. N. Brovikova, N.V. Kholodkova, I.V. Kholodkov, R.M. Kol'tsov, 2008, published in Elektronnaya Obrabotka Materialov, 2008, No. 4, pp. 51–54.

ELECTRICAL PROCESSES IN ENGINEERING AND CHEMISTRY

Probabilities of the Heterogeneous Recombination of Oxygen Atoms in O_2–Ar Plasma

I. N. Brovikova, N. V. Kholodkova, I. V. Kholodkov, and R. M. Kol'tsov

GOUVPO Ivanovo State Chemical and Technological University, pr. F. Engel'sa 7, Ivanovo, 153000 Russia

E-mail: kholodkova@isuct.ru

Received January 21, 2008

Abstract—The probabilities of the heterogeneous recombination of oxygen atoms in the positive glow gap and afterglow for O_2–Ar (0–90%) mixtures were determined for the pressure range of 50–300 Pa and discharge currents of 10–80 mA. A molybdenum glass was used as the recombination surface in the first case, while a quartz glass surface was used in the second case.

DOI: 10.3103/S106837550804008X

Low-temperature oxygen-containing plasma is widely applied both in etching technology and for surface modification of various materials. Application of mixtures of chemically active gases with argon is of great interest from the engineering point of view. The choice and evaluation of the working parameters of plasmachemical reactors must take into account many factors. The kinetic characteristics of the loss processes of active particles on various surfaces occupy an important place among them. Quartz and molybdenum glasses are widely used as construction materials for plasmachemical reactors. At the same time, despite the great number of works devoted to the investigation of plasma in O_2–Ar mixtures [1–3], there is lack of systematic data in the literature related to the probability of the heterogeneous recombination of oxygen atoms on the surface of these materials.

EXPERIMENTAL METHOD

Experimental measurements were performed using the setup whose schematic diagram is presented in Fig. 1. The cylindrical reactor with an internal diameter of 1.5×10^{-2} m was made of S-52 electron-tube molybdenum glass. The maximal anode–cathode distance was 1.5 m. The length of the positive glow gap (PGG) of the DC glow discharge could be varied by the anode displacement along the discharge tube. The atoms generated by the discharge were transported by the gas flow through the quartz tube with a diameter of 0.96×10^{-2} m

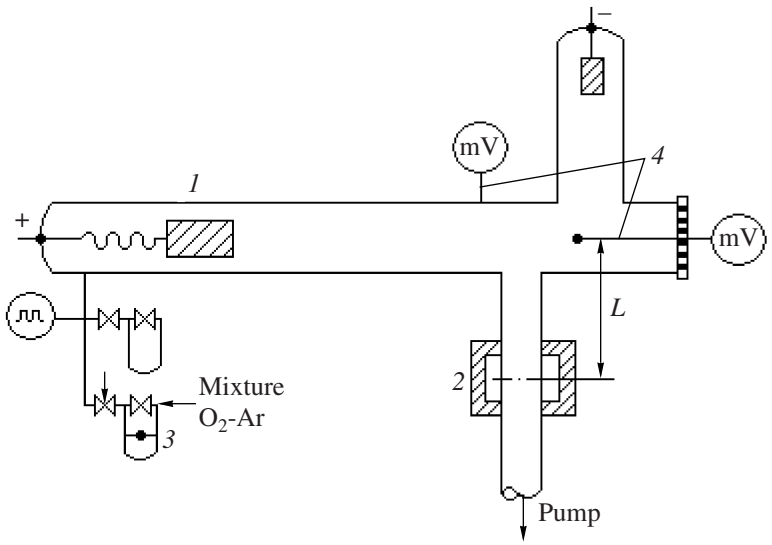

Fig. 1. Schematic diagram of the experimental setup. (*1*) Reactor, (*2*) resonator of the EPR microwave spectrometer, (*3*) flow meter, (*4*) thermocouple.

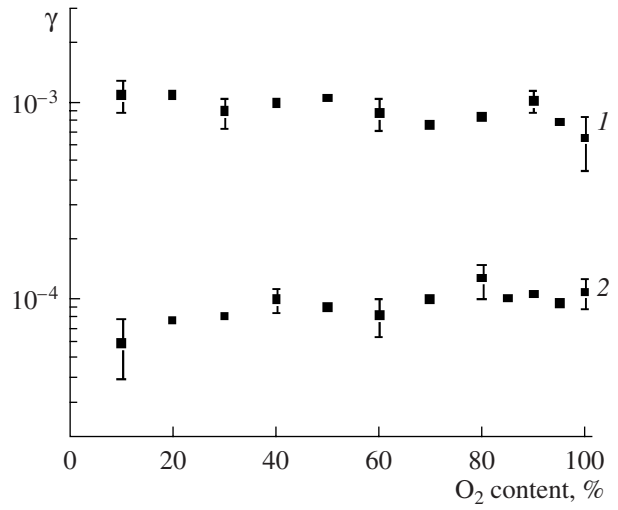

Fig. 2. Dependence of the probability of the heterogeneous loss of oxygen atoms in the PGG (*1*) and afterglow (*2*) of O_2–Ar plasma on the composition of the O_2–Ar mixture (P = 200 Pa, I_d = 50 mA).

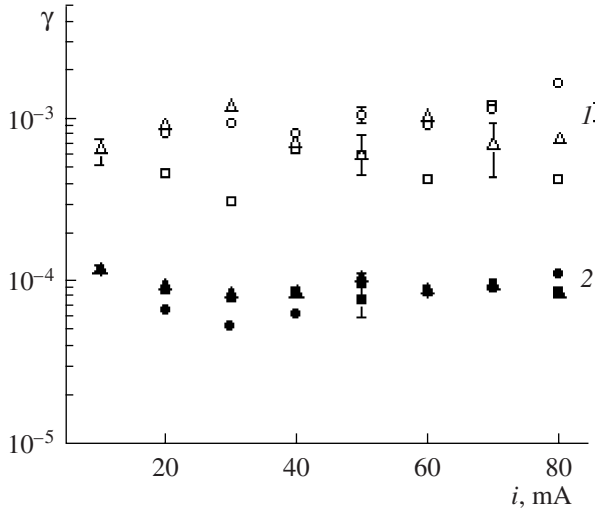

Fig. 3. Dependence of the probability of a heterogeneous loss of oxygen atoms in the PGG (*1*) and afterglow (*2*) of O_2–Ar plasma on the discharge current (P = 200 Pa). ○, ● 20% O_2 + 80% Ar; △, ▲ 80% O_2 + 20% Ar; □, ■ 100% O_2.

and a length of 0.3 m and were registered by the EPR method using an RE 1301 radiospectrometer.

The pressure of the gas mixture was in the range of 50–300 Pa; the discharge current was varied in the limits of 10–80 mA. The plasma-forming gas was prepared by mixing known volumes of argon and oxygen; a mass spectrometer was used to control the accuracy of the preparation. Copper-constantan thermocouples were employed to measure the gas temperature on the axis of the positive glow gap T_0 and the temperature of the discharge tube wall T_w [4].

The jet method was used during the experiments, which allowed us to obtain data related to the loss process of the atoms both in the plasma zone and outside its limits in the afterglow region.

The kinetic dependences for the oxygen atoms were obtained by variation of the contact time with the studied surface (quartz or electron-tube glass). In the afterglow case, the gas flow rate was varied at the constant discharge parameters; in the case of the plasma zone, the length of the discharge zone was varied at a constant flow rate; that is, the distribution of the relative atom concentrations was determined. Linearization of these dependences in a semilogarithmic scale allows us to suggest that the reaction of the heterogeneous recombination of atoms on the surface of the quartz glass (afterglow) and on the electron-tube glass (plasma) occurs according the first kinetic order; this agrees with the published data [5, 6].

The solution for the continuity equation for the density of the flow of atoms gives the following equation for the concentration of atoms n in the resonator of the EPR spectrometer:

$$n = [W\tau(1 - e^{-\alpha_1 z}) + n_0 e^{-\alpha_1 z}]e^{-\alpha_2 L}. \quad (1)$$

Here, W is the dissociation rate averaged over the tube cross section, τ is the time of the heterogeneous recombination of oxygen atoms in the PGG zone, z is the coordinate counted from the place where the resonator enters the tube to the anode, L is the distance between the PGG and the resonator (Fig. 1), and n_0 is the concentration of atoms for $z = 0$.

The α_1 and α_2 values were determined using the equation

$$\alpha = 0.5\left(\frac{V}{D}\right)\left[\sqrt{1 + \frac{4D}{V^2\tau}} - 1\right], \quad (2)$$

where V is the mass average velocity, and D is the diffusion coefficient for the atoms. To determine the α_1 and α_2 parameters V, D and τ were taken for the PGG and afterglow zones, respectively; the bulk processes of the loss of the atoms can be neglected for our experimental conditions. The preliminary measurements showed that the characteristic time for the radial diffusion was at least an order of magnitude less than τ, and the variation of the mass average velocity owing to dissociation did not exceed 5%. The probability of the heterogeneous loss of the atoms was determined as

$$\gamma = (2R/V_T)\tau,$$

where R is the tube radius, and V_T is the thermal velocity of the atoms near the wall.

RESULTS AND DISCUSSION

The results of measurements of the probabilities of the loss of oxygen atoms $O(^3P)$ in the plasma zone and in the region of the flowing afterglow are shown in Fig. 2, Fig. 3, and in the table. For all the cases, the measure-

Influence of the plasma-forming gas pressure on the probability of the heterogeneous recombination of atoms (discharge current of 50 mA)

Plasma (molybdenum glass)								
P, Pa		50	75	100	150	200	250	300
20% O_2 + 80% Ar	T_w, K	322	327	331	334	339	345	352
	τ, 10^{-2} s	2.3	0.8	1.2	2.7	2.1	2.0	2.2
	γ, 10^{-3}	1.00 ± 0.11	2.73 ± 0.30	1.95 ± 0.21	0.85 ± 0.09	1.08 ± 0.12	1.12 ± 0.12	1.00 ± 0.11
80% O_2 + 20% Ar	T_w, K	327	331	332	346	351	362	369
	τ, 10^{-2} s	1.5	2.2	3.9	3.1	3.7	6.4	5.6
	γ, 10^{-3}	1.56 ± 0.42	1.01 ± 0.27	0.59 ± 0.09	0.72 ± 0.11	0.63 ± 0.17	0.34 ± 0.05	0.38 ± 0.06
100% O_2	T_w, K	327	332	336	344	357	359	362
	τ, 10^{-2} s	1.3	1.3	2.7	4.8	3.4	4.6	6.9
	γ, 10^{-3}	1.04 ± 0.62	1.75 ± 0.28	0.87 ± 0.14	0.48 ± 0.14	0.65 ± 0.04	0.48 ± 0.07	0.32 ± 0.05
Afterglow (quartz)								
P, Pa		50	75	100	150	200	250	300
20% O_2 + 80% Ar	T_w, K	325	326	327	335	338	346	348
	τ, 10^{-2} s	7.4	6.6	4.9	2.2	2.0	1.4	1.2
	γ, 10^{-3}	2.07 ± 0.31	2.31 ± 0.22	3.09 ± 0.46	6.92 ± 0.76	7.85 ± 1.84	10.83 ± 1.62	12.57 ± 1.89
80% O_2 + 20% Ar	T_w, K	333	334	342	348	351	363	371
	τ, 10^{-2} s	17.3	5.3	3.2	1.7	1.5	1.4	0.8
	γ, 10^{-3}	0.88 ± 0.13	2.93 ± 0.27	5.21 ± 2.04	9.22 ± 1.01	10.08 ± 0.48	11.03 ± 1.32	20.28 ± 2.88
100% O_2	T_w, K	329	335	340	344	358	361	352
	τ, 10^{-2} s	6.3	4.9	2.9	1.8	1.5	0.7	0.6
	γ, 10^{-3}	2.54 ± 0.51	3.18 ± 0.36	5.32 ± 0.21	8.81 ± 0.81	10.70 ± 080	23.61 ± 3.54	24.80 ± 3.62

ments were performed under the conditions of natural heat exchange with the ambient medium.

The addition of argon did not markedly change the probability of the heterogeneous recombination of oxygen atoms in the plasma zone; an insignificant increase in γ was only observed when argon was introduced into the plasma-forming gas (Fig. 2). Within the limits of the experimental accuracy, the obtained γ value was of the order of 1×10^{-3} for all the O_2–Ar (0–90%) compositions. This γ value is less than the probability of the heterogeneous recombination of $O(^3P)$ atoms in the pure oxygen plasma measured in [6]; however, it well coincides with the data reported in [1, 2, 7].

In the afterglow region, the probability of the heterogeneous recombination increases insignificantly with the growth in the oxygen content in the mixture (Fig. 2), as well as with the increase in the pressure of the plasma-forming mixture (see the table); this agrees with the results [5] for the pure oxygen plasma.

A definite influence of the discharge current on the γ value in the PGG region was not found (Fig. 3). In the afterglow region, a tendency was observed that γ increased when the discharge current decreased below 30 mA independent of the mixture composition.

CONCLUSIONS

As a result of the experimental investigations, data were obtained related to the probability of the heterogeneous loss of oxygen atoms in the positive glow gap of a DC glowing discharge on the surface of S-52 electron-tube glass and in the region of the flowing afterglow on a quartz glass surface in O_2–Ar mixtures of various composition. It was shown that a monotonous decrease in the probability of the heterogeneous recombination of oxygen atoms was observed in the plasma afterglow region in an O_2–Ar (10–90%) mixture; however, the γ value did not change in the PGG region for the same content of argon atoms in the mixture.

REFERENCES

1. Smirnov, S.A., Rybkin, V.V., Ivanov, A.N., and Titov, V.A., The Simulation of the Processes of Formation and Decay of Neutral Particles in DC Discharge Plasma in an

Argon-Oxygen Mixture, *High Temp.*, 2007, vol. 45, no. 3, pp. 291–297.

2. Rybkin, V.V., Smirnov, S.A., and Ivanov, A.N., The Kinetic Model of Formation and Loss of Neutral Particles in Plasma of O_2–Ar Mixture, *Trudy IV mezhdunarodnogo simpoziuma po teor. i prikl. plazmokhimii* (Proc. IV Int. Symp. on Teor. and Applied Plasmachemistry), Ivanovo, 2005, vol. 1, pp 247–250.
3. Morscheidt, W., Hassouni, K., Bauduin, N., Arefi-Khonsari, F. and Amouroux J. On the Use of Global Kinetics Models for the Investigation of Energy Deposition and Chemistry in RF Argon–Oxygen Plasmas Working in the Torr Regime, *Plasma Chem. Plasma Process.*, 2003, vol. 23, no. 1, pp. 117–140.
4. Maksimov, A.I., Sergienko, A.F., and Slovetskii, D.I. Measuring Gas Temperature in the Glow Discharge Using a Thermocouple Method, *Fiz. Plazmy*, 1978, vol. 4, no. 2, pp. 347–351.
5. Brovikova, I.N., and Rybkin, V.V., Temperature Dependence of the probability of Heterogenelous Recombination of $O(^3P)$ Atoms on the Quartz Glass Surface, *Khim. Vys. Energ.*, 1993, vol. 27, no. 4, pp. 89–92.
6. Brovikova, I.N., Rybkin, V.V., and Shukurov, A.L., Kinetic Characteristics of Dissociation of Oxygen Molecules in the Positive DC Glow Gap, *Khim. Vys. Energ.*, 1997, vol. 31, no. 2, p. 146.
7. Gordiets, B., Ferreira, C. M., Nahorny, J., Pagnon, D., Touzeau, M., and Vialle, M. Surface Kinetics of N and O Atoms in N_2–O_2 Discharges, *J. Phys. D: Appl. Phys.*, 1996, no. 29, pp. 1021–1031.

ISSN 1068-3755, Surface Engineering and Applied Electrochemistry, 2008, Vol. 44, No. 4, pp. 297–300. © Allerton Press, Inc., 2008.
Original Russian Text © I.I. Beril, M.K. Bologa, S.I. Beril, 2008, published in Elektronnaya Obrabotka Materialov, 2008, No. 4, pp. 55–59.

ELECTRICAL PROCESSES IN ENGINEERING AND CHEMISTRY

On the Theory of Dielectric Liquid Electric Conductivity in a Field of Injecting Electrodes (Concentration Dependence)

I. I. Beril[a], M. K. Bologa[b], and S. I. Beril[a]

[a] *Shevchenko State University, Pridnestrovie, ul. 25 Oktyabrya 128, Tiraspol, Republic of Moldova*

[b] *Institute of Applied Physics, Academy of Sciences of Moldova, ul. Academiei 5, Chisinau, MD-2028 Republic of Moldova*

E-mail: mbologa@phys.asm.md

Received February 6, 2008

Abstract—Calculation of the free electron concentration in a weakly conducting liquid at injection of electrons from high voltage needle electrodes on the liquid surface is given. Methods of solid state physics have been substantiated and applied. The concentration of free electrons does not depend on the electric field intensity up to prebreakdown voltages.

DOI: 10.3103/S1068375508040091

In the development of the theory of electric conductivity of weakly conducting liquids, in the majority of cases [1, 2] the absence of free electrons is assumed and the electron electric conductivity is not taken into account; this is incorrect, since, in studying problems of heat and mass transfer in strong electric fields, intense injection of electrons in liquid from electrodes is nearly always observed [3, 5].* In some cases, the electron electric conductivity is comparable with the ionic conductivity or exceeds it [4].

In strong electric fields in weakly conducting liquids, as well as in solid-state semiconductors and dielectrics, nonlinear current–voltage characteristics are observed; both ionic and electron components contribute to it.

Let us consider the electron electric conductivity of a weakly conducting liquid in a strong electric field of injecting electrodes. Weakly conducting liquids are similar to solid-state semiconductors and dielectrics in many instances. For example, sunflower oil is a solution of many fatty acids and impurities, such as proteins, waxes, and sterines, which are in a dissolved or colloid–dissolved state at room temperature; the atoms in it are bound between each other by covalent bonds, the electron orbits overlap, and the band theory holds for the electrons. The solution of the problem on minimization of the dipole system energy in a strong electromagnetic field, which the considered liquids are, leads to the subcrystalline, i.e., cluster liquid model. A significant difference is the liquid fluidity caused by weaker intercluster bonds than that of the atoms and molecules inside the cluster. As well as in the solid state, electrons, atoms, and molecules execute heat oscillations with their kinetic energy being on the order of 3/2kT; at room temperature, this is on the order of 0.04 eV. The liquid fluidity is explained by hopping of cluster–crystals containing several thousands of atoms each. The adiabatic approximation in the physics of semiconductors used in the solution of the Schrodinger equation for a system of particles is made for the reason that the rate of the nuclei motion at oscillations is less by 2 orders than the rate of the electron motion; that is, nuclei are "frozen in" and the variables in the Schrodinger equation are divided. Similar to the adiabatic approximation, the estimation shows that the time of the cluster hopping from one equilibrium position to another is on the order of 3×10^{-12} s; the period of the oscillations or orbital revolution of the valence electrons is about 10^{-16} to 10^{-18} s; therefore, at the time of hopping, the cluster is as if "frozen in"; the electron runs through all the states many times at a nearly constant cluster position. In addition, the considered liquids are characterized by translation symmetry, as well as semiconductors, due to the liquid isotropy in the electrophysical characteristics. Earlier [5], in studying the kinetics of weakly conducting liquid electrization by the method of thermally stimulated discharge, it was shown that thermal ionization of deep impurity centers of weakly conducting liquids takes place at strict temperatures; this testifies to the regularly periodic position of impurity centers that does not give a spread in the frequency of the absorption and radiation of the impurities.

By analogy, the one-electron approximation and the method of effective mass are applicable for weakly conducting liquids; thus, the many-particle problem is reduced to the one-particle one: to the motion of a free electron with effective mass in a strong electric field, which was considered in [6].

The nonlinearity of the current–voltage characteristic of a weakly conducting liquid, in particular, of its

* A liquid is considered weakly conducting if its activation energy is similar to that of dielectric liquids but its dielectric loss tangent is high.

electron components, can be explained by the dependence of the concentration and the mobility of the conduction band electrons on the electric field intensity. The electron electric conductivity is written as

$$\sigma = en(\mathrm{E})\mu(\mathrm{E}) \tag{1}$$

where e, n, and μ are the charge, concentration, and mobility of the electrons; $n(\mathrm{E})$ is proportional to the initial number of impurity centers and to the number of transitions in unit time from the impurity band into the conduction band. The mobility $\mu(\mathrm{E})$ also depends on the probability of the transition between the electron states in the conduction band; that is, in both cases, the matrix elements must be calculated

for $n(\mathrm{E})$

$$M_1 = \iiint \Psi_n(r)\,\widehat{V}\,\Psi_k(\xi) r^2 dr \sin(\nu) d\nu d\varphi; \tag{2}$$

for $\mu(\mathrm{E})$

$$M_2 = \iiint \Psi_n(\xi)\,\widehat{V}\,\Psi_k(\xi) r^2 dr \sin(\nu) d\nu d\varphi. \tag{3}$$

In the present paper, we calculate the concentration of free electrons $n(\mathrm{E})$. For a deep impurity center, the wave function is taken in the form [6]

$$\Psi(r) = \frac{A\sqrt{\chi}}{r} e^{-\chi r}. \tag{4}$$

For electrons in the conduction band, the wave function is

$$\Psi(\xi) = A\Phi(-\xi), \tag{5}$$

where $A = \dfrac{1}{\sqrt{2\pi}}$, $\chi = \dfrac{\sqrt{2m\Delta E}}{\hbar}$, $\widehat{V} = -e\mathrm{E}x$, $A' = \dfrac{(2m^*)^{1/3}}{T^{1/2}(e\mathrm{E})^{1/2}\hbar^{2/3}}$, $\xi = \left(x + \dfrac{E}{e\mathrm{E}}\right)\left(\dfrac{2m^*\mathrm{E}}{\hbar^2}\right)^{1/3}$,

m^* is the electron effective mass, $\hbar$ is the Planck constant, ΔE is the impurity center activation energy, and

$$\Phi(\xi) = \frac{1}{\sqrt{\pi}} \int_0^\infty \cos\left(\frac{u^3}{3} + u\xi\right) du.$$

The results of the integrals of the product and square of the Airy function in the form of the Airy function and its derivatives are given in [7]. Since the obtained results must be averaged over the electron energy distributions, the calculations become significantly more complicated. It is more advantageous to neglect less than 1% accuracy and to obtain results on matrix elements in the form of elementary functions.

After integrating over φ in (2), we obtain

$$M_1 = -2AA'e\mathrm{E}\sqrt{\frac{\chi}{u}} \int_0^\infty \int_0^\infty \int_0^\pi e^{-\chi r} \sin(\nu) \times \left[\cos\frac{u^3}{3} + \sin(uba)\pi J_1(\alpha) + \sin\frac{u^3}{3}\pi J_1(\alpha)\cos(uba) - \right] dur^2 dr \sin(\nu) d\nu,$$

where $b = \left(\dfrac{2me\mathrm{E}}{\hbar^2}\right)^{1/3}$, $a = \dfrac{E}{e\mathrm{E}}$, $z = ubz$, $\alpha = ubz\sin(\nu)$, $J_1(\alpha)$ is the Bessel function.

After integrating over ν, we obtain

$$M_1 = \frac{4AA'e\mathrm{E}\sqrt{\pi\chi}}{b} \int_0^\infty \int_0^\infty e^{\chi^2} (J_4 - J_5)(dur) dr,$$

where

$$J_4 = \int_0^\infty \frac{1}{u} \sin\left(\frac{u^3}{3} + uab\right) du$$

$$= \frac{1}{3}\sum_{k=0}^{\infty} \frac{(-1)^k (ab)^{k+1}}{(k+1)!} \left(\frac{1}{3}\right)^{\frac{k+1}{3}} \Gamma\left(\frac{k+1}{3}\right) \cos(-2k+1)\frac{\pi}{6};$$

$$J_5 = \frac{1}{6br}\sum_{k=0}^{\infty} \frac{(-1)^k}{(k+2)!} \left(\frac{1}{3}\right)^{\frac{k+1}{3}} \Gamma\left(\frac{k+1}{3}\right) \cos(-2k+1)\frac{\pi}{6} \times [(ab+br)^{k+r} - (ab-br)^{k+r}].$$

After integrating over u and r, we obtain

$$M_1 = \frac{a^{k+2}}{\chi} - \sum_{i=1}^{k+2} \frac{(-1)^i (k+2)(k+1)\ldots(k+3-i)}{(-1)^{i+3}\chi^{i+1}} a^{k+2-i}.$$

Since a^{k+2}/χ is a rapidly decreasing function, then an error of less than 1% only in terms with $k = 0$ and $i = 1; 2$ may be taken into account:

$$M_1 = \frac{4AA'}{\chi^{3/2}}\left(a^2 + \frac{1}{3\chi^2}\right). \tag{6}$$

The transition probability is

$$W = \frac{2\pi}{\hbar}|M_1|^2 \delta(E_\mathrm{K} - E_\mathrm{H} - \Delta E).$$

After calculations, we obtain the probability of electric ionization of the impurity center

$$W_{\mathrm{E.I.}} = \frac{16(e\mathrm{E})^{7/3}}{\hbar^{2/3} m^{1/6} \Delta E^{3/2}} \left[\frac{\Delta E^2}{(e\mathrm{E})^2} + \frac{\hbar^2}{6m\Delta E}\right]. \tag{7}$$

The first term weakly depends on the electric field; the second term gives the dependence on the field intensity, being slightly higher than the quadratic one; therefore,

$$W_{\text{E.I.}} \approx \frac{8\hbar^{4/3}(e\text{E})^{7/3}}{3m^{7/6}\Delta E^{5/2}}. \quad (8)$$

Substitution of numerical data at $\text{E} = 3 \times 10^5$ V/m, $\Delta E = 0.6$ eV gives $W_{\text{E.I.}} = 0.5 \times 10^{-15}$ s^{-1}; this corresponds to the carried out estimation.

Applying the obtained expressions for the probability of ionization of a deep impurity center in a strong electric field, we derive the balance equation for the three processes: injected electron capture by impurity centers, thermal ionization of impurity centers, and electric ionization of impurity centers in the conduction band

$$R_{\text{C}} = G_{\text{T.I.}} + G_{\text{E.I.}}, \quad (9)$$

where R_{C}, $G_{\text{T.I.}}$, and $G_{\text{E.I.}}$ are the rate of the injected electron capture and the thermal and electric ionization, respectively.

Let us define the rate of the injected electron capture by impurity centers as [8]

$$R_{\text{C}} = N\langle VG\rangle(N_{\text{I.C.}} - N_{\text{C.I.C.}}), \quad (10)$$

where N is the free electron concentration, V is the absolute value of the free electron rate, $G = G(V)$ is the cross section of the electron capture by the impurity center, $\langle VG\rangle$ is the VG value averaged over free electron rates, $N_{\text{I.C.}}$ is the impurity center concentration, and $N_{\text{C.I.C.}}$ is the charged impurity center concentration.

The rate of the thermal ionization of the impurity centers is

$$G_{\text{T.I.}} = N_{\text{C.I.C.}} \sum_k W^k_{\text{T.I.}} = N_{\text{C.I.C.}} W_{\text{T.I.}} N_{\text{S}}, \quad (11)$$

where N_{S} is the number of free electron states, and $\sum_k$ is the summation over the final states.

The rate of the electric ionization of the impurity centers is

$$G_{\text{E.I.}} = N_{\text{C.I.C.}} \sum_k W^k_{\text{E.I.}} = N_{\text{C.I.C.}} W_{\text{E.I.}} N_{\text{S}}. \quad (12)$$

The probability of thermal ionization of impurity centers after summation over the final states of the free electrons is

$$W_{\text{T.I.}} = N_{\text{S}} \exp\left(\frac{-\Delta E}{kT}\right). \quad (13)$$

For the injected electron capture rate in (9), it is necessary to calculate $\langle VG\rangle$, to determine the capture cross section, and to average the VG product over the rate distribution of the electron number.

The determination of the capture cross section by the classical formula

$$G(\Theta) = \frac{e_i^r e^r}{4m^2 v^4}[Z - F(\Theta)]^2 \cos es\left(\frac{4\Theta}{2}\right)$$

gives a complex expression; therefore, let us assume $G_{\text{T.I.}} \gg G_{\text{E.I.}}$; this is fulfilled for the fields being less than or equal to 10^6 V/m, where Z is the number of electrons in the atom; a is the scattering center radius; e_i, e are the charges of the scattering center and the electron; and k is the wave vector.

Then, from the equation,

$$N_{\text{C.I.C.}} = \frac{N_{\text{I.C.}}}{1 + \dfrac{W_{\text{T.I.}}}{\langle VG\rangle}\dfrac{N_{\text{S}}}{N}}. \quad (14)$$

In the heat equilibrium

$$N = N_0, \quad N_{\text{C.I.C.}} = N^0_{\text{C.I.C.}}, \quad N^0_{\text{C.I.C.}} = \frac{N_{\text{I.C.}}}{1 + N/N_{0\partial}}. \quad (15)$$

Comparing (14) and (15), we obtain

$$\frac{W_{\text{T.I.}}}{\langle VG\rangle} = \frac{N}{N_S} = \exp\left(\frac{\Delta E}{kT}\right), \quad (16)$$

Hence,

$$\langle VG\rangle = W_{\text{T.I.}} \exp\left(-\frac{\Delta E}{kT}\right). \quad (17)$$

From balance equation (8), we find the concentration of free electrons

$$N = \frac{N_{\text{I.C.}} N_S}{N_{\text{I.C.}} - N_{\text{C.I.C.}}}\left[\exp\left(-\frac{\Delta E}{kT}\right) + \frac{8\hbar^{4/3}(e\text{E})^{7/3}}{3m^{7/6}\Delta E^{5/2}}\right]. \quad (18)$$

At $\Delta E = 0.6$ eV, $\text{E} = 3 \times 10^5$ V/m, and $T = 293$ K, we find that the contribution of the second term in square brackets is significantly less than that of the first term; that is, the electric field influence on the energy distribution of the free electron number is weaker and N depends on the temperature.

Taking into account that the concentration of free electrons and the number of impurities is low, the states on free electron energies are not degenerate, and the distribution function $f_0(\varepsilon) \ll 1$ has the form of the Maxwell–Boltzmann distribution.

REFERENCES

1. Ostroumov, G.A., *Vzaimodeistvie elektricheskikh i gidrodinamicheskikh polei* (Interaction of the Electric and Hydrodynamic Fields), Moscow, 1979.
2. Stishkov, Yu.K., Electrohydrodynamic Model of Conductivity of Isomering Liquids, *Extended Abstract of Cand. Sci. Dissertation*, Leningrad, 1971.
3. Bologa, M.K. and Beril, I.I., *Rafinatsiya podsolnechnogo masla v elektricheskom pole* (Refinement of Sunflower Oil in Electric Filed), Chisinau, 2004.
4. Bologa, M.K., Beril, I.I., Tsulyanu, K.I., and Tsiulyanu, I.I., Thermally Stimulated Discharge in Suspension of a Weakly Conducting Liquid, *Elektron. Obrab. Mater.*, 1991, no. 6, pp. 47–50.
5. Bologa, M.K., Beril, I.I., Tsiulyanu, K.I., and Tsiulyanu, I.I., Kinetics of Charging of the Waxes–Sunflower Oil Suspension in the Injecting Electrode Field, *Elektron. Obrab. Mater.*, 1991, no. 5, pp. 57–59.
6. Landau, L.D. and Lifshits, E.M., *Kvantovaya mekhanika* (Quantum Mechanics), Moscow, 1989.
7. Aspnes, D.E., Electric–Field Effects on Optical Absorption near Thresholds in Solids, *Phys. Rev.*, 1966, vol. 147, issue 2, pp. 554–566.
8. Lampert, M. and Mark, T., *Inzhektsionnye toki v tverdykh telakh* (Injection Currents in Solids), Moscow, 1973.

ISSN 1068-3755, Surface Engineering and Applied Electrochemistry, 2008, Vol. 44, No. 4, pp. 301–305. © Allerton Press, Inc., 2008.
Original Russian Text © V.L. Lanin, 2008, published in Elektronnaya Obrabotka Materialov, 2008, No. 4, pp. 60–65.

ELECTRICAL PROCESSES IN ENGINEERING AND CHEMISTRY

Increasing the Efficiency of Ultrasonic Cleaning by Means of Directed Action of an Electric Field in Liquid Media

V. L. Lanin

State University of Informatics and Radioelectronics of Belarus,
ul. P. Brovki 6, Minsk, 220013 Republic of Belarus
E-mail: vlanin@bsuir.by

Received January 16, 2008

Abstract—The directed action of an electric field on liquid media at ultrasonic cleaning was investigated. This allowed adjusting the intensity of the cavitation process, accelerating the processes of transport and dissolution of pollutants, and facilitated more effective clearing of products with microrelief surfaces.

DOI: 10.3103/S1068375508040108

Cavitation processes in liquid media generated in strong ultrasonic fields are accompanied by electric phenomena. Electric discharges in collapsing cavities, sonoluminescence, and electrokinetic processes can be referred to the latter phenomena [1–3]. The mass transfer in liquid media under the action of an ultrasonic (US) field is associated with the appearance of the electrokinetic effect. It consists of the phenomenon that the mobility of the charge carriers in a liquid increases in the US field, and the directed mass transfer of the carriers occurs from the radiator under the action of the US wave [4]. At the collapse of cavitation cavities, formation of additional carriers (negatively charged cavitation bubbles) is possible, which also take part in the mass transfer. Because the charged particles of various concentration and mobility are present simultaneously in the liquid medium, the sum density of the flow of the particles in a unit of time amounts to

$$J_{эп} = \sum_{i=1}^{n} B_{ui} C_{ui} F, \quad (1)$$

where B_u is the ion mobility, C_u is the concentration of ions of the reaction active component, and F is the force of the US field.

The magnitude of the current owing to the generation of the electric field in the liquid medium is

$$I = \sum_{i=1}^{n} B_{ui} C_{ui} Q_{ui} F S, \quad (2)$$

where Q_u is the ion charge, and S is the cross section area of the action of the electric field.

The force of the US field, which produces the motion of the charged particles, is determined as

$$F = \rho c \omega A S, \quad (3)$$

where ρc is the wave resistance of the medium, ω is the circular frequency of the vibrations, and A is the amplitude of the vibrations.

Then, the value of the electric transfer current in the US field equals

$$I = \sum_{i=1}^{n} B_{ui} C_{ui} Q_{ui} \rho c \varpi A S^2, \quad (4)$$

The obtained equation does not take into account the temporal dynamics of the electric transfer process; however, it allows one to determine the maximal current value for various parameters of the US field and properties of the liquid medium. For the concentration of ions in the aqueous solution in the zone of action of US vibrations up to 3×10^5, the ion mobility is $(1.8–3.2) \times 10^{-7}$ m^2/s V and the amplitude of the vibrations is 10 μm; the maximal value of the electric transfer current in the polar solutions amounts to 20–30 mA, and, in the weakly polar solutions, it is an order of magnitude lower.

With the aim to investigate the electrokinetic effect, US vibrations with a frequency of 22 kHz were excited in liquids with an amplitude of 10–12 μm using a piston-type generator. The value of the direct current that appeared in the liquid was registered by an F166/1 microamperemeter connected between the generator and the stainless steel electrode located at the bottom of the reservoir with the studied liquid. The greatest action of the electrokinetic effect was that an increase in the value of the direct current was observed for the liquids with the least electric resistance and viscosity [5]. The analysis of the data (see the table) showed that the time for which the current in the liquid attained equilibrium was proportional to the viscosity of the liquid. The maximal effect of the current increase was noted for the interelectrode distance of 5–7 mm, because, in this

Characteristics of the electrokinetic effect in liquid media in the US field

Liquid medium	Resistance; Ohm m	Viscosity, Pa s	Current variation ΔI, mA	Time to attain the equilibrium state, s
Mineral oil	10^{13}	3.2–3.3	0	–
Glycerin	10^{12}	1.5–1.6	0.06	70
Distilled water	10^{3}	0.32–0.33	0.6	50
Ethyl alcohol	10^{4}	0.24–0.25	1.4	10
Organic acid	10	0.24–0.25	2.0	5
Water with Cl ions	0.3	0.32–0.33	3.4	3

case, the entire interelectrode zone was filled with cavitation bubbles (Fig. 1). For less interelectrode distances, the charge carriers are partly repulsed out of the zone owing to the microflows. The electrokinetic effect in liquids weakens at distances exceeding 7 mm, because the dimensions of the cavitation region are limited for the specified generator type.

The flow of the direct electric current in a liquid in an US field can be explained as follows. Under the action of the field forces, the mobility of the charge carriers in the liquid increases; a directed mass transfer from the generator appears under the action of the US pressure, and additional carriers (negatively charged cavitation bubbles) are generated at the collapse of the cavitation bubbles [6]. The time during which the current attains its maximal value depends on the amplitude of the US vibrations, the interelectrode distance, and the polarity of the molecules of the liquid. To verify the hypothesis related to the polarity of the ions that take part in the current generation, a third grid electrode was placed near the generator, and a DC voltage of 400–500 mV was applied to it from an external power source. The character of the temporal current change depended on the grid potential. The current value increased on average by a factor of three at the positive potential at the grid electrode. The current changed its direction, and the current amplitude decreased for the negative potential. This can be explained by the fact that positive hydrogen ions situated in the liquid medium mainly took part in the charge transfer [7].

The influence of the electric transfer current that appeared at the US activation of the liquid media on the cavitation and diffusion processes is rather limited owing to the low current densities. With the aim to

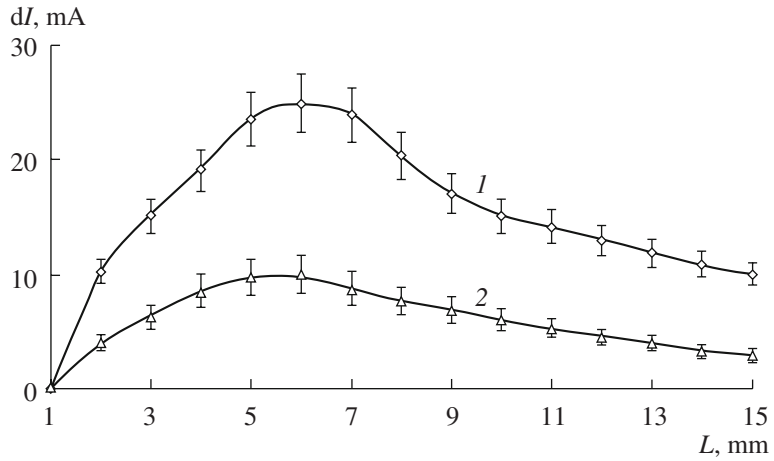

Fig. 1. Dependence of the current variation in the liquid in the US field vs. the interelectrode distance. (*1*) Water with chlorine ions; (*2*) organic acid.

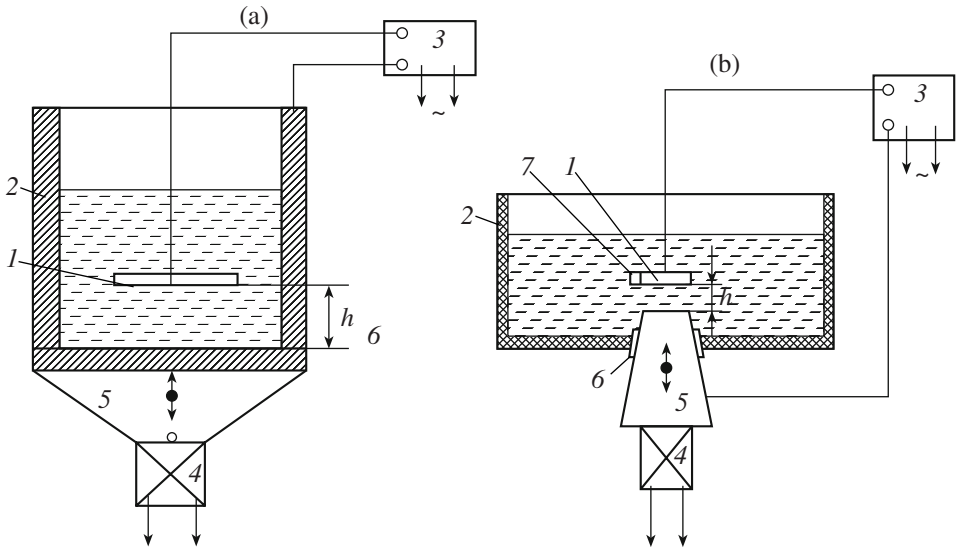

Fig. 2. Diagrams of the combined activation using the energy of US and electric fields.

increase the intensity of the cavitation processes in the liquid media, it was proposed to pass an electric current with a density of 10–100 A/m^2 from an external source through the liquid medium in the direction that coincides with the direction of motion of the most mobile ions to the generating surface of the US generator [8]. The mass transfer of the ions increases under the action of the direct electric current in the polar liquid, and the reduction of hydrogen ions occurs in the form of gas bubbles with dimensions of 50–100 μm, which are the nuclei of cavitation. The continuous accumulation of the cavitation nuclei in the working zone and their collapse under the action of the US vibrations increase the intensity of the cavitation processes; this facilitates the process of disruption of fat films and increases the cleaning quality owing to the more uniform spreading of the cavitation nuclei over the treated surface under the action of the force lines of the electric field.

With the aim to increase the locality and productivity of the activation, the electric field was oriented in such a way that the hydrogen ions moved to the generator and reduced in the form of gas bubbles. Fast growth of the bubbles to the critical dimensions and their collapse occurs near the generator surface; this is accompanied by intensive cavitation phenomena. The value of the electric current through the liquid depends on the degree of its polarity and the dimensions of the processed workpiece. The greatest increase in the cavitation pressure (by a factor of 2–2.5), which was measured using a cavitometer, was registered for the optimal current density of 10–100 A/m^2 and the negative generator potential.

The diagrams of the directed action of the electric field at the US cleaning for metallic (a) and nonmetallic (b) materials are shown in Fig. 2. The workpiece *1* is immersed in the liquid to the distance *h* from the bottom of the bath *2*, and it is connected with a wire to one of the poles of the external power source *3*. The other pole of the source is connected to the bath. When the electric vibrations are supplied from the US generator to the transducer *4*, mechanical vibrations with the amplitude A_1 are excited in the transducer, which are transferred to the bath through the diaphragm generator *5*. Under the action of the direct electric current, the positive ions in the liquid move to the generator; their reduction and formation of gas bubbles occur, which enhances the cavitation process.

At the local introduction of the US vibrations in the bath, workpiece *1* is located in bath *2* at the distance *h* from the working end surface of the generator. The nonmetal bath *2* has a hole in its base, and a condenser type generator is mounted on it with a gasket *6*. The contact ring *7* is connected to one of the poles of the external source *3*, and the other pole is connected to the generator *5*. When mechanical vibrations are excited in the transducer *4*, they are amplified by the generator to the amplitude A_2 and transferred to the liquid medium. This significantly increases the intensity of the cavitation effects owing to the deposition of the cavitation nuclei on the processed workpiece and the local introduction of the US vibrations.

The density of the electric current that passed through the liquid medium was chosen in the range of 10–100 A/m^2, because these values are necessary for effective motion of the gas cavitation bubbles to the zone of treatment and increasing of the cavitation pressure at their collapse. For the current density less than 10 A/m^2, the quantity of the moving hydrogen atoms is

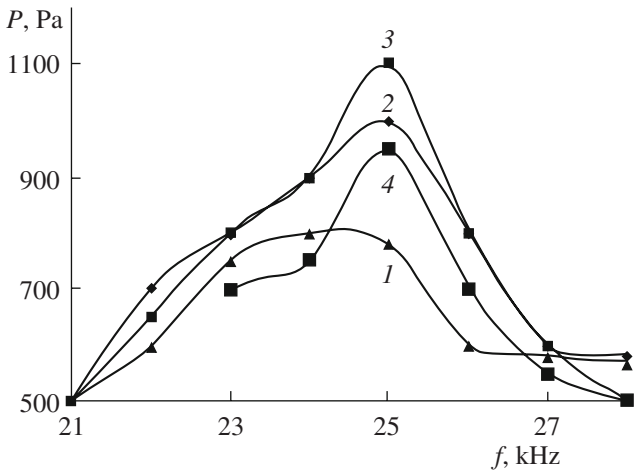

Fig. 3. Dependences of the cavitation pressure vs. the frequency for various electric current values. *I*, mA: (*1*) 0, (*2*) 5, (*3*) 30, (*4*) 40.

not enough to facilitate the cavitation process; at the current density greater that 100 A/m^2, the quantity of cavitation bubbles increases to a high degree; this leads to their merging into greater gas cavities, which do not collapse at the amplitudes of vibrations of 10–15 μm but float to the liquid surface.

In the case when it is necessary to lower the cavitation intensity to avoid considerable destruction of the treated surface, one can change the direction of the passing current (the positive pole is on the generator) and apply a version of cathode protection of the product.

The dependence of the cavitation pressure in the liquid washing media vs. the frequency of the vibrations, the amplitude, and the polarity of the electric current passing through the medium was studied. The maximal value of the cavitation pressure of 1100 Pa corresponds to a frequency of 25 kHz in the case when a positive potential is applied to the cleaned metal sample. The value of the cavitation pressure lowers when the frequency increases or decreases. When the negative potential was applied, the cavitation pressure value lowered to 900 Pa. The minimal pressure value of 850 Pa at the resonance frequency was observed when the current was absent. The maximal cavitation pressure of 1100 Pa was reached for the current value equal to 30 mA (Fig. 3).

While performing the experimental research related to the US cleaning, the dependences were investigated of the values of the destruction coefficient for the aluminum foil vs. the immersion depth, the current polarity, and the properties of the liquid medium. The maximal values of the destruction coefficient were obtained when the positive potential was applied to the cleaned product (Fig. 4). The lowering of the destruction coefficient was observed with the increase in the immersion depth. When the negative potential was applied, the value of the destruction coefficient lowered by 20–25%, but it remained relatively constant (stable). Thus, by changing the direction of the electric field action, we can to a certain degree control the intensity of the cavitation effects.

While investigating the dependences of the destruction coefficient on the immersion depth in water and in the SAS aqueous solution, we observed that the destruction in water was greater than that in the SAS aqueous solution (Fig. 5). Both in water and in the SAS aqueous solution at the various current densities (Fig. 6), the max-

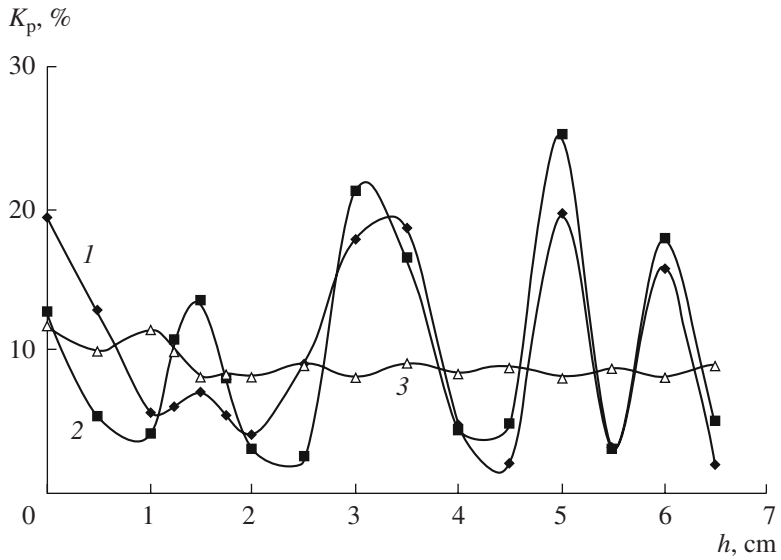

Fig. 4. Dependences of the destruction coefficient vs. the immersion depth and the current density in water. j, A/m^2: (*1*) 0, (*2*) 21, (*3*) –21.

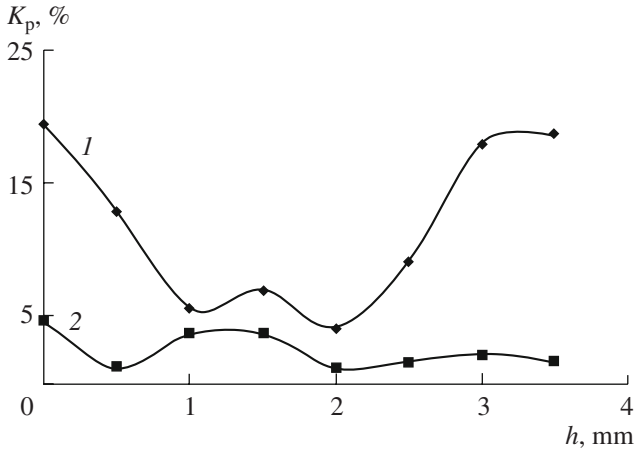

Fig. 5. Dependences of the destruction coefficient vs. the immersion depth in various liquid media. (*1*) Water, (*2*) SAS solution.

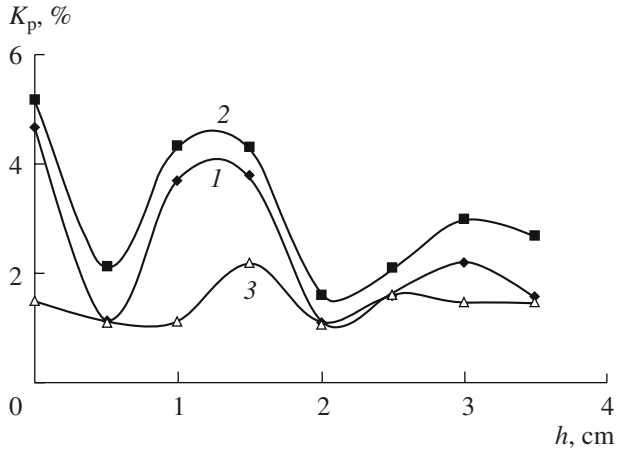

Fig. 6. Dependences of the destruction coefficient vs. the immersion depth and current density in the SAS solution. j, A/m^2: (*1*) 0, (*2*) 21, (*3*) –21.

imal values of the destruction coefficient were reached when the positive potential was applied to the product; when the negative potential was applied, the values remained relatively constant.

The obtained results can be explained by the following processes. In the process of treatment of a workpiece with a great surface area, the minus {pole} of the external source is connected to the workpiece and the plus {pole} is connected to the generator with the aim to increase the uniformity of the treatment. In polar liquids (aqueous solutions), the migration of hydrogen ions to the treated surface enhances. When the ions give off their positive charge, they are eliminated in the form of gas bubbles of atomized hydrogen, which serve as the cavitation nuclei.

In the case when a localized or more productive treatment is needed, the minus of the external source is connected to the generator of the US vibrations, and the plus is connected to the workpiece. In this case, the hydrogen ions move to the generaor and reduce in the form of gas bubbles. Owing to significant amplitudes of the vibrations, near the generator, a fast growth of the bubbles to their critical dimensions and their collapse occur, and this is accompanied by intensive cavitation effects.

The magnitude of the current that passes through the liquid depends on the polarity of the liquid and the dimensions of the processed workpiece. The greatest increase in the cavitation pressure (by a factor of 2.0–2.5) measured using a cavitometer was noted for the optimal current density of 1–2 mA/cm^2 [9].

Hence, the directed action of the electric field on the liquid media at the US treatment allows one to adjust the intensity of the cavitation processes, to accelerate the processes of mass transfer and dissolution of pollutants, and facilitates more effective clearing of products with microrelief surfaces.

REFERENCES

1. Lazarenko, B.R., Paukov, Yu.N., and Bologa, M.K., Problems of Cavitation Physics, *Elektron. Obrab. Mater.*, 1965, no. 2, pp. 35–50.
2. Margulis, M.A., *Zvukokhimicheskiye reaktsii i sonoluminestsentsiya* (Acoustochemical Reactions and Sonoluminescence), Moscow: Khimiya, 1986.
3. Maisonhaute, E., and Prado, C., Surface Acoustic Cavitation Understood via Nanosecond Electrochemistry, *Ultrason. Sonochem.*, 2002, no. 9, pp. 297–303.
4. *Ul'trazvukovye protsessy v proizvodstve izdelii elektronnoi tehniki* (Ultrasonic processes in the production of electronic components), Dostanko, A.P., Ed., Minsk, 2002, vol. 1, pp. 267–285.
5. Rumak, N.V., Bondarik, V.M., and Lanin, V.L., Electric Effects in Liquids and Melts under the Action of Ultrasonic Vibrations, *Dokl. AN Belarusi*, 1994, vol. 38, no. 2, pp. 115–118.
6. Lanin, V.L. Electrical Phenomena in Liquids and Melts by Ultrasound Processing, *Proc. 3rd Conf. on Applications of Power Ultrasound in Physical and Chemical Processing*, Paris, 2001, pp. 143–146.
7. Lanin V.L., Mass Transfer in Liquid Media under the Combined Action of Ultrasonic and Electric Fields, *Vestn. Polotskogo Gos. Univ., Ser. C. Findamental'nye Nauki. Fizika*, 2005, no. 4, pp. 117–121.
8. Lanin, V.L., Anufriev, L.P., Method of Ultrasonic Cleaning, Belarus Patent 7318, *Afits. Byull., Dzyrzh. Pat. Ved. Resp. Belarus'*, 2005, no. 3(46), p. 135.
9. Lanin, V.L., and Tomal', V.S., Optimization of Cavitation Fields in the Ultrasonic Cleaning Baths, *Dokl. NAN Belarusi*, 2007, vol. 51, no. 3, pp. 119–121.

ISSN 1068-3755, Surface Engineering and Applied Electrochemistry, 2008, Vol. 44, No. 4, pp. 306–310. © Allerton Press, Inc., 2008.
© Published in Russian in Elektronnaya Obrabotka Materialov, 2008, No. 4, pp. 66–71.

ELECTRICAL PROCESSES IN ENGINEERING AND CHEMISTRY

Gas Analogue of the Ganna Effect under Conditions of Two-Electrode Discharge of Continuous Current[1]

A. I. Gerasimov, I. V. Gerasimov, and T. P. Kopeikina

Kostroma State University, 1 May Str. 14, Kostroma, 156961 Russia

E-mail: igor_valerger@mail.ru

Received February 12, 2008

Abstract—The existence of a mode of periodic movement of a volumetric charge of negative sign from an electrode with a negative potential (600–4500 V) in the direction of the other earthed electrode was discovered. The experiments were carried out with the discharge of a constant current in the presence of the pressure of air (10^{-3}–10 Torr) in tubes with various internal diameters (3.8, 6.6, 15.5, 20.1, and 25.8 mm) but with the same (510 mm) distance between the electrodes. The opportunity for the appearance of the mode of periodic discharge was provided by the connection to the potential output of a source of several condensers of large capacity (300 μF). It is supposed that the discovered periodic mode of the gas discharge is similar to the Gann effect—the movement of a volumetric charge of negative sign in the volume of a semiconductor.

DOI: 10.3103/S106837550804011X

INTRODUCTION

The action of a strong electrical field of constant value by means of ohmic contacts on a semiconductor volume of any orientation gives rise to fluctuations of the current through the semiconductor (effect of Gann, 1963 [1–5]). The nature of these fluctuations [5, 6]—processes of periodic movement through the sample in the area of the strong electrical field—occurs in the domain nearby the cathode of the sample. The period t_D of these fluctuations was approximately equal the time of the electrons' flight from the cathode to the anode. The repeated cycle of the appearance of the new domain and its movements in the volume of the semiconductor occur only after the elimination of the previous domain on the anode. The new domain arises only when the time of its formation t_F is less than the time t_L of the leaving of the electrons in the anode from the place of formation of the domain, i.e., at $t_F < t_L = L/\vartheta_E$. Here, L is the distance from the cathode to the anode, and $\vec{\vartheta}_E$ is the velocity of the electron-drift in the field (about 10^5 ms^{-1}) at which formation of the domain begins.

In a long model of the semiconductor, the domain can arise in various areas of its volume; i.e., in this case, L is the distance from the anode of the birth to the place of the domain. The density of the current through the exemplar in which the domain moves is $\vec{j}_e = en_E\mu_E\vec{E}_{K-A}$, μ_E is the mobility of the electrons, and $\vec{E}_{K-A}$ is the field outside of the domain. The result of the consecutive repetition of the processes of the appearance of the domains and their subsequent elimination on the anode becomes the reason for the generation of the fluctuations of the current in the circuit of the cathode and anode with a frequency of $f_D = t_D^{-1} = \vec{\vartheta}_D/L$.

In semiconductor devices, the movement of electric charges is located only in the area of *p–n–p* (or *n–p–n*) transitions, while, in the work of Gann devices, all the volume of the semiconductor elements takes part. This explains, in particular, the high power of such devices.

1. EXPERIMENTAL SETUP

In a rarefied gas, a mode similar to the effect of Gann in semiconductors is realized by supplying a regulated direct voltage of 600—4500 V to electrodes of five discharge tubes of various internal diameters (3.8, 6.6, 15.5, 20.1, and 25.8 mm). One of the ends of all the tubes (with an equal distance between the electrodes of 510 mm) is joined to a common vacuum system (the range of the pressure p of the forevacuum is 10^{-3}–10 Torr), and the second electrode of all the tubes is earthed (Fig. 1). Four accumulating condensers (300 μF) were joined to the output of the source of a constant voltage. At realization of the periodic discharge, they were joined either in parallel or in series [7, 8].

For registration of the time of the longitudinal moving of the domains (Fig. 2), a circuit with two photo cells (or photomultiplier tubes) was used. One of them was placed near the electrode with the negative high-voltage potential, and the second photo cell was mobile—it moved along the tube surface. The signals from both photo cells were connected to a two channel

[1] The text was submitted by the authors in English.

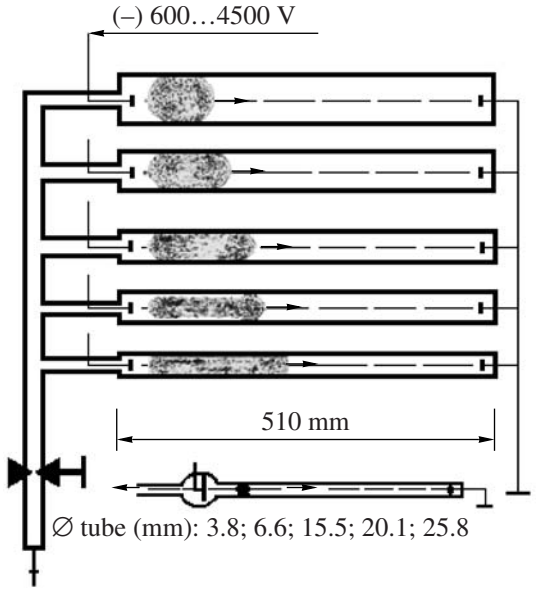

Fig. 1. The block of the discharge tubes for research of the aperiodic mode of the discharge.

memorizing oscillograph and a frequency meter working in the mode of measurement of intervals of time. The change of temperature of the gas in the longitudinal direction of the volumes of the tubes was estimated using a removable thermopair on the external surface of the glass wall of the tubes.

2. EXPERIMENTAL RESULTS

In the experiments, the area of existence of the periodic mode of breakdown of the gas was established at the coordinates $V(p)$ (a dependence similar to the curve of Pashen $V(p)$ for the discharges of constant current [9]) (Fig. 3). The experiments have shown that the character of this dependence as a whole is the same as the curve of Pashen $V(p)$ for the discharges of constant current and for the discharge of unipolar breakdown of the gas (UBG) [10, 11]: with reduction of the diameter of the tubes $2r_{TUB}$, the border of the breakdown of the gas is displaced in the area of the large valuations of p and V. However, the threshold of the breakdown for the maximum of pressure is practically identical for all the radiuses of the tubes. The dependence of the frequency of the appearance of the domains on the pressure $f_D(p)$ has a maximum that (for all the significant diameters of the tubes $2r_{TUB}$) is related to the area of the pressure p = 0.1–0.3 Torr (Fig. 3, curve *6*).

In the same coordinates ($V(p)$), the frequency f_D of formation of the domain near the cathode was determined; the dependence of the voltage V of the electrodes and the duration of the process of the time of flight of the domain on the fixed distance (i.e., the time of its displacement t_D and its velocity $\vec{\vartheta}_D$) was established; the dependence of the frequency f_D of formation

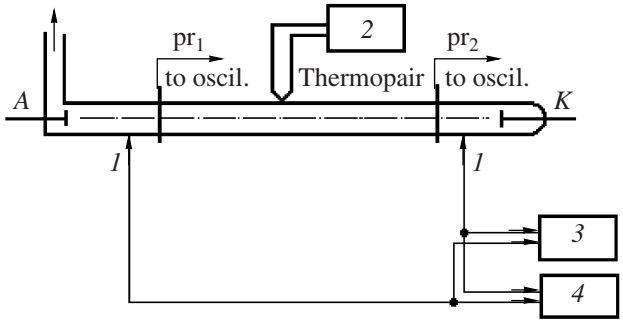

Fig. 2. Setup for registration of longitudinal moving of domains. *1*—Photoelectric detector; *2*—plotter; *3*—oscillograph; *4*—frequency meter.

of the domain on the length L_D of the volume of the tube with the discharge and on its diameter ($2r_{TUB}$) was defined; and the temperature parameters of the gas volume at moving of the domain were measured.

The maximum velocity of moving of the domain between the electrodes is displaced to the border of the greater pressure of the area of the existence of the pulse mode of breakdown of the gas in coordinates (Fig. 3, curve *7*). In Fig. 4 are shown the results of measurement of the time of flight of the domain at a fixed distance between the photocells (505 mm) in dependence on the duration of the process and the voltage of the electrodes.

The velocity $\vec{\vartheta}_D$ of the displacement of the domains becomes maximal ($\approx 4.0 \times 10^6$ ms^{-1}) at some distance from the cathode; it does not change at further longitudinal movement of the domains (the inclination of the curves *1, 2,* and *3* in Fig. 4 to the axis of the distances was constant and rather small). The results of Fig. 4

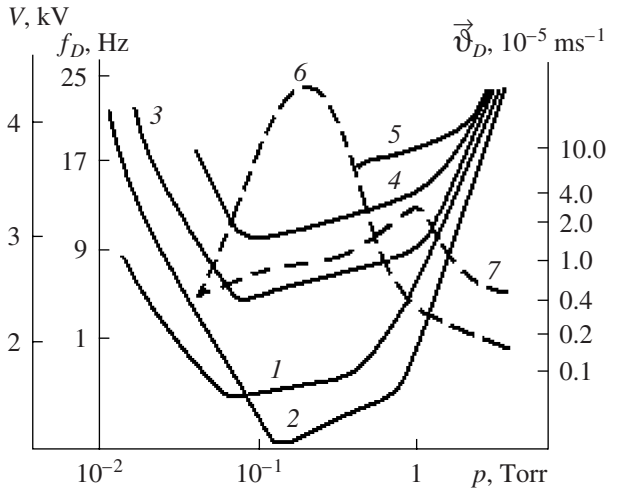

Fig. 3. Dependence $V(p)$ determining the area of existence of a periodic mode of the discharge at its various parameters. The curves 1–5 concern the dependences for tubes with a diameter of $2r_{TUB}$ = 25.8, 20.1, 15.5, 6.6, 3.8 mm, respectively.

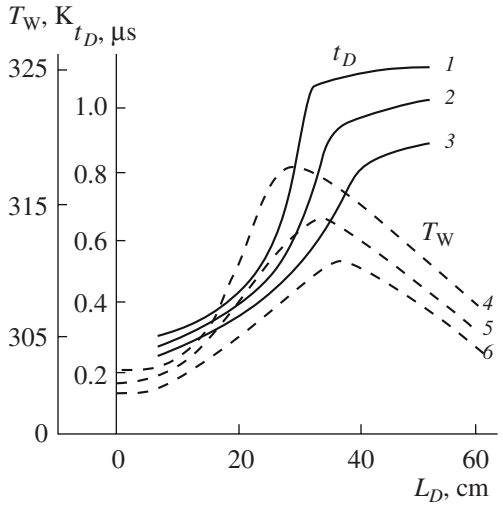

Fig. 4. Time of moving of domains on the length of the tubes and the temperature of their walls at various values of the negative potential on the cathode. *1*—4.3; *2*—3.7; *3*—4.3 kV. ∅ = 6.6 mm; f_D = 0.7 Hz; p = 0.8 Ton.

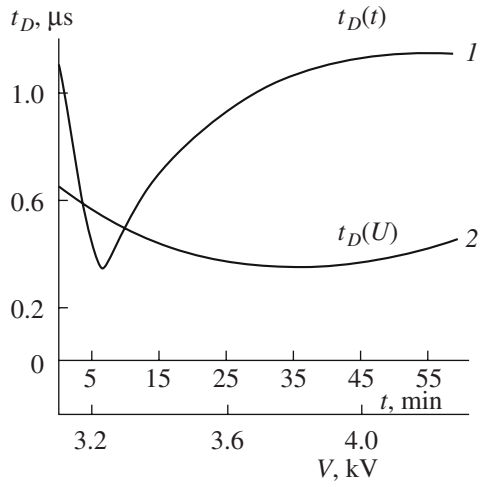

Fig. 5. Dependence of the duration of the process of the movement of domains on their periodic occurrence and on the value of the negative potential on the cathode. L_D = 50.5 cm; p = 0.7 Torr.

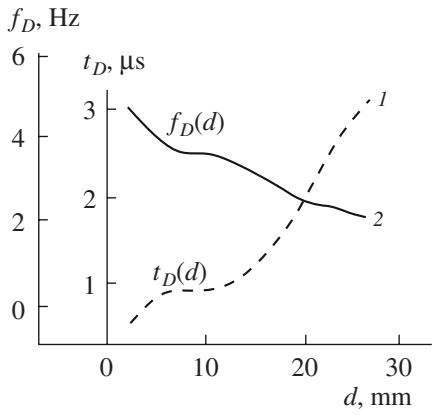

Fig. 6. Dependence of the frequency of the appearance of domains on the diameter of the tubes and the time of their moving. L_D = 28 cm; V = 4.3 kV; p = 1.8 Torr.

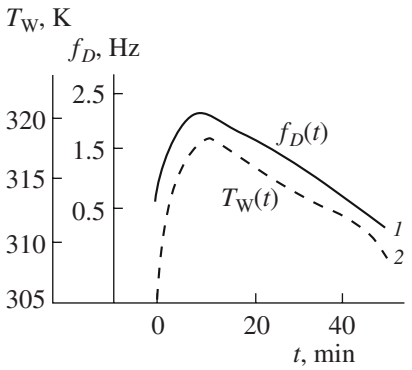

Fig. 7. Dependence of the temperature of the walls of the tubes and the frequency of the formation of the domains on the duration of the aperiodic mode of the discharge. V = 4.3 kV; L_D = 25 cm.

were achieved at p = 0.8 Torr and for the frequency of formation of the domains f_D = 0.7 Hz.

6.5 minutes after the beginning of the process of the formation of the domain (the dependence $t_D(t)$; curve *1*, Fig. 5), a velocity of the displacement of the domains of $\vec{\vartheta}_D = 1.44 \times 10^6$ ms^{-1} is observed.

~50 minutes from the beginning of the process, the velocity of the movement of the domain $\vec{\vartheta}_D$ increases up to $\approx 4.4 \times 10^6$ ms^{-1} and remains without change.

The area of the maximal temperature of the gas in the volume of the tube (the temperature of its wall was measured) is observed at the distance of 25–35 cm from the electrode with the negative potential in the field of the maximal speed of moving of the domains $\vec{\vartheta}_D$ (curves *4* and *6* in Fig. 4 for 4.26 kV and 3.4 kV, respectively; they are received at the same parameters of the discharge as curves *1*, *2*, and *3* in Fig. 5).

The increase of the diameter of the tubes from 3.8 mm up to 25.8 mm (at preservation of the other parameters of the discharge: V = 4.255 kV, p = 1.8 Torr, and L_{DIS} = 28.5 cm) reduced the following: (1) the velocity of moving of the domains (curve 1, Fig. 6) with $\vec{\vartheta}_D$ = $(0.285/5 \times 10^{-7}) = 5.7 \times 10^5$ ms^{-1} up to $\vec{\vartheta}_D$ = $(0.285/3 \times 10^{-6}) = 9.5 \times 10^4$ ms^{-1}; (2) the frequency f_D of formation of the domains with 5.0 up to 2.5 Hz (curve *2*, Fig. 6).

The frequency of appearance of the domains f_D depends on the time interval from the beginning of the process of their formation (Fig. 7). The maximal value f_D was observed ~9 minutes from the moment of the

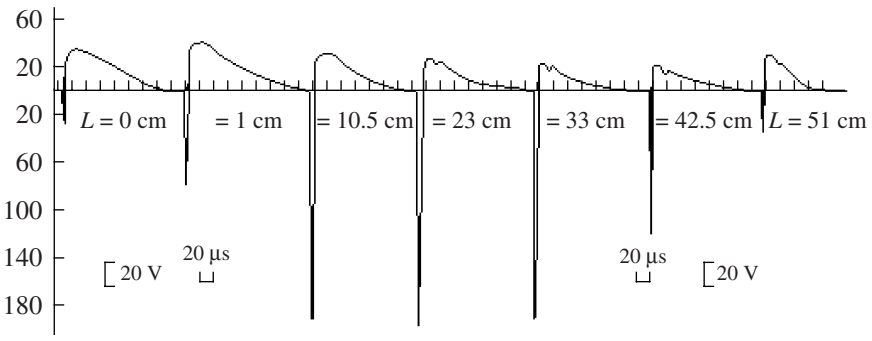

Fig. 8. Dependence of the form of the oscillograms from probes at movement of the volumetric charges (domains) on the length of the volume of the tube.

appearance of the periodic mode. In the subsequent time (a time interval of 50 minutes), the frequency of the fluctuations f_D fell down to a value that was less than the initial one (curve *1*, Fig. 7; p = 1.7 Torr, L_{DIS} = 28.5 cm).

The local temperature of the wall of the discharge chamber (T_W, K) (curve *2*, Fig. 7; V = 4.255 kV) varies in the same way, as well as f_D. The initial volume of the domain V_D near to the cathode and during its displacement to the anode was fixed in two ways: (1) using the mobile pair of photo diodes on the border of the luminous covering protected from ionized and exited molecules of gas; (2) using two mobile ring probes on sharp changes of the potential on the surface of the tube. At a certain distance from the cathode L_{MAX}, the volume of the driven domain V_D was increased up to the maximal. The distance L_{MAX} decreased with an increase of the radius of the tube. At V = 4.255 kV and the diameter of the tube $2r_{TUB}$ = 6.6 mm, L_{MAX} = 21–23 cm, and, at $2r_{TUB}$ = 25.8 mm, L_{MAX} = 5–6 cm.

3. DISCUSSION AND CONCLUSION

Using electrical probes on the surface of the discharged tube, the negative charge inside of the tube was fixed in a time of about several microseconds (the oscillograms of Fig. 8). These charged volumes were inside of the tube from the moment of the formation of the domain nearby to the cathode and the beginning of its passage inside of the tube. The same information from the probes was gained at their input inside of the volume of the tube. The signals of the probes were fixed by the recession of the positive charge of ions that arose under the percussion action of the field of the domains $\vec{\nabla}\vec{E} = \rho/\varepsilon_0$ on the atoms and molecules of the gas [12, 13] (the top part of the oscillograms in Fig. 8).

In the oscillograms in Fig. 8, the changes in the volume of the domains are clearly visible during their removal from the cathode (the change of duration $t_{(-)}$ of the signal of negative polarity); i.e., the volume of the domain at its moving to the anode in the tube with radius r_{TUB} with velocity $\vec{\vartheta}_D$ is defined from $V_D = \pi r_{TUB}^2 L_D = \pi r_{TUB}^2 \vec{\vartheta}_D t_{(-)}$.

The experiments with the pulsed-periodic discharge have shown the following:

—The borders of the moving volumes of the domains are rather precisely fixed optically (photocells, multiplier phototubes, and photodiodes) and by electrical methods of research (by electrical probes inside and on the surface of the discharge tubes); i.e., the charge of the negative sign is located at the borders of the moving domain [13, 14].

—In the discharge tubes with various radiuses but with an equal square of the surface of the potential electrode and equal pressure of the gas (maximal for the pulsed-periodic mode of the discharge in the tube with the minimal radius), the maximum primary volume of the domains was also equal (Fig. 1).

—The form of the domain looked like an ellipsoid of rotation; at a small radius of the tube, the width of the domain in the direction of its moving was less than for the tube with a large radius.

—A spherical form of the domain is observed only at the border of the existence of the periodic discharge at the maximal pressure and only at the square of the surface of the potential electrode much exceeding the square of the cross section of the discharged tube (the circuit in the bottom of Fig. 1); i.e., the appearance of the domain in the form of a sphere required simultaneous realization of the following conditions: (1) a well-defined value of the pressure of the gas, (2) a fixed minimal value of the potential of negative polarity on the cathode, and (3) a large surface of the cathode (greater than the square of the cross section of the tube).

—The frequency of the formation of domains near the cathode increased proportionally with the growth of the negative potential of the cathode and decreased with the increase of the diameter of the tube and with the growth of the duration of the discharge process.

—The volume of the domains increased proportionally to the growth of the value of the potential of the negative polarity on the cathode, but the time of the formation of the domains decreased and the velocity of their passage from the cathode increased (up to $\approx 6.59 \times 10^6$ ms^{-1}).

On the whole, the experiments have also shown that the periodic mode of the discharge was eliminated at switching off of the condensers; after that, the usual stratified discharge of a constant current is observed. From this, a conclusion can be drawn: the condensers connected to the output of the source carry out the role of a storage device of such a quantity of negative electrical charge that provides its continuous and inseparable filling of such part of the volume of the rarefied gas of the discharge tube at which the electrostatic field of the volumetric negative charge (that has appeared in the rarefied gas) itself stops the further process of continuous filling of the negative charge in the volume of the gas inside of the tube. This process will be repeated only in the interval of time necessary for continuous draining of the charge that entered into the gas volume through the earthed electrode.

Is obvious that the frequency of the reiteration of this process in the experiments depends on the following: (1) on the possibility of accumulation in the condensers of a certain value of the charge (i.e., on the value of the potential of the output of the source and the value of the electrical capacity of the condensers connected to its output); (2) on the pressure of the gas in the tube and on its volume (i.e., on the defined value of the charge of negative sign that exhibits continuous spatial localization in the rarefied gas of the tube, which, firstly, depends on the defined square of the surface of the potential electrode that participates in the continuous filling of the energy of the electrical pulses in the rarefied gas and, secondly, depends on the fixed volume that provides the opportunity for allocation of the defined value of the negative charge in the rarefied gas depending on its pressure and on its total volume, i.e., on the sizes of the tubes); (3) on the moving of the volumetric negative charge in the rarefied gas in the condition of its indissoluble continuous spatial localization, which occurs by resistance on the part of the molecules of gas, which results in its heating; and (4) on the electrical circuit of the earthed electrode, which should provide the minimal possible time of continuous running off of the volumetric negative charge into the ground.

ACKNOWLEGMENTS

This work was supported by grant no. 96-26-3.6-3 of the Ministry of General and Professional Education of the Russian Federation.

The authors express their gratitude to A.A. Rukhadse for constant attention and interest in the plasma research at the Laboratory of Physical (plasma) Electronics of Kostroma State University.

REFERENCES

1. Gunn, J.B., High-Electric Field Effects in Semiconductors, *Progr. Semicond.*, 1957, vol. 2, p. 211.
2. Gunn, J.B., Microwave Oscillations of Current in III–V Semiconductors, *Sol.-St.Comm.*, 1963, vol. 1, no. 4, p. 88.
3. Gunn, J.B., Electron Transport Properties Relevant to Instabilities in GaAs, *J. Phys. Soc. Japan (Suppl.)*, 1966, p. 509.
4. Gunn, J.B., Instabilities of Current in III–V Semiconductors, *IBM J. Res. Dev.*, 1964, vol. 8, no. 2, p. 141.
5. Knight, B.W. and Peterson, G.A., Theory of the Ganna Effect, *Phys. Rev.*, 1967, vol. 155, no. 2, p. 393.
6. Bonch-Bruevich, V.L., Zvjagin, I.P., and Mironov, A.Ch., *About Electrical Instability of Domains in Semiconductors*, Moscow.: Nauka, 1972.
7. Gerasimov, I.V. and Mavlonov, Sh., About Movement of the Volumetric Charge at Pulsed-Periodic Breakdown of Gas by a Constant Voltage, *Theses of III All-Union Conferences on Physics of the Gas Discharge*, Kiev, 1986, p. 22.
8. Gerasimov, A.I. and Gerasimov, I.V., Gas Analogue of the Ganna Effect in Conditions of Two-Electrode Discharge of Continuous Current, *Theses of the 20th Symposium on Plasma Physics and Technology*, Czech Republic., Prague, 2002, p. 89.
9. Raiser, Y.P., *Physics of the Gas Discharge*, Moscow.: Nauka, 1987.
10. Gerasimov, A.I., Gerasimov, I.V., Guseev, R.K., and Kukushkin, C.A., The Community and Differences of Generation of Free Volumetric Charges of a Negative Sign in Conditions of Gas Analogue of Effect Gann and the Discharge of Unipolar Breakdown of Gas (UBG), *Proc. III All-Russian Scientific Conferences "Molecular Physics of Nonequilibrium Systems"* (Ivanovo, 2001), p. 20.
11. Gerasimov A.I. and Gerasimov I.V., Necessity of the New Approach to Explanation of a Nature of Discharges, *Theses of the XXX Conf. on Plasma Physics and Controlled Thermonuclear Synthesis in Zvenigorod* (Moscow, 2003), p. 27.
12. Gerasimov, I.V., RF Patent 2076381*, Bull. Izobr.*, 1997, no. 9, p. 1227.
13. Gerasimov, I.V., Radiative Properties of the Volume with the Discharge of Unipolar Breakdown of Gas, *Zh. Tekh. Fiz.,* 1994, vol. 65, p. 30.
14. Gerasimov, I.V., About Distribution of the Electrodeless Discharge of Unipolar Breakdown of Gas, *Plasma Physics* (Russia), 1988, vol. 14, p. 1214.

ISSN 1068-3755, Surface Engineering and Applied Electrochemistry, 2008, Vol. 44, No. 4, pp. 311–319. © Allerton Press, Inc., 2008.
Original Russian Text © O.N. Sizonenko, R.I. Malaya, E.I. Taftai, R.P. Kolmogorova, 2008, published in Elektronnaya Obrabotka Materialov, 2008, No. 4, pp. 72–81.

ELECTRICAL PROCESSES IN ENGINEERING AND CHEMISTRY

Influence of Pulse Electric Field Parameters on the Physicochemical Properties and Structure of Liquid Disperse Systems

O. N. Sizonenko, R. I. Malaya, E. I. Taftai, and R. P. Kolmogorova

Institute of Pulse Processes and Technologies, National Academy of Sciences of Ukraine, pr. Oktyabr'skii 43-a, Nikolaev, 54018 Ukraine

Email: dioo@iipt.com.ua

Received March 10, 2008

Abstract—The results of experimental research of the influence of pulse electric field parameters on the physicochemical properties and structure of highly stable emulsions are presented. It is found that the optimum values of the electric field peak intensity, the current, and the pulse duration at which the maximum effect is achieved depend on the physicochemical characteristics of the disperse medium and the salinity of the disperse phase. It is revealed that the aggregative stability of the emulsion decreases and the separation rate increases in the process of exposure. The disperse phase varies most substantially at the beginning of the exposure. It is found that electric discharge (ED) exposure causes structural changes of highly stable emulsions, which is shown in the destruction of asphaltenes, resins, and paraffins that constitute the disperse medium.

DOI: 10.3103/S1068375508040121

INTRODUCTION

The possibility to influence the physicochemical properties and structure of heterogeneous systems—mixtures of bodies of different physical and chemical nature—is of great importance for the control of disperse system properties; it requires the development of principles for control of the properties taking into account the laws of physicochemical phenomena and the processes in these media [1]. The development of principles for the control of the physicochemical, physicomechanical, and other properties of disperse systems of natural, technogenic, and synthetic origin is of high priority due to their importance for the majority of present-day technologies and for process engineering.

Problems appearing in the course of oil-field operation at the stage of oil treatment and in refineries are of extra urgency. In particular, these are the problems caused by complications in the treatment of oil wherein fine highly stable emulsions are formed. The formation of highly stable emulsions is attributed to the wide application of efficient chemical and physicochemical technologies for increasing reservoir recovery connected with application of surface-active substances leading to formation of fine highly stable emulsions.

One of the most efficient and routine methods for breaking of oil emulsions is electric field exposure [2–4]. However, in electric dehydrators, in the course of separation of oil and aqueous phases, an intermediate layer appears between them; it is a fine highly stable emulsion contaminated with mechanical impurities, which is removed into special storage pits. The storage pits aggregating so-called "trapped oils" are an environmental safety hazard.

The work of many leading companies in the United States, England, Japan, Russia, etc., is focused on the solution of this urgent problem. However, they do not have sufficiently powerful methods for control of highly stable emulsion properties either: for decreasing viscosity, increasing the degree of dispersion of solid inclusions, and for weakening colloidal systems by weakening the interaction between their building agents without changing the initial chemical composition of the medium. An analysis of current literature sources shows that research on the application of pulse electric discharge (ED) exposure in the processes of control of oil disperse system properties (in particular, of highly stable emulsions) is practically absent at present.

At the same time, studies of ED exposure on various disperse systems carried out by specialists of the Institute of Pulse Processes and Technologies of the National Academy of Sciences of Ukraine have proved the possibility in principle to vary and control the physicochemical properties of the systems. Thus, papers [5–7] present the results of experiments on the study of ED exposure on highly viscous heterogeneous poor-dispersion systems with a great amount of free carbon. It is found that there is the possibility of stable weakening of the colloidal system due to dispersion of coarse free carbon particles of 10–25 μm up to dimensions

Table 1. Physicochemical characteristics of oil

Oil origin	Oil parameters		
	Water content, *O*, %	Density at 50°C, kg/m^3	Salinity, %
Malodevitsk oil field (Ukraine, Chernigov Region)	24	876	35
Karazhanbass oil field (Kazakhstan)	Dry crude oil	920	–

Table 2. Physicochemical characteristics of emulsions

Characteristics	Emulsions	
	no. 1	no. 2
Salinity, %	15.0	35.0
Water content, *O*, %	25.0	25.0
Electrical conductivity of the disperse phase, Ohm^{-1} m^{-1}	3.21	5.02
Emulsion density at 50°C, kg/m^3	971	934

below 5 μm and viscosity reduction approximately by a factor of 2.

The aim of the present paper is to study the influence of the pulse electric field parameters on the physicochemical properties and structure of highly stable emulsions.

EXPERIMENTAL

Two types of oil were selected for the studies; their characteristics are presented in Table 1.

Highly stable emulsions of the converse type were prepared from the oil; the value of the globules of the polar fluid—the water in the oil—was close to the dimensions of the colloidal particles; it was approximately 10 μm. This emulsion type was selected for the studies as it is the most characteristic of real conditions of crude-oil production and oil treatment process operations.

The physicochemical characteristics of the emulsions are given in Table 2. The emulsion numbers in Table 2 coincide with the oil numbers of Table 1, on whose basis the emulsions were prepared.

The emulsion preparation was realized by the method of component intermixing, while taking into account the optimum rate and time of the intermixing [8]. It is known [8] that, for preparation of highly concentrated emulsions, it is necessary to introduce a third substance (an emulsifying or stabilizing agent) into the system. However, since the disperse medium in the studied emulsions is oil that already contains substances (asphaltenes, resins, paraffins, etc.) that are emulsion stabilizing agents, additional emulsifying agents were not introduced.

Emulsion no. 1 was of natural origin (from a producing well) and had a salinity of 35% (σ_1 = 5.2 Ohm^{-1}m^{-1}). Water with a salinity of 15% (electrical conductivity σ_1 = 1.035 Ohm^{-1}m^{-1}) was used for the preparation of emulsion no. 2. Before intermixing, the components were heated up to a temperature of 60°C and poured into a mixer with a volume of 450 cm^3; then, they were intermixed for 120 s at a rotation rate of 12000 r/min. Then, the emulsion was placed into a thermostat at 60°C, since, at heating of the liquid disperse system, its kinetic energy increases, which leads to a total increase in the rate of motion of the molecules and particles. The emulsion was considered stable if its aggregative stability was more than 120 h, that is, if the emulsion did not break down after five days of retention.

After the treatment, the emulsion was poured into a glass reservoir and placed into a thermostat where it was kept from 24 to 48 hours at a temperature of 60°C; afterwards, the residual water content O_1, which quantifies the disperse phase residue, was determined.

A Study of the laws of ED exposure on the variation of highly stable emulsion properties was carried out using the apparatus shown in Fig. 1. Autotransformer *1* (RTT–25/05 type) and high-ohmic rectifier transformer *2* (VTM–20/50–72 type) were applied as the power supply for the ED circuit. The VTM–20/50–72 output voltage was varied by means of the RTT–25/05 autotransformer, which was fed from control board *3*. The voltage set by virtue of the high-ohmic rectifier transformer was applied to one of ED circuits *4*, wherefrom pulses passed into the operating chamber.

The measurement of system *6* consisted of a current-limiting resistor; a potential divider; and a kilovoltmeter, which was used for setting and control of the operating voltage applied to the ED circuit. In addition, the measurement system contained a potential divider, a shunt resistor, and an oscillograph of the S 9–8 type. By virtue of them, the voltage between the operating chamber electrodes and the current through the emulsion were registered. The number of realized discharges in each experiment was registered by means of a pulse meter of the PSO2–08A type. The discharge of pulse capacitors through the resistor and short-circuiting of the ED circuit at power dumping were realized by

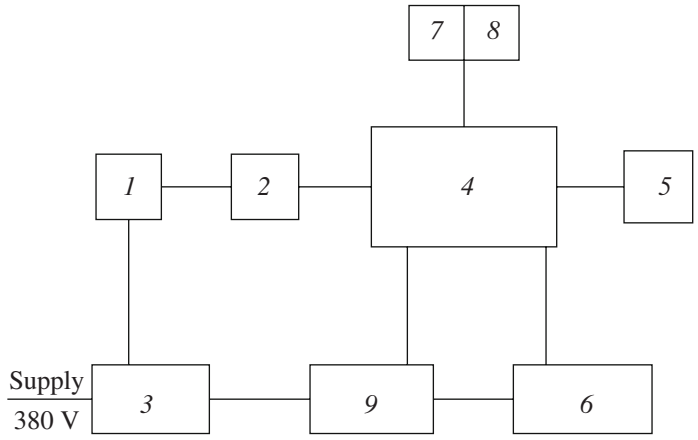

Fig. 1. Schematic diagram of the experimental bedstead: (*1*) autotransformer RTT–25/05, ES 16–517.739–76; (*2*) high-ohmic rectifier transformer VTM–20/50–72, ES 16.529.743–76; (*3*) control board; (*4*) ED circuit; (*5*) operating chamber; (*6*) measurement system; (*7*, *8*) electric interlocks; (*9*) control desk

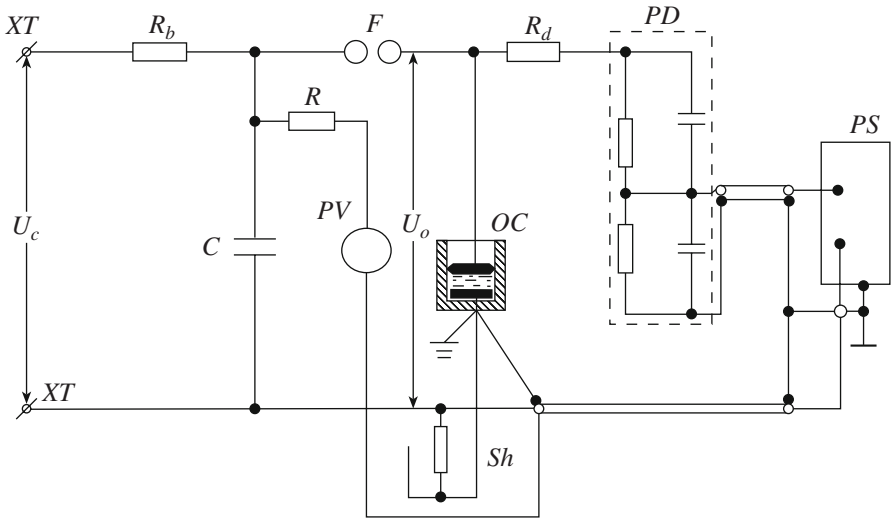

Fig. 2. Circuit of ED exposure: U_c is the power supply voltage; R_b is the ballast resistor (from 0.109 to 200 MOhm); *F* is the spark gap; *C* is the operating capacitance (0.025; 0.05; 0.1; 0.2; 0.4; 0.8 μF); U_o is the operation voltage (30.5; 22.5; 15; 12; 10; 7.5 kV); *R* is the current–limiting resistor; *PV* is the kilovoltmeter; *Sh* is the coaxial shunt resistor; *PD* is the potential divider; *OC* is the operating chamber (technological unit); *PS* is the oscillograph; R_d is the damping resistor.

means of electric interlocks *7* and *8*. The experimental apparatus was controlled from control desk *9*.

The ED exposure was realized by means of the electric circuit shown in Fig. 2. The rate of the exposure wave front steepness was controlled by virtue of replaceable inductors in the discharge circuit of reserve capacity *C*, and the pulse duration was controlled by variation of the capacity *C* and by the replaceable inductors *L*. The pulse amplitude was set by controlling the voltage of the self-breakdown of the spark gap *F*, and the pulse repetition frequency was set by controlling the voltage U_c. Alternation of the pulse polarities took place at interchanging of the capacitor *C* and the spark gap *F*. In this case, the current through the emulsion in the course of charging of the capacitor *C* passed in one direction; at breakdown of the spark gap *F*, the capacitor *C* discharged current through the emulsion thus changing its direction.

The quantitative content of the water in the oil emulsions *O* was determined by the Dean and Stark method [9]; it consisted of the following. A certain amount of emulsion is heated in a solvent mixture in the Dean and Stark apparatus. The solvent, being evaporated, carries moisture contained in the oil product. The vapors of the water and solvent are condensed in a refrigerator, and the distilled off water gravitates to the bottom of a receiver with a calibrated trap. According to the water

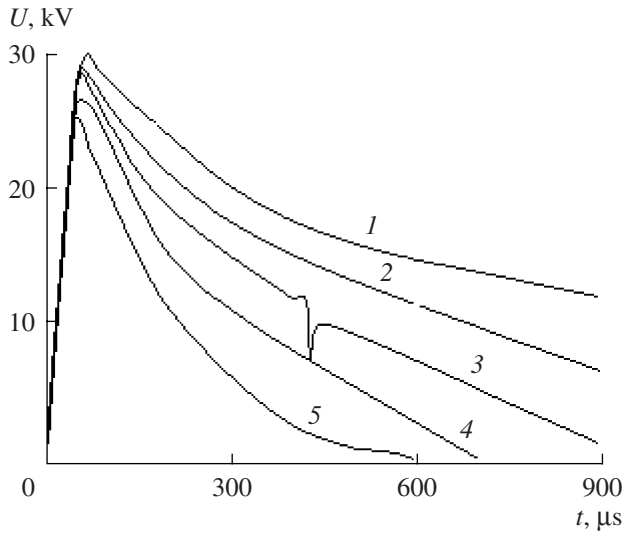

Fig. 3. Form of the discharge voltage in the emulsion at the beginning of the treatment: *1–5* are the pulse series numbers.

amount in the trap, the water percentage in the emulsion is calculated.

The mass (O^1) or volume (O) concentration of the water in the emulsion is determined from the relations

$$O^1 = \frac{V_0}{m}100\%; \quad (1)$$

$$O = \frac{V_0}{V}100\%, \quad (2)$$

where V_0 is the water sample volume in the receiver–trap, cm^3; m is the sample weight, g; and V_1 is the sample volume, cm^3.

A water amount in the receiver–trap of 0.03 cm^3 or less is as considered traces. The absence of water in a studied oil product is determined by the state at which water drops are not observed in the bottom part of the receiver–trap. The method accuracy is 0.1 cm^3, or 2% of the mean value, at a water amount up to 1.0 cm^3.

The microstructure of the solid inclusion dispersion was studied by means of an optical microscope (Neofit-32).

For the qualitative analysis of the inclusion dispersion, the precise method of A.A. Glagolev was applied [10]. Using this method, the analyzed structure is covered with an ensemble of points; then, their number occurring on each of these structural constituents is calculated separately. The studies were carried out by the method of a moving section with applying a micrometer eyepiece with a reticle with 64 nodal points.

In order to determine the size distribution of the inclusions, at first the size of the inclusions was measured using the linear method [9]. The studies were carried out using the method of a moving section with applying a micrometer eyepiece with a scale divided into 100 parts. The linear method consists of measurement of the length of the segment of a straight line passing through the nominal particle diameter. The values obtained by this means are distributed in size groups. The values of the particle sizes in each group are selected to include all the sizes from the minimum to the maximum. The statistical sample amount in all the cases is selected so that the error does not exceed 5% at a confidence level $P = 0.95$.

RESULTS AND DISCUSSION

The study of the influence of the pulse electric field parameters on the aggregative stability of the emulsions was realized by varying the pulse duration from tens and hundreds of microseconds, the peak values of the field intensity from 0.3×10^6 to 1.2×10^6 V/m, the peak values of the current by fractions of a kiloampere, and the pulse form was nonperiodic (unipolar). This range was provided by variation of the circuit parameters at constant stored energy of 22.5 J:

—the reserve capacity C_r from 0.05×10^{-6} to 0.8×10^{-6} F,

—the inductance L_k from 10^{-5} to 9.4×10^{-2} H,

—the operation voltage U_o from 7.5 to 30 kV,

—the pulse number n from 50 to 8000, and

—the pulse frequency f from 0.5 to 4 Hz.

The system analysis of the results of the experimental series allowed us to find the 17 most characteristic ones among them; they are presented in Table 3.

The experiments have shown that, at the beginning of the pulse exposure, the voltage form on the electrode (being at positive potential) has a complex curve due to the reserve capacity discharge on the nonlinear resistance of the emulsion and the induction. At first, a highly stable emulsion is characterized by high resistance, since the fine globules of mineralized water are situated chaotically and do not form ohmic bridges yet. As soon as water globules, being stretched along flux lines of the electric field, begin to form ohmic bridges, the emulsion resistance decreases and the current in it increases. Therefore, after several pulses, the voltage takes the form shown in Fig. 3. Herein, the voltage that affects the emulsion is formed by the voltage on the capacitator and inductor; this leads to an increase in the voltage on the discharge chamber electrodes (curve *5* with respect to curve *4*) in comparison with the voltage of the spark gap discharge.

After a certain number of pulses, the coalescing globules of water coalesce so that they form a conducting medium between the electrodes in the electric field; as a result, at the capacity discharge, the emulsion breakdown takes place (a discharge channel is formed).

Table 3. Results of the studies of the influence of the pulse electric field parameters on the residual water content O_1 of the emulsion

Experiment no.	Emulsion no.	C, μF	U_o, kV	n, pulses	f, Hz	L, mH	O_1,%	W_Σ, kJ
1	1	0.5	30	50	0.5	0.63	5.3	1.125
2	1	0.5	30	270	0.5	0.63	7.7	6.075
3	1	0.5	30	300	1	0.63	6	6.75
4	1	0.1	22.2	100	0.5	0.63	4.3	2.94
5	2	0.2	15	4000	0.5	0.63	10.5	90.0
6	2	0.2	15	4000	0.5	10	11	90.0
7	2	0.2	15	4000	0.5	94	9.5	90.0
8	2	0.2	15	6000	0.5	94	7.5	135.0
9	2	0.1	25	6000	0.5	94	9	135.0
10	2	0.2	15	6000	4	10	4.5	135.0
11	2	0.4	10	6000	4	10	2.5	135.0
12	2	0.8	7.5	4350	4	10	8.5	97.875
13	2	0.8	7.5	6000	4	10	6	135.0
14	2	0.8	7.5	8000	4	10	3.5	180.0
15	2	0.2	10	8000	4	10	4.2	80.0
16	2	0.4	10	4000	4	10	5.3	80.0
17	2	0.8	10	2000	4	10	6.5	80.0

Thus, the disperse phase coalescence and the conducting system formation lead to a decrease in the emulsion resistance. Herein, the form of the voltage applied to the emulsion changes as well.

The research results have shown that, in the studied parameter range (see Table 3) with relatively low energy consumption (1125 J), a decrease in the water content of emulsion no. 1 from the maximum of 25.0 to 3.5% is possible. The continuation of the treatment after the breakdown occurrence worsened the results: the residual water content was 7.7%. Herein, the electric energy consumption increased by approximately by a factor of 5. An increase by a factor of 2 in the discharge pulse repetition frequency practically did not lead to variation of the results. These results can be explained by the fact that the electric field intensity in the emulsion was above the limiting value (E_{lim}) and, as a consequence, the inverse process—dispersion of coalesced globules—appeared.

A decrease of the voltage from 30.0 to 22.2 kV and, respectively, of the peak values of the field intensity from 1.20×10^6 to 0.88×10^6 V/m at an increase in the pulse duration and the value of the current passing through the emulsion due to an increase in the reserve capacity by a factor of 2 (from 0.1 to 0.2 μF) makes it possible to somewhat improve the result. In comparison with all the previous experiments, the water content decreases to 4.3% at relatively low energy consumption (2.94 kJ).

Studies of the influence on emulsion no. 2, which is characterized by its viscosity being less by approximately a factor of 3 than that of emulsion no. 1, have shown that a decrease in the operation voltage to 15 kV at a reserve capacity of 0.2 μF leads to worsening of the results (O_1 = 10.5%); in addition, the energy consumption in some experiments increased by almost a factor of 30.

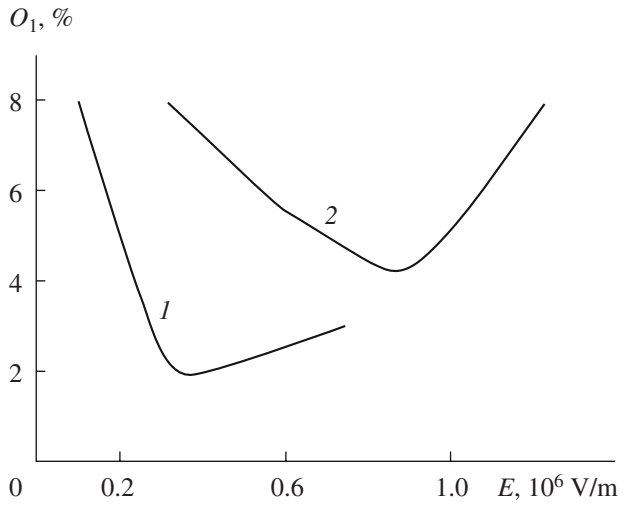

Fig. 4. Dependence of the residual water content of the oil emulsion on the peak intensity of the pulse electric field at different salinities of the water: (*1*) emulsion no. 1, salinity of 35%; (*2*) emulsion no. 2, salinity of 15%.

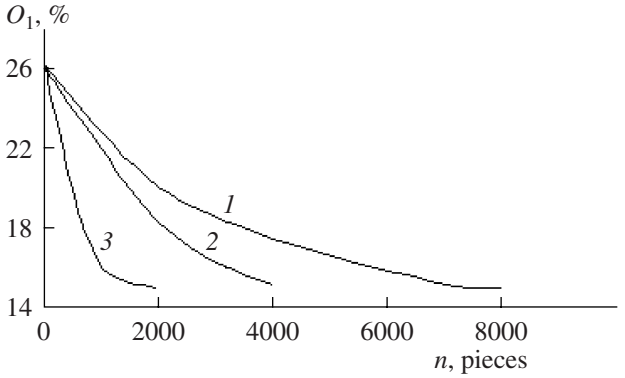

Fig. 5. Variation in the water content of emulsion no. 2 in the treatment process: (*1*) exposure pulse duration $\tau = 1.3 \times 10^{-4}$ s; (*2*) exposure pulse duration $\tau = 1.9 \times 10^{-4}$ s; (*3*) exposure pulse duration $\tau = 2.8 \times 10^{-4}$ s.

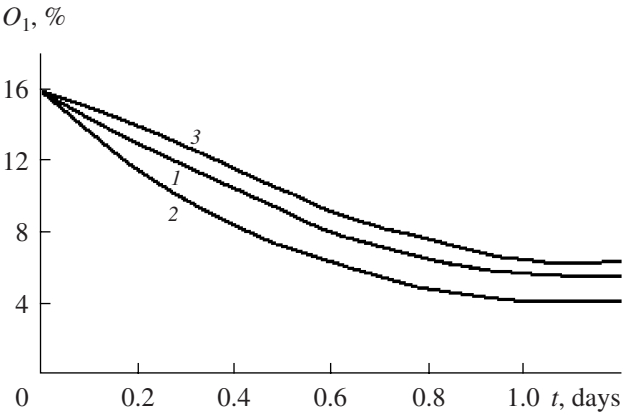

Fig. 6. Dependence of the variation in the residual water content of emulsion no. 2 on the retention time: (*1*) exposure pulse duration $\tau = 1.9 \times 10^{-4}$ s ($C = 0.2$ μF); (*2*) exposure pulse duration $\tau = 1.3 \times 10^{-4}$ s ($C = 0.4$ μF); (*3*) exposure pulse duration $\tau = 2.8 \times 10^{-4}$ s ($C = 0.8$ μF).

An increase in the pulse duration and a significant decrease in the discharge current amplitude (due to an increase by a factor of 15 of the inductance in the discharge circuit) do not exert a positive influence on the final result.

An increase by a factor of 1.5 of the pulse number and, therefore, in the exposure period at a simultaneous increase in the electric field intensity up to 1×10^6 V/m, as well as a decrease in the pulse duration and discharge current value due to a decrease in the reverse capacity by a factor of 2, worsen the result: it becomes comparable with the experiment where the energy consumption was lower by a factor of 2.

A comparison of the results shows that the pulse duration decrease from 3.5×10^{-4} to 1.1×10^{-4} s, due to the inductance decrease from 94 to 10 mH at increasing the pulse repetition frequency from 0.5 to 4 Hz, exerts a stronger influence on the structure processes in the disperse medium ($O_1 = 4.5\%$). An increase in the pulse duration up to 1.3×10^{-4} s and in the current at a decrease by a factor of 2 of the capacity and the peak intensity of the electric field to 0.4×10^6 V/m leads to a better result: in this case, the residual water content of the emulsion is 2.5%.

The experimental research allowed determining the degree of variation of the aggregative stability of the disperse system in its dynamics by the sequential sampling method. It follows from the presented results that the total energy increase by a factor of 2 allows increasing the exposure efficiency by a factor of 2.5.

The results of the analysis show that the optimum values of the peak intensity of the electric field, the current value, and the pulse duration at which the most efficient loss of the aggregative stability is obtained depend on the physicochemical properties of the disperse medium and the salinity of the disperse phase at identical water contents (Fig. 4).

The dynamics of the variation of the water content in the process of exposure at a constant field intensity of 10 kV/cm and evolved energy in the emulsion of 80 kJ is illustrated in Fig. 5.

The dependence of the residual water content on the retention time (Fig. 6) shows that the emulsion breaking continues after the exposure; the water content in all the samples decreases by almost a factor of 3. This counts in favor of the fact that, in the pulse exposure process, there occur coalescence and coarsening of aqueous phase globules and their consequent slow precipitation, i.e., separation of the oil–water emulsion. This is confirmed by the results of the microstructure analysis of the oil–water emulsion (Fig. 7).

Therefore, it is of interest to observe how the aggregative stability of the emulsion varies in the exposure process and to determine rate of its separation. According to [8], the emulsion aggregative stability is deter-

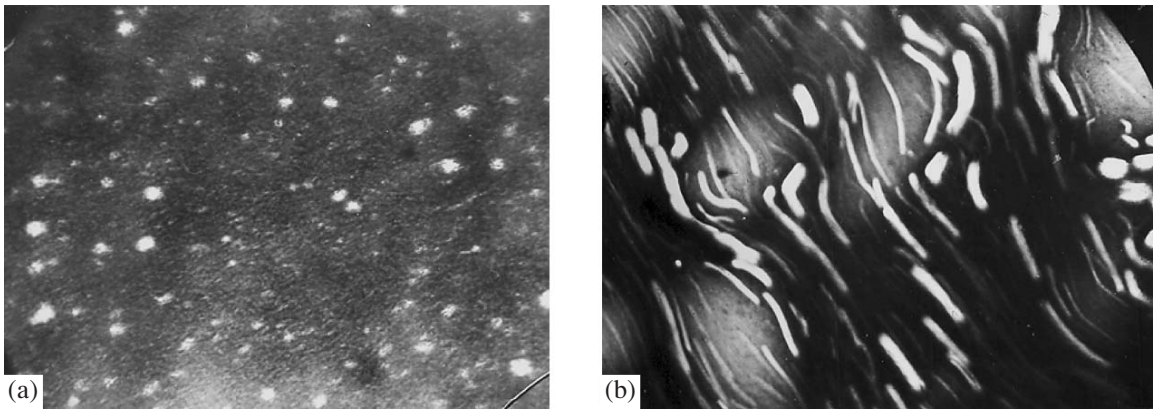

Fig. 7. Microstructure of oil emulsion no. 2: (a) the emulsion before exposure ×100; (b) the emulsion after exposure ×100.

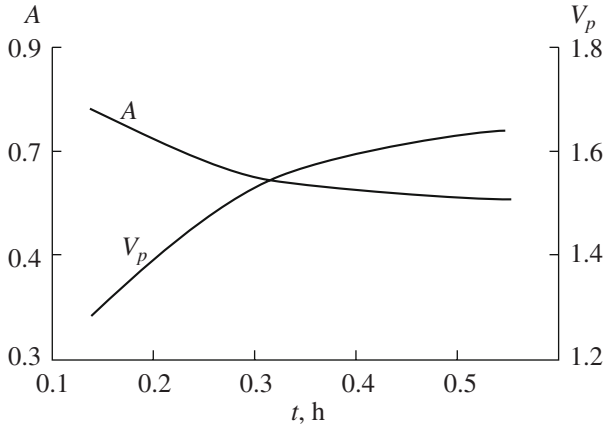

Fig. 8. Dependence of the aggregative stability and the rate of separation of oil emulsion no. 2 on the exposure time in the treatment process (Table 3, experiment no. 15).

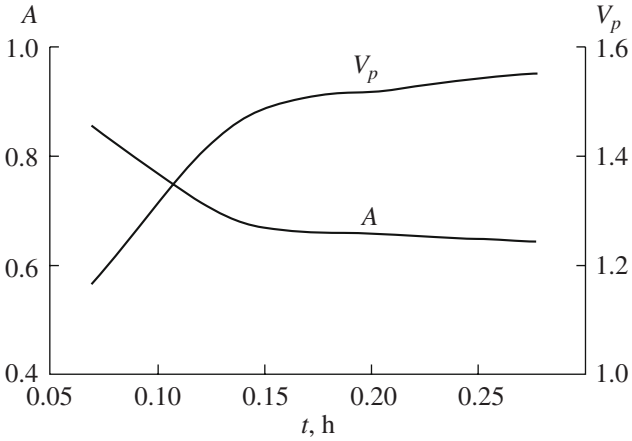

Fig. 9. Dependence of the aggregative stability and the rate of separation of oil emulsion no. 2 on the exposure time in the treatment process (Table 3, experiment no. 16).

mined by the time of its complete separation into constituent phases at retention. Hence, for estimation of the aggregative stability variation in the exposure process, we proceeded as follows.

Let us present the emulsion aggregative stability in the exposure process as a measure of the elementary stability in relative units by estimation of the water content variation after a certain number of pulses at an identical amount of impressed energy for all the treatment time

$$A = \frac{O - O_2}{O}, \tag{3}$$

where O_2 is the precipitated water, and $O_2 = O - O_1$.

The value opposite to the aggregative stability under exposure will characterize the rate of its separation:

$$V_p = \frac{1}{A}. \tag{4}$$

The experimental data on the measurement of the water content under exposure and calculated data on the aggregative stability and the rate of separation of emulsion no. 2 in experiments nos. 15–17 (Table 3) are presented in Figs. 8–10, respectively. It should be noted that all the emulsion samples were taken from the upper layer of the operating chamber at an identical amount of impressed energy but at different exposure times (number of pulses). In all the experiments, the total energy value was 80 kJ.

The data on the aggregative stability and the emulsion separation rate presented in Figs. 8–10 testify to the fact that the emulsion aggregative stability decreases in the exposure process; the separation rate increases. The aggregative stability varies most signifi-

Table 4. Results of microstructure analyses of the disperse systems before and after ED exposure

Medium type	Asphaltenes, resins, and paraffins		Water	
	Amount, %	Size, μm^2	Amount, %	Size, μm^2
Emulsion no. 1 before treatment	6.1	455.6	1.8	5.2
Emulsion no. 1 after treatment (Table 3, experiment no. 1)	5.9	43.5	0.8	177.2
Emulsion no. 2 before treatment	3.7	392.8	1.7	12.0
Emulsion no. 2 after treatment (Table 3, experiment no. 14)	3.5	32.7	0.9	320.0

cantly at the beginning of the exposure, that is, when the first fine water globules begin to coalesce.

The microstructure analyses of the emulsion samples before and after the exposure allowed revealing the size distribution of the water drops characterizing degree of dispersion of the emulsion (the degree of subdivision of the disperse phase). The water drop size in initial emulsion no. 1 is from 5 to 10 μm; in emulsion no. 2, it is from 10 to 15 μm; and the distribution is chaotic (Fig. 11). After the exposure, small water drops coalesce into greater ones with their sizes being from 60 to 240 μm (Table 3, experiment nos. 1 and 4) and from 80 to 480 μm (experiment nos. 14 and 15) and the structure becomes ordered (Fig. 12).

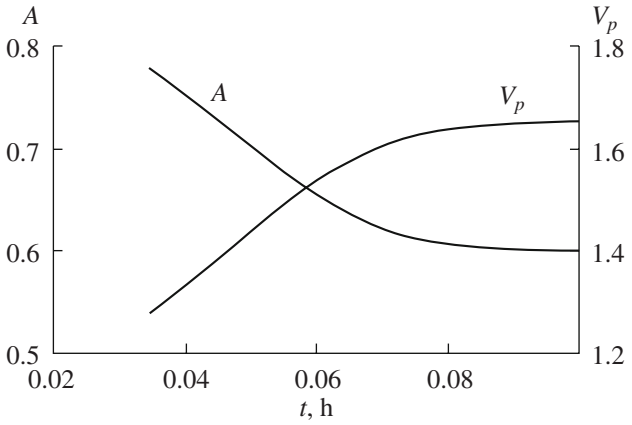

Fig. 10. Dependence of the aggregative stability and the rate of separation of oil emulsion no. 2 on the exposure time in the treatment process (Table 4, experiment no. 17).

The optical microscopy allowed finding that, in addition to oil and water, foreign inclusions are present in all the samples. In all the cases, these inclusions are conglomerates of asphaltenes, resins, and paraffins, which influence the rheological properties of the emulsions; moreover, their percentage was higher by approximately a factor of 2 than that of water, and their sizes before the treatment were greater by approximately an order of magnitude (see Table 4). As one can see from Table 4, after the ED treatments, the loss of the aggregative stability of the disperse systems occurs not only due to the disperse phase coagulation but also due

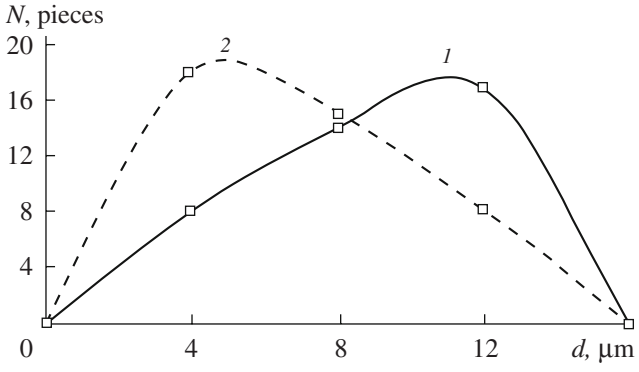

Fig. 11. Size distribution of the water in the oil before ED exposure (*d* is the globule diameter, *N* is the globule number): (*1*) emulsion no. 1; (*2*) emulsion no. 2.

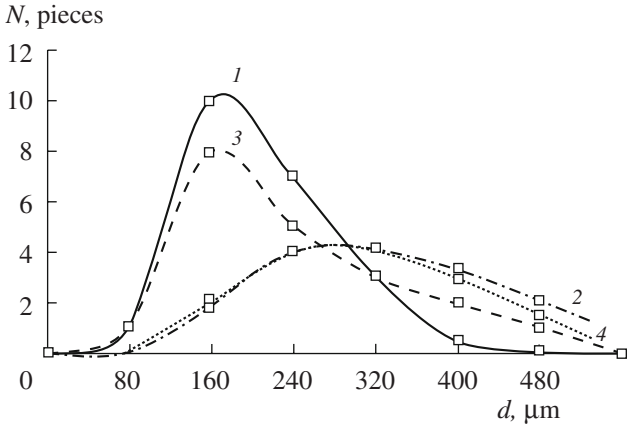

Fig. 12. Size distribution of the water in the oil after ED exposure (*d* is the globule diameter, *N* is the globule number): (*1*) emulsion no. 2, experiment no. 14; (*2*) emulsion no. 1, experiment no. 1; (*3*) emulsion no. 2, experiment no. 15; (*4*) emulsion no. 1, experiment no. 4.

to the disintegration of conglomerates of asphaltenes, resins, and paraffins.

CONCLUSIONS

The experimental studies of the influence of the pulse electric field parameters on the variation of the aggregative stability, the disperse composition, and the structure of highly viscous oil disperse systems allowed reaching the following conclusions:

—The optimum values of the electric field peak intensity, the current, and the pulse duration at which the most efficient loss of aggregative stability is achieved depend on the physicochemical characteristics of the disperse medium and the salinity of the disperse phase at identical water contents.

—The aggregative stability of the emulsion decreases and the separation rate increases under the exposure. Herein, the disperse phase varies most substantially at the starting exposure, when the first fine water globules begin to coalesce.

—ED exposure leads to qualitative changes of highly stable emulsions, which is shown in the destruction of supermolecular structures of asphaltenes, resins, and paraffins.

REFERENCES

1. Ur'ev, N.B., *Fiziko–khimicheskie osnovy tekhnologii dispersnykh sistem i materialov* (Physicochemical Principles of Technology of Disperse Systems and Materials), Moscow: Khimiya, 1988.
2. Levchenko D.N., Bernshtein, N.V., and Nikolavea, N.M., *Tekhnologiya obessolivaniya nefti na neftepererabatyvayushchikh predpriyatiakh* (Technology of Oil Desalting at Oil Refinery), Moscow: Khimiya, 1985.
3. Proskuryakov, V.A. and Smirnov, O.V., *Ochistka nefteproduktov i neftesoderzhashchikh vod elektroobrabotkoi* (Refining of Oil Products and Oil Containing Water by Electric Treatment), St. Petersburg: Khimiya, 1992.
4. Martynenko, A.G., Konoplev, V.P., and Shiryaev, G.P., *Ochistka nefteproduktov v elektricheskom pole* (Refining of Oil Products in Electric Field), Moscow: Khimiya, 1974.
5. Sizonenko, O.N., Shvets, I.S., Dudukin, L.S., and Golovashchenko, A.F., Ukraine Patent 67828, C2 7 C10L1/32, *Byull.*, 2004, no. 7.
6. Sizonenko, O.N., Taftai, E.I., Tkachenko, A.K., and Shvets, I.S., Peculiarities of ED Exposure on Highly Viscous Media, *Elektron. Obrab. Mater.*, 2004, no. 6, pp. 37–43.
7. Sizonenko, O.N., Taftai, E.I., Tkachenko, A.K., and Shvets, I.S., Influence of ED Exposure on Physicochemical Properties of Highly Viscous Media, in *Natsional'nyi Universitet Korablebuduvannya: Zbirnik Naukovykh Pratsi*, 2004, no. 1, pp. 154–162.
8. Clayton, W., *Emul'sii, ikh teoriya i tekhnicheskoe primenenie* (Emulsions, their Theory and Engineering Application), Rebinder, P.A., Ed., Moscow: Inostrannaya Literatura, 1950 (in Russian).
9. Borovaya, M.S., *Laborant neftyanoi i gazovoi laboratorii* (Laboratory Assistant of Oil and Gas Laboratory), Moscow: Nedra, 1968.
10. Saltykov, S.A., *Stereometricheskaya metallografiya* (Stereometric Metallography), Moscow: Metallurgiya, 1976.

ISSN 1068-3755, Surface Engineering and Applied Electrochemistry, 2008, Vol. 44, No. 4, pp. 320–329. © Allerton Press, Inc., 2008.
Original Russian Text © V.N. Tsurkin, A.V. Mel'nik, 2008, published in Elektronnaya Obrabotka Materialov, 2008, No. 4, pp. 82–92.

EQUIPMENT AND INSTALLATIONS

Processes and Character of Melt Loading by an Electric Discharge Generator of Vibrations on Resilient Elements: Part I (Waveguide Dynamics)

V. N. Tsurkin and A. V. Mel'nik

Institute of Pulse Processes and Technologies, National Academy of Sciences of Ukraine, Oktyabr'skii 43-A, Nikolaev, 54018 Ukraine

E-mail:iipt@iipt.com.ua

Received January 31, 2008

Abstract—The results of numerical modeling of the waveguide-radiating system dynamics for the electrical discharge generator of vibrations with resilient elements are presented. The possibility of the metal structure changing due to the choice of the optimal resilient elements rigidity and application of the waveguide nozzles is shown. It was found out that the share of the dissipation energy is stipulated by the nozzle configuration and the properties of the processed metal.

DOI: 10.3103/S1068375508040133

INTRODUCTION

The development of new and the perfection of the existing methods of processing liquid and crystallizing metals using physical fields, which enable one to increase the melt quality, have current importance for foundries. Among the great number of methods, there is electrohydropulse processing (EHPP) of the melt in a ladle, which is distinguished by its high efficiency. A more detailed description of the method, its functional possibilities, and the mechanisms of its action on the melt are presented in [1–4]. The source of disturbances in the melt of such a processing method is an electric discharge generator of resilient vibrations (EDGRV), which produces a field of resilient waves in a liquid metal by means of a membrane and a waveguide. We should note that the choice of the EDGRV type, of the constructional dimensions, and the configurations of its component elements is a complicated and not quite solved problem. The known project solutions are based mainly on the experimental investigations and statistical data of the practical application of the design projects in the production field.

The operating properties of the ready metal products are defined by both the magnitude and character of the load being applied; hence, the problems of the dynamics of the wave system in EHPP of a melt in a ladle are of scientific and practical interest.

In the technological devices of the EHPP of a melt, while assembling the discharge chamber, they usually use a rigid attachment, but, as was found out in the course of experiments and exploitation of the equipment, the degree of the low frequency vibrations impacting the object being processed considerably increases provided the EDGRV frames have a resilient mounting employing disk spring sets (GOST 3057-90). The low frequency action ensures favorable conditions for the melt agitation, which provides the volume homogenization of the liquid bath.

It is known that the efficiency of EHPP of a melt in a ladle is considerably influenced by the constructive peculiarities of the waveguides immersed into the melt, their form, the presence of various extension pieces, the depth of their immersion into the liquid metal, etc. [5]. The experiments on the physical modeling of the electric explosion action on the melt in a ladle [5] showed that the utilization of cylindrical waveguides with a plate nozzle ensures that the hydroflow rate increase up to 40%. This promotes more active melt agitation and a significant reduction of the temperature drop with respect to the ladle height and gas content in the processed metal. In addition, such a constructive solution intensifies the cavitation processes in the melt, which are crucial for the structural changes in the metal.

A number of publications [1, 2, and 6] are devoted to investigations of the dynamic characteristics of waveguide-radiating EDGRV systems at various stages of the discharge. Their spectral analysis was carried out as well [7 and 8]. At the same time, the calculation schemes presented in the above works failed to consider the possibility of the resilient movement of the discharge chamber frame and the presence of the nozzles on the vibrator. Thus, the introduction of the additional resilient and damping elements into the vibration system of the EDGRV–liquid metal will enable one to expand the design concepts of the EHPP melting process in a ladle and to display its qualitatively new mechanisms of development.

In the general case, the spectrum of the wave disturbances generated into the melt includes three frequency ranges, which correspond to the three stages of processing:

I stage. In the region of high frequencies, the load from the widening channel of the discharge and its adjacent area is transferred to the melt by means of the waveguide (the active stage of discharge).

II stage. The region of medium frequencies is characterized by the melt being loaded due to the pressure wave focusing by the walls of the discharge chamber with respect to its form and the pulsation of a vapor–gas cavity (VGC).

III stage. In the region of low frequencies, the source of the disturbances is the EDGRV itself, which can be regarded, with certain allowances, as an oscillation system with lumped constants.

The purpose of the present work is a complex study of the dynamics of the waveguide radiating system of EDGRV based on the resilient elements and the hydrodynamic processes occurring in the liquid metal under the action of EHPP of the melt in a ladle. At the first stage, the dynamic characteristics of the waveguides with nozzles are examined with regard to the damping properties of the melt. Further on, there will be solved the problems connected with the definition of the nonstationary field of pressures, which occurs in the metal being processed at various stages of its processing.

THEORETICAL INVESTIGATION

For the modeling of the vibratory motion of the waveguide-radiating system of the EDGRV based on the resilient elements at the EHPP of the melt in a ladle (the general scheme of which is presented in Fig. 1), the following physical allowances should be accepted:

—the water in the discharge chamber is assumed to be an ideal and compressible liquid;

—the membrane deformation is described by Hooke's law for isotropic media;

—in the places of the membrane fastening to the chamber frame, there should be a rigid fixing;

—the load is distributed axis-symmetrically across the membrane surface;

—30% of the energy evolved in the discharge channel [5] is transferred to the VGC energy;

—heat transfer from the melt to the waveguide-radiating system is absent.

The initial conditions are as follows:

—the movement of the mass centers of the waveguide radiating system and the discharge chamber starts from the position of static equilibrium and a quiescent state.

The boundary conditions are as follows:

—the pressure in the VGC and in the water on the media interface is identical;

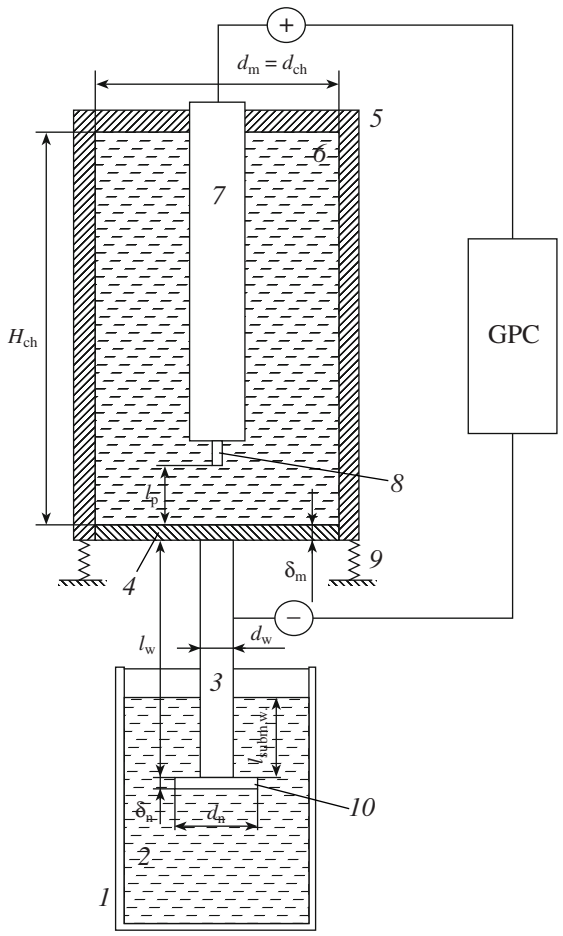

Fig. 1. The general scheme of the EHPP melt in a ladle and the EDGRV of the resilient elements: *1*—ladle; *2*—melt; *3*—waveguide; *4*—membrane; *5*—discharge chamber; *6*—operation liquid; *7*—electrode; *8*—current lead; *9*—resilient element; *10*—circular nozzle.

—on the interface of the water, the membrane, and the walls of the discharge chamber frame is maintained the water nonpenetration condition.

The external load from the pressure created by the widening VGC is assumed to be in the form of a sinusoid half-wave:

$$F(t) = F_{max} \sin \frac{\pi}{\tau} t, \quad (1)$$

where F_{max} is the amplitude value of the load, τ is the period of the load, and t is the time.

The value F_{max} affecting the membrane can be obtained from the equation of the water state in the form of Theta.

The maximal radius of the widening VGC makes up 25% of the radius of the VGC pulsation in the open volume, and the duration of the load τ is 10% of the pulsation period of the VGC in the open volume [9], which can be defined by the Willis formula.

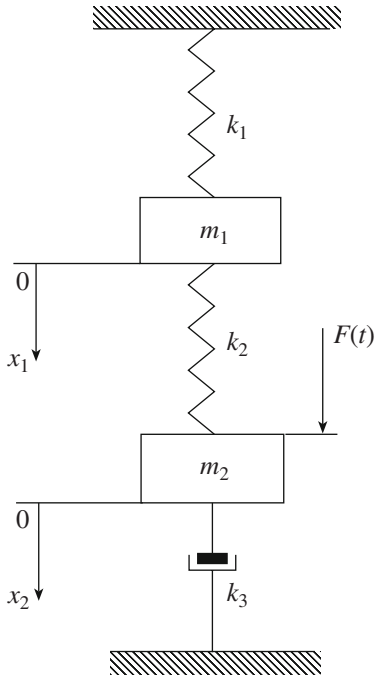

Fig. 2. The dynamic model of the EDGRV on the resilient elements at the EHPP melt.

The damping properties of the melt are characterized by the dissipative forces of the wave and viscous resistance. The added mass of the liquid metal and the regenerating Archimedean force were taken into account. The resiliency coefficient of the plate was determined according to Hook's law by the methods of [1].

Then, the dynamic model of the EDGRV on the resilient elements at EHPP of a melt in a ladle can be presented as a vibration system with two stages of freedom, two resilient elements, and a damper (Fig. 2). The disturbing force corresponds to the axis-symmetrical load (1) of the widening VGC. The one-dimensional problem of the vibrations of a membrane with a waveguide that was supposed to be absolutely rigid is being solved. In such a formulation, according to [6], it can be considered that the motion of the waveguide end corresponds to the shifts of the membrane pole.

The motion of the dynamic model with two stages of freedom is described by a system of differential equations of the second order:

$$\begin{cases} m_1 \dfrac{d^2x_1}{dt^2} = -k_1 m_1 - k_2(x_1 - x_2); \\ m_2 \dfrac{d^2x_2}{dt^2} = -c_1\left(\dfrac{dx_2}{dt}\right)^2 - c_2\dfrac{dx_2}{dt} - c_3 x_2 \\ -k_2(x_2 - x_1) + F(t), \end{cases} \quad (2)$$

where m_1 is the mass of the discharge chamber with water without considering the mobile part of the waveguide-radiating system; m_2 is the mass of the mobile part of the membrane with a waveguide taking into account the added mass of the liquid metal; k_1 is the sum coefficient of the rigidity of the resilient element sets; k_2 is the membrane rigidity coefficient; x_1 is the shift of mass center of the discharge chamber in the operating state; x_2 is the shift of the membrane pole; c_1, c_2, and c_3 are the coefficients of the viscous and wave resistances and of the regenerating force, correspondingly; and $F(t)$ is the disturbing force. On the basis of the numerical solution by the Runge–Kutta method of system (2), there were carried out the calculations of the amplitude of the damped vibrations of the waveguide end without a nozzle and with a circular one with respect to its diameter at various values of the ratio between the rigidity of the EDGRV resilient elements and that of the membrane.

RESULTS AND DISCUSSION

The numerical experiment was carried out at the value of the stored energy of the capacitor battery of 1 kJ. The geometric parameters of the EDGRV (Fig. 1) correspond to the ones used in the existing experimental industrial devices for the EHPP of metal in a ladle: the height of the discharge chamber is H_{ch} = 270 mm, the internal diameter of the discharge chamber is d_{ch} = 230 mm, the operation length of the discharge channel is l_p = 30 mm, the diameter of the mobile part of the membrane was considered to equal d_k, the membrane thickness is δ_m = 16.5 mm, the waveguide diameter is d_w = 20 mm, and the waveguide length is l_w = 900 mm. The calculations were carried out for three diameter values of the circular nozzles d_{ex}: 30, 50, and 70 mm. The material of the membrane and the waveguide was St3, and the objects of the processing were melts of aluminum, iron, and lead. The ratio of the sum rigidity of the resilient elements to the membrane rigidity k_1/k_2 equaled the following: 0.1; 0.5; 1.

The results of the numerical modeling are presented in figures 3, 4, and 5 as graphic dependences of the waveguide end shift in the melt upon the time. In general, the motion of the waveguide end should be regarded as damped harmonic vibrations that can be explained by the sinusoidal law (1) of changes of the disturbing force $F(t)$. The presence of the circular nozzle on the end ensures more intensive damping of the vibrations; moreover, the greater the diameter of the end is, the faster the return of the system to the state of static balance. For instance, for the aluminum melt (Fig. 3) at d_{ex} equal to 30 mm, the oscillations are actually being damped after 200 ms, and, with the d_{ex} increased up to 70 mm, the amplitude drops to zero already after 40 ms. The damping properties of the melt are determined by its density; therefore, with its

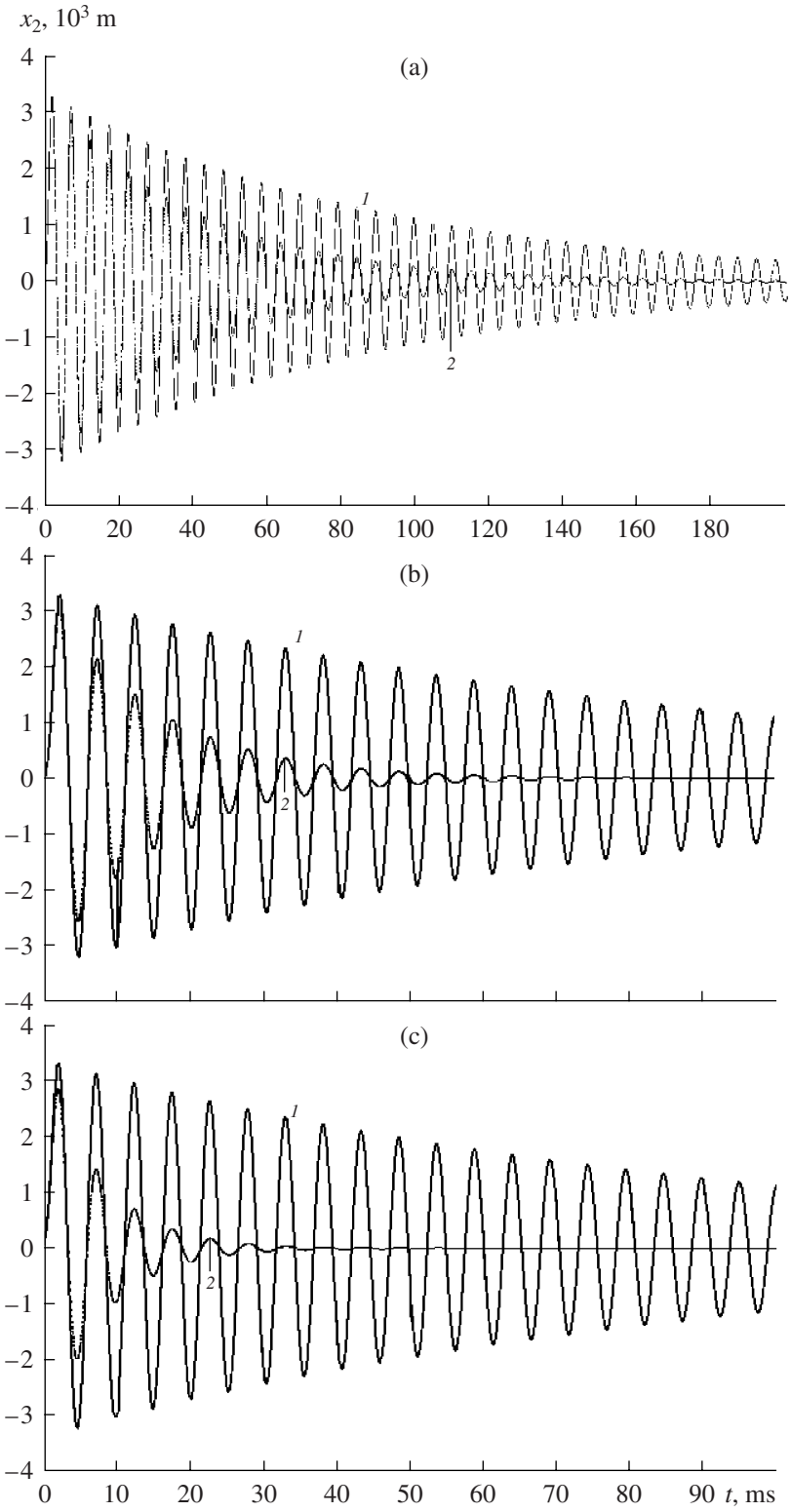

Fig. 3. The waveguide travel in the melt of aluminum at $k_1 = k_2$ and the different diameter values of the circular nozzle d_n, mm: a—30; b—50; c—70. *1*—without the nozzle; *2*—with the nozzle.

increase, the amplitude drop becomes more evident. Thus, for the aluminum melt at the waveguide vibrations without a nozzle, the amplitude drops up to 1 mm in about 110 ms (Fig. 3); for the iron melt, this amplitude value is observed in 38 ms (Fig. 4); and, for the lead, correspondingly, in 35 ms (Fig. 5).

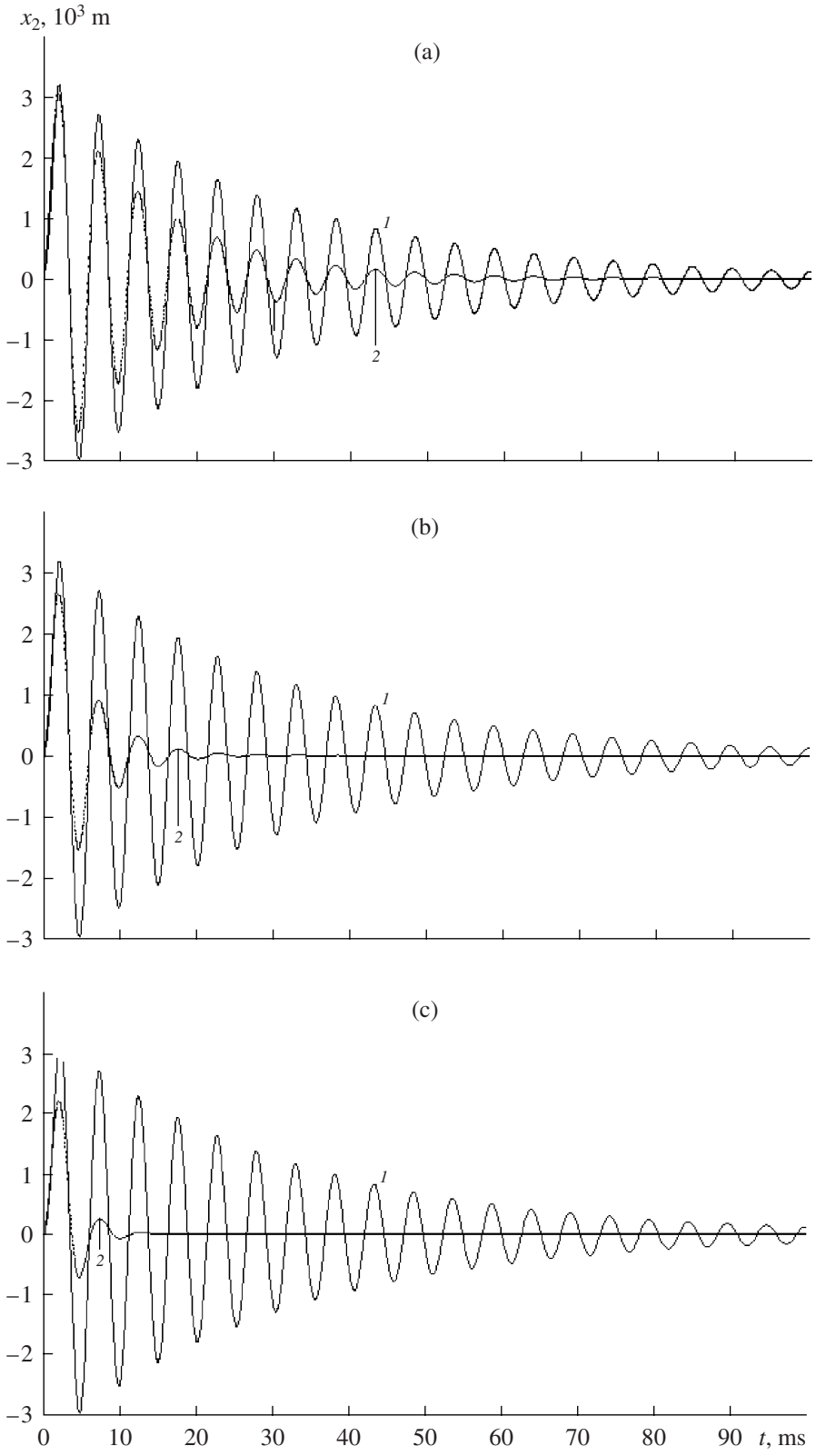

Fig. 4. The waveguide travel in the iron melt at $k_1 = k_2$ and different diameter values of the circular nozzle d_n, mm: a—30; b—50; c—70. *1*—without the nozzle; *2*—with the nozzle.

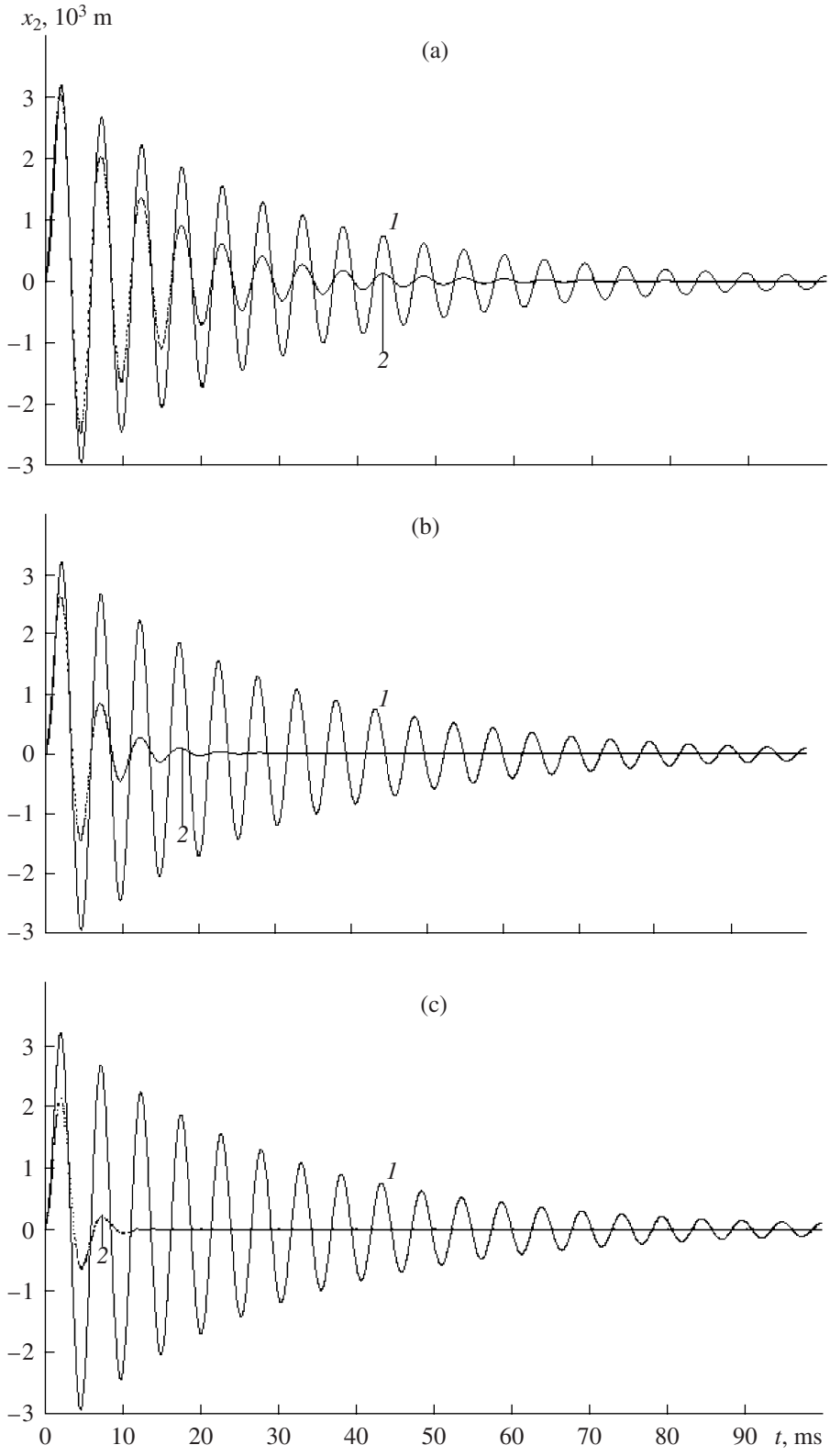

Fig. 5. The waveguide travel in the lead melt at $k = k_2$ and different diameter values of the circular nozzle d_n, mm: a—30; b—50; c—70. *1*—without the nozzle; *2*—with the nozzle.

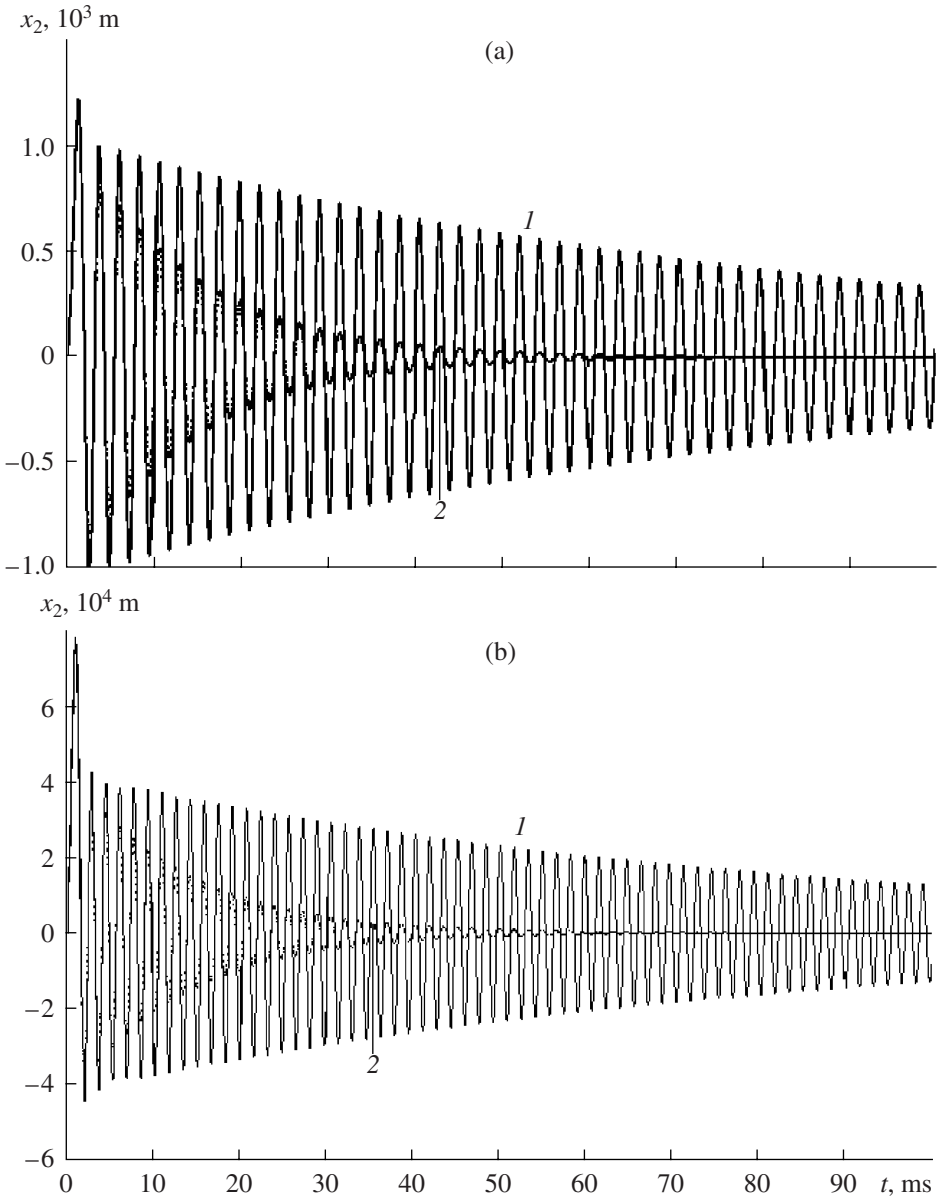

Fig. 6. The waveguide travel in the aluminum melt with the diameter d_n = 50 mm of the circular nozzle and different values of k_1/k_2: a—0.5; b—1. *1*—without the nozzle; *2*—with the nozzle.

The influence of the rigidity of the EDGRV flexible elements is shown in Fig. 6. The nearer the rigidity value of the flexible elements is to the membrane rigidity value, the greater the waveguide vibration frequency becomes, but the amplitude value considerably decreases in this situation. It should be noted that the first amplitude maximum significantly exceeds the subsequent values at $k_1 = k_2$.

The travel of the waveguide end within the period of the loading action, which was 1.63 ms, is depicted in Fig. 7. In the time interval corresponding to half the period of the loading, there are high frequency components during the major part of the travel. Moreover, the waveguides without a nozzle display this characteristic to a greater extent. The rigidity of the resilient elements also influences the process of the vibratory motion. The higher its value is, the more significantly the period of the waveguide travel approaches the period of the loading action at this stage (Fig. 7, c).

In the technical appendices, one of the main technological parameters of EHPP is the frequency of the pulse sequence in the range of 0.5 to 20 Hz. As has been shown in the present work, the duration of the loading processes lies within the millisecond range; therefore, by adjusting the rigidity of the resilient elements and the damper (nozzle) dimensions, one can provide the loading conditions with or without a pause. In the first case, we shall obtain more active metal degassing, since the gas bubbles will have time to leave the processing

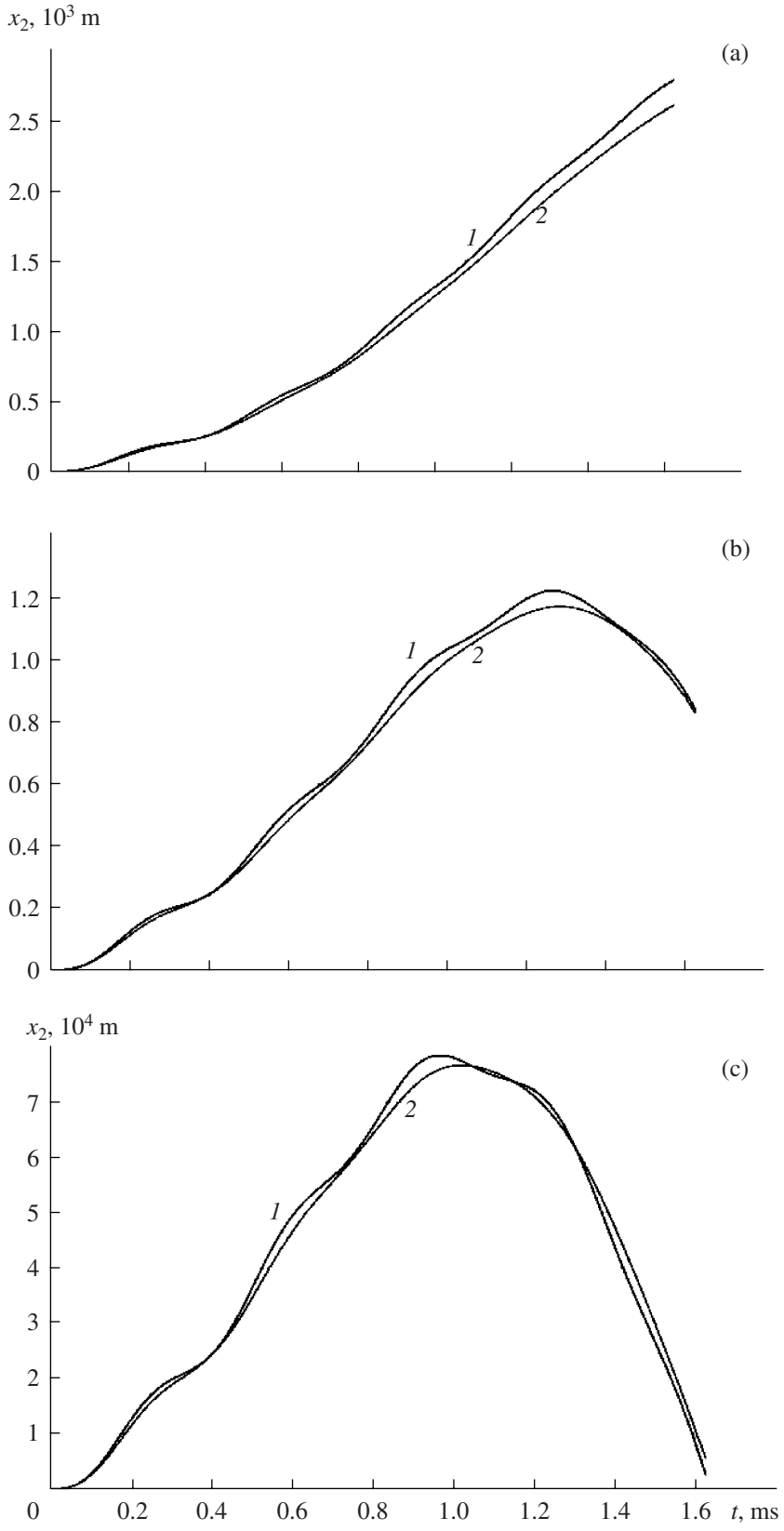

Fig. 7. The waveguide travel in the aluminum melt during the loading action with the diameter d_n = 50 mm of the circular nozzle and different values of k_1/k_2: a—0.1; b—0.5; c—1. *1*—without the nozzle; *2*—with the nozzle.

The values of the absorption coefficient ψ at EHPP of the melts

The melt Al		The melt Fe		The melt Pb	
The waveguide without a nozzle	The waveguide with a nozzle, d_n = 30 mm	The waveguide without a nozzle	The waveguide with a nozzle, d_n = 30 mm	The waveguide without a nozzle	The waveguide with a nozzle, d_n = 30 mm
0.112	0.268	0.325	0.75	0.355	0.81

area [10]. In the second case, there is provided more intensive melt agitation and a change of its structure.

As a characteristic of the dissipative properties of the vibration system, there is used the logarithmic decrement of the vibrations, which equals the Naperian logarithm of the relation of two successive peak shift magnitudes separated in time by one period. On the other hand, the relation of the dissipated energy (during one cycle) to the mean cycle energy also characterizes the agility of the vibration process damping, which actually is a coefficient of the absorption ψ, and, at a moderate damping, it is two times more than the logarithmic decrement [11]. Let us estimate the magnitudes of ψ for the given melts assuming that the vibration damping of the waveguide without a nozzle and with a circular nozzle at d_n equal to 30 mm is moderate (Figs. 3; 4; and 5, a), i.e., ψ = const for the entire process of the motion. The obtained results are presented in the table.

Using the waveguide with a circular nozzle with a diameter of d_n = 30 mm, the ψ magnitude increases by about 2.3 times in comparison with the waveguide without a nozzle for all the given melts. With the d_n increase, the waveguide vibrations are damped more intensively (Figs. 3; 4; and 5 b, c) and the ψ will change in accordance with another law and will increase significantly. The share of the dissipative energy is defined also by the melt physical properties. Thus, for the iron and lead melts, the magnitude of the ψ is approximately 3 times more than that for the aluminum melt, both in the case of the waveguide with a nozzle and without one (see the table).

The analysis of the obtained results show that the utilization of the waveguide nozzles at the EHPP of the melt promotes fast vibration damping, i.e., considerable dissipation of the consumed energy with respect to the processed metal properties.

At any kind of the loading, the consumed energy can be presented as a sum of two components; i.e., the energy E_0 transferred to the melt through the operation element of the EDGRV passes into a certain energy E_n and a dissipation energy E_{dis}:

$$E_0 = E_n + E_{dis}.$$

The E_n energy is spent for the generation of a nonstationary field of pressures, ultrasonic cavitation, the development of the local acoustic flows and streams, etc., that provide the degassing, refining of harmful impurities, homogenization of the melt, and activation of the potential centers of nucleation.

The influence of the dissipation energy on the metal structure is ambiguous and is determined by the processing method. It should be noted that, until recently, researchers neglected the contribution of the E_{dis} share to the formation of the new structure of the processed object. Moreover, as the latest investigations in the field of synergy show [12 and 13], the role of the energy dissipated in a material can be determining in the structure formation of a new quality.

CONCLUSIONS

1. The EHPP of a melt by EDGRV on the resilient elements with the application of the waveguide nozzles increases the share of the energy being dissipated, which, in turn, along with the E_n energy causing the internal structure-kinetic changes, will influence the processes of self-organization in the melt and formation of a qualitatively new structure.

2. The absorption coefficient ψ of the Fe and Pb melts at EHPP by the waveguides, both with a nozzle and without one, exceeds the ψ value of the Al melt by around 3 times; i.e., the dissipated energy share significantly depends on the processed metal's properties.

3. By adjusting the value of the rigidity ratio of the resilient elements of the EDGRV and the membrane, it is possible (at high rates of the hydroflows in the melt) to attain a considerable share of the dissipated energy, which is comparable with the E_n value.

4. The optimal selection of the resilient elements' rigidity and the geometrical dimensions of the waveguide nozzles allows one to provide more active degassing, intense agitation, and changing of the melt structure.

REFERENCES

1. Tsurkin, V. N. and Mel'nik, A. V., Investigation of the Amplitude of the Transmitting Element Drift of the Electric Discharge Generator of the Resilient Vibrations, *Elektron. Obrab. Mater.*, 2003, no. 6 (224), pp. 63–69.
2. Tsurkin, V. N. and Mel'nik, A. V., The Influence of the Geometric Characteristics of the Electric Discharge Generator of the Resilient Vibrations on the Operation Element Drift at the Afterdischarge Stage, *Elektron. Obrab. Mater.*, 2006, no. 1, pp. 63–69 (*Surf. Eng. Appl. Electrochem.* (Engl. Transl.), 2006, no. 1).
3. Tsurkin, V. N., Grabovyi, V. M. and Sinchuk, A. V., The Functional Possibilities of the Electrohydropulse Processing of the Melt in a Ladle, *Elektron. Obrab. Mater.*,

2006, no. 5, pp. 55–61 (*Surf. Eng. Appl. Electrochem.* (Engl. Transl.), 2006, no. 5).

4. Grabovyi, V. M., Sinchuk, A. V. and Tsurkin, V. N., The Mechanism of the Influence of the Electrohydropulse Processing on the Melt State Prior to the Ladling and on the High-carbon Alloys Crystallization, *Teoriya i Praktika Metallurgii*, 2000, no. 6 (20), pp. 28–31.
5. Gulyi, G. A., *Nauchnye Osnovy Razryadno-Impul'snykh Tekhnologii* (Scientific Bases of the Discharge – Pulse Technologies), Kiev: Naukova Dumka, 1990.
6. Galiev, Sh. U., Barbashova, G. A., Bilyanskii, Yu. S., Zhirnov, M. V. and Kosenkov, V. M., The Interaction of the Electric Discharge Generator of Vibrations with the Liquid Metal in a Ladle, *Problemy Prochnosti*, 1991, no. 11, pp. 78–82.
7. Tsurkin, V. N., Mel'nik, A. V. and Gabovyi, V. M., The Analysis of Spectral Characteristics of the Electric Discharge Generator, *Zb. Nauk. Prats' NUK*, 2005, no. 2 (401), pp. 106–112.
8. Pozdeev, V. A., Tsarenko, P. I., Butakov, B. I. and Malyushevskii, P. P., *Elektrorazryadnye generatory uprugikh kolebanii* (Electric Discharge Generators of Resilient Vibrations), Kiev: Naukova dumka, 1985.
9. Litvinenko, V. P., Shamko, V. V. and Derevyanko, Yu. I., *Vliyanie zhestkoi obolochki na dinamiku parogazovoi polosti. Osnovnye problemy razryadnoimpulsnoi tekhnologii* (The Influence of a Rigid Shell on the Vapor-Gas Cavity Dynamics. The Main Problems of the Discharge-Pulse Technology), Kiev: Naukova dumka, 1980, pp. 50–61.
10. Tsurkin, V. N. and Mel'nik, A. V., Estimation of the Rational Time of the Dead Pre-Cast Melt, *Zb. Nauk. Prats' NUK*, 2006, no, 6 (411), pp. 75–81.
11. Panovko, Ya. G., *Osnovy prikladnoi teorii kolebanii i udara* (The Basis of the Application Theory of Vibration and Shock), L. : Mashinostroenie, 1976.
12. Semenov, B. I. and Ivanova, V. S., Conception and Means of Monitoring the Formation of the Cast Crystal Structure in New Methods of Casting, *Liteinoe proizvodstvo*, 2001, no. 5, pp. 20–25.
13. Ivanova, V. S., Balankin, A. S., Bunin, I. Zh. and Oksogoev, A. A., *Sinergetika i fraktaly v materialovedenii* (Synergy and Fractals in Physical Metallurgy), Moscow: Nauka, 1994.

ISSN 1068-3755, Surface Engineering and Applied Electrochemistry, 2008, Vol. 44, No. 4, pp. 330–334. © Allerton Press, Inc., 2008.
Original Russian Text © V.D. Polovinko, E.S. Yurchenko, 2008, published in Elektronnaya Obrabotka Materialov, 2008, No. 4, pp. 93–97.

OPERATING EXPERIENCE

Solid-State Welding of Metals with Application of High Density Current Pulses

V. D. Polovinko and E. S. Yurchenko

Institute of Pulse Processes and Technologies, National Academy of Sciences of Ukraine, pr. Oktyabr'skii 43-a, Nikolaev, 54018 Ukraine

E-mail: iipt@iipt.com.ua

Received February 6, 2008

Abstract—The results of solid-state welding of homogeneous and heterogeneous metals with application of high density current pulses are presented. A chart of the current treatment allowing obtaining of the welded joint at its heating in an air atmosphere is proposed. The influence of alternating and unipolar current on the deformation of contact surface microroughnesses in the welding zone is considered. The basic parameters of the pulse current and the specific energy of the treatment of steel and copper samples that ensure obtaining of the welded joint are determined.

DOI: 10.3103/S1068375508040145

The studies carried out in the field of diffusion welding of ferrites with metals with application of conductor electric explosion [1] and discharge-pulse welding of ceramic materials [2, 3] have shown the high efficiency of application of pulse methods for treatment of welding surfaces.

A similar method of treatment of welding surfaces with application of the electroplastic effect (EPE) in metals [4, 5] is proposed in paper [6]. Preliminary treatment of compressed welding surfaces by means of passing of high density current pulses through them appeared to allow heating and isothermal holding of steel pieces in an air atmosphere.

The given paper presents the results of experimental studies of the influence of the basic parameters and the form of the high density current pulses on the quality of welding of planar samples of homogeneous and heterogeneous metals in the course of their heat treatment in air.

The studies were carried out by means of a laboratory installation (Fig. 1) that was a surge–current generator (SCG) with the charge voltage U = (20–40) kV and the capacitor capacitance C = (2–32) μF, which allowed the required form, amplitude, and duration of the current pulse on studied sample *5*.

The discharge circuit of the SCG was assembled circuitwise with time-controlled short-circuiting of the load [7]; this makes it possible to let the required amount of discharge current half-wave pass in load and to control the time of the current. The discharge circuit electric parameters were registered by virtue of high-ohmic divider *2* and current sensor *3*, with application of a double-beam memory oscillograph S9–6.

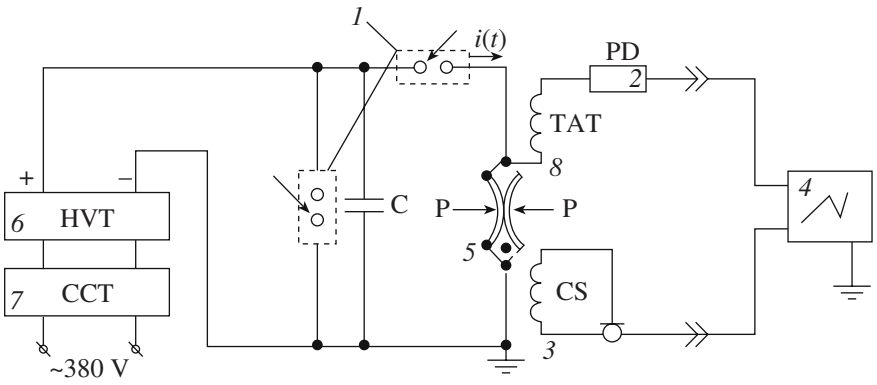

Fig. 1. Diagram of the laboratory installation: (*1*) controlled air gap; (*2*) potential divider; (*3*) current sensor; (*4*) double-beam memory oscillograph; (*5*) welding pieces; (*6*) high-voltage transformer; (*7*) current controller–transformer; (*8*) toroidal air transformer.

The influence of two forms of current pulses—unipolar and alternating with the oscillation frequency f = 10 kHz (Fig. 2)—on the microroughness deformation value was determined by the final value of the gap between the welding surfaces.

The criterion of the required value of the electric current treatment was the approach of the contacting surfaces until the gap was h = (1–0.5) μm. As was shown in earlier studies [8], this gap ensures the obtaining of a welded joint of axisymmetric pieces at their heating in an air atmosphere.

The amplitude current density j_m varied from 0.8×10^9 to 1.6×10^9 A/m^2, the pulse duration τ fluctuated from 50×10^{-6} to 500×10^{-6} s, and the pulse number n ranged within 5 and 40; this made it possible to vary the specific energy of the metal treatment in the welding zone q_{sp} from 0.3 to 1.5 J/mm^3. The pulse repetition frequency was 0.2 Hz in all the cases.

The experiments were carried out for planar steel (St 3) and copper (M-3M) samples with the dimensions $170 \times 15 \times 3.0$ mm. The preparation of the welding surfaces consisted of treatment by sand paper of M 280 grit, which allows the height of the microroughnesses to be not more than 6 μm, and fat removal with industrial white spirit. The samples were pressed together in a device until a contact pressure in the welding zone of 40 MPa (Fig. 3); then, each plate in turn was treated with a series of high density current pulses. The treated samples, together with the device, were heated in an electric furnace in an air medium up to a temperature of 810°C with holding for 10 min. The samples were cooled with the furnace to a temperature of 200°C.

The heat deformation cycle of the welding was constant in all the cases; this allowed determining the influence of the high density current pulse on the value of the total microroughness deformation according to the final value of the gap between the welding surfaces. The gap was determined by the results of metallographical tests. Microsections were prepared of the middle part of the welding zone, and they were studied at 250-fold magnification by means of an optical microscope (Neofot-32). The gap value was measured at 20 points along the welding zone length.

As a result, it was found that, at the current density $j_m \geq 1.2 \times 10^9$ A/m^2 and at the pulse duration $\tau_u \geq 200 \times 10^{-6}$ s, significant collapsing of the microroughnesses of the contacting surfaces takes place; for decreasing of the gap h from 6.0 to 0.5–1.0 μm, the minimum specific electric energy of the metal treatment is at least q_{st} = 0.8 J/mm^3 for the steel samples and q_{Cu} = 0.65 J/mm^3 for the copper ones. Herein, the value of this energy of the treatment of both the steel and copper does not depend on form of the current pulse (unipolar or alternating). This allowed presenting the obtained results in the form of a dependence that made it possible to determine the number of pulses in a series required for collapsing of the microroughnesses on the contact surface:

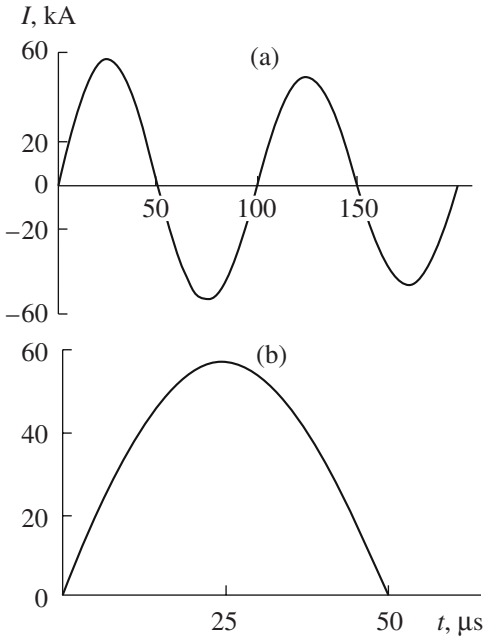

Fig. 2. Form of the current pulse applied in the experiments: (a) alternating; (b) unipolar.

$$n = \frac{q \cdot V_{wz}}{W_u}; \quad (1)$$

where q is the specific electric energy of the metal treatment ensuring collapsing of the microroughnesses, J/mm^3; V_{wz} is the volume of the welding zone of one piece, mm^3; and W_u is the electric energy of the unit pulse in the welding zone, J.

The energy of the unit pulse W_u is determined by the dependence

$$W_u = \frac{1}{2} J_0^2 \cdot R_{wz} \cdot \tau_u, \quad (2)$$

where R_{wz} is the electric resistance of the sample along the welding zone length, Ohm; and J_0 is the current pulse amplitude, A.

The specific energy of the metal treatment was defined as a ratio of the total heat energy released in the welding zone at passing of a series of current pulses to the volume of the welding zone of one piece (Fig. 3).

Taking into account the obtained dependences, planar steel and copper samples were welded. The geometrical characteristics of the samples and the preparation of the welding surfaces were similar to those of the previous experiments. For the selected values of the density j_m and the current pulse duration τ_u, according to formula (2), the unit pulse energy was calculated for determination of the generator parameters allowing this mode. Then, according to formula (1), the current pulse number was found, and the pieces were treated in turn. Afterwards, the samples were heated at a temperature

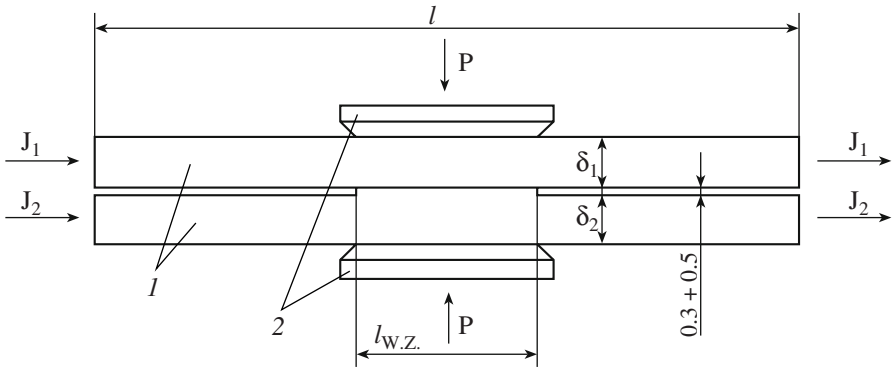

Fig. 3. Diagram of pulse current treatment of welding pieces: (*1*) samples; (*2*) device clamp; $l_{W.Z.}$ is the welding zone length; l is the sample length; and δ_1 and δ_2 are the sample thickness.

of 850°C for 15 min. The samples were cooled with the furnace to a temperature of 200°C.

The quality of the welding was estimated by the results of tensile mechanical tests of the samples, according to the technique proposed in paper [9], and by the results of metallographical tests.

The analysis of the influence of the pulse current treatment modes on the results of the mechanical tests of the samples (see the table) has shown that, under the conditions (the amplitude current density $j_m \geq 1.2 \times 10^9$ A/m^2, the pulse duration $\tau_u \geq 200 \times 10^{-6}$ s, and the specific energy of the metal treatment $q_{st} = 0.8$ J/mm^3 for the steel and $q_{Cu} = 0.65$ J/mm^3 for the copper), this method allows qualitative welding at different forms of current pulse for both homogeneous (tests 1, 6, 7) and heterogeneous metals (tests 5, 8).

In tests 2, 3, and 4, the values of the duration, the amplitude of the current pulse, and the specific energy of the treatment were lower than the calculated ones; this decreased the quality of the welding, and destruction occurred along the contact zone.

However, also in this case, tack welds are situated over the whole contact zone, and oxidized surfaces are absent on the steel plate; that is, sealing of the welding zone was achieved, but, apparently, the energy was not sufficient for activation of diffusion processes on the contact surface. The dimensions of the welding zone

Results of mechanical tests of welded joints

No.	Sample material	Current density $j_m \times 10^{-9}$, A/m^2	Pulse duration $\tau \times 10^6$, s	Current pulse form	Tensile mechanical tests	Specific energy of treatment q, J/mm^3	Treatment pulse number n
1	St3	1.2	200	Unipolar	with respect to the parent metal	0.8	25
	St3	1.2	200	″		0.8	25
2	St3	1.2	100	″	with respect to the compound	0.8	50
	St3	1.2	100	″		0.8	50
3	St3	1.0	200	″	with respect to the compound	0.8	36
	St3	1.0	200	″		0.8	36
4	St3	1.2	200	″	with respect to the compound	0.55	17
	St3	1.2	200	″		0.55	17
5	St3	1.2	200	″	with respect to the parent metal	0.8	25
	copper	1.2	200	″		0.65	60
6	St3	1.2	200	Alternating	with respect to the parent metal	0.8	25
	St3	1.2	200	″		0.8	25
7	copper	1.2	350	″	with respect to the parent metal	0.65	34
	copper	1.2	350	″		0.65	34
8	St3	1.2	350	″	with respect to the copper sample	0.8	15
	copper	1.2	350	″		0.65	34

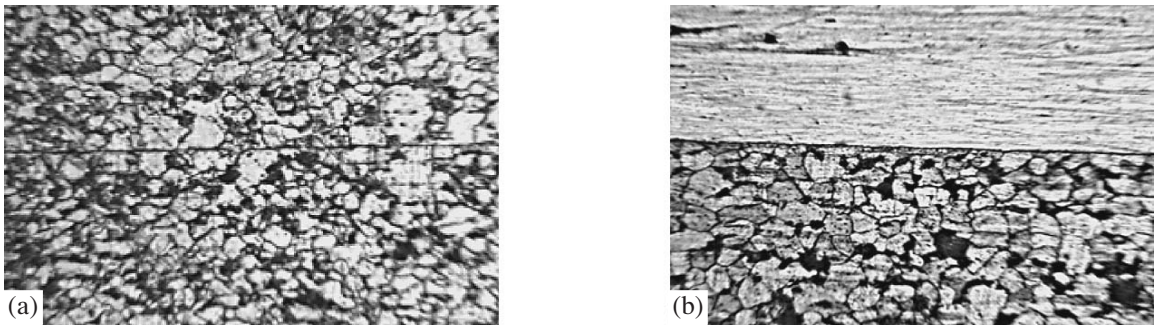

Fig. 4. Microstructure of the welding zone (×250): (a) steel–steel; (b) steel–copper.

corresponded to the surface area of the contact pressures produced by the device.

In addition, we should note the results of welding of the steel and copper (tests 5, 8), which have shown that strength joints with breaking on the copper plate (σ_b = 160–170 MPa) are obtained in the mode of T = 850°C and t = 15 min. In the case of diffusion welding of steel and copper in vacuum [10], the optimum treatment mode is T = 900–950°C, t = 20 min, and B = (10^{-3}–10^{-4}) mm Hg. This apparently shows that treatment by high density current pulses makes it possible not only to approach surfaces in the welding zone at the preliminary stage but also to significantly influence the diffusion processes at heat treatment.

The steel sample welding zone (Fig. 4a) is characterized by formation of common grains, and the contact zone is a broken line with a width of not more than 0.4 μm. In the zone of welding of the steel and copper (Fig. 4b), an unbroken contact line is observed; it has a width close to the grain boundary width in the steel. Intermetallic interlayers are absent; that is, diffusing elements merge into the base metal lattice, thus forming solid solutions.

Discussing the results obtained in the present work, the following should be mentioned. In addition to protection of the welding zone from oxidation by ambient air, the approach of the surfaces up to a gap of 0.5–1.0 μm leads to the fact that the air located between the microroughnesses is expulsed outside, and, by the end of treatment, the air volume in the welding zone significantly decreases in comparison with the initial volume. These conditions in the process of heat treatment result in automatic evacuation of the contact surface [11], since the remaining insignificant amount of air diffuses into the metal, and new portions of air do not come into the welding zone due to the small gaps between the contact surfaces. There occur cleaning of the welding surface from fatty and oxide films and further collapsing of microroughnesses due to an increase in the thermal plasticity of the materials; this leads to approaching of the surfaces up to the level of interatomic interaction of the metals, to activation of interdiffusion, and to formation of a joint with the predominance of metallic bonding.

In addition, the diffusion processes in the welding zone must intensify due to an increase in the emergence of mobile dislocations on the contact surface, which allow formation of additional activation centers. At the current densities causing the EPE, there occurs approximately a tenfold increase in the density of the mobile dislocations tending to leave the metal with the current [4]. Thus, treatment by current pulses gives the possibility to obtain additional activation centers on both welding surfaces.

The conditions of current treatment of welding pieces determined in the present paper are the lower boundary of the parameters (both in the amplitude current density and the pulse duration and in the specific energy of the metal treatment), which ensure formation of a welded joint.

In terms of electroinduced plastic deformation, on the contact surface, the obtained values of the specific electric energy of the treatment for steel (0.8 J/mm^3) and copper (0.65 J/mm^3) correspond to the lower boundary of the specific electric energy range q = (0.5–4.0) J/mm^3, wherein the EPE is shown in metals [4, 5]. Herein, the metal plasticity increases in the whole energy range for carbon steels, copper, and titanium and aluminum alloys.

Thus, the studied approach and method of diffusion welding of metals in air are promising in terms of both the enhancement of the processing capabilities and additional activation of diffusion processes in the welding zone.

CONCLUSIONS

1. Treatment of welding pieces with high density current pulses causes electroinduced plastic deformation of microroughnesses and leads to a significant decrease in the gap (up to 0.5–1.0 μm) between the contacting surfaces; this allows further treatment of the joint in air.

2. Qualitative welding of samples of homogeneous (steel–steel, copper–copper) and heterogeneous (cop-

per–steel) metals is ensured at treatment of samples by a series of current pulses with the amplitude current density $j_m \geq 1.2 \times 10^9$ A/m^2 and the pulse duration $\tau_u \geq 200 \times 10^{-6}$ s. Herein, the minimum specific energy of the metal treatment in the welding zone is q_{st} = 0.8 J/mm^3 for the steel samples and q_{Cu} = 0.65 J/mm^3 for the copper ones.

3. The conditions of pulse current treatment of pieces determined in the present paper with respect to the value of the specific energy of the metal treatment correspond to the lower boundary of the specific energy range in which EPE is shown in metals.

REFERENCES

1. Konyushkov, G.V., Zhevalev, O.Yu., Koblov, A.I., and Kotina, N.M., Possibilities of Diffusion Welding for Obtaining of Ferrite Compounds with Metals., *Avtom. Svarka*, 1991, no. 5, pp. 54–55.
2. Yushchenko, K.A., Nesmikh, V.S., Dubovetskii, I.V., and Kutsenko, I.V., Ceramics Welding by the Method of Conductor Electric Explosion, *Avtom. Svarka*, 1990, no. 3, pp. 32–36.
3. Shevchuk, T.V., Dubovetskii, I.V., Nesmikh, V.S. et al., Influence of Intermediate Interlayer Composition on Structure and Properties of Nitride Ceramics at Discharge–Pulse Welding, *Avtom. Svarka*, 1991, no. 5, pp. 66–69.
4. Spitsin, V.I. and Troitskii, O.A., *Elektroplasticheskaya deformatsiya metallov* (Electroplastic Deformation of Metals), Moscow: Nauka, 1985.
5. Beklemeshev, N.N., Baranov, Yu.V., Doronin, Yu. L. et al., Influence of Pulse Electric Current on Characteristics of Structural Strength of Metallic Materials, *Fiz. Khim. Obrab. Mater.*, 1990, no. 4, pp. 108–112.
6. Polovinko, V.D. and Yurchenko, E.S., Study of Influence of High Density Current Pulses on Diffusion Welding of Metals, Abstracts of Papers, *VI Mezhdunarodnaya shkola–seminar "Impul'snye protsessy v mekhanike sploshnykh sred"* (VI Int. School–Seminar "Pulse Processes in Mechanics of Continua"), Nikolaev: Inst. Pulse Processes Technol., Nation. Akad. Nauk Ukrainy, 2005, pp. 39–41.
7. Dashchuk, P.N., Zaients, S.L., and Komel'kov, V.S., *Tekhnika bol'shikh impul'snykh tokov i magnitnykh polei* (Technique of High Pulse Currents and Magnetic Fields), Moscow: Atomizdat, 1970, p. 472.
8. Demidenko, L.Yu., Onatskaya, N.A., and Yurchenko, E.S., Press–Thermal Electrohydropulse Pipe Coupling with Tube Sheets of Heavily Alloyed Steels, *Avtom. Svarka*, 2003, no. 5, pp. 53–54.
9. Samsonova, T.S., Ternovskii, A.P., and Karakozov, E.S., Peculiarities of Diffusion Welding of Alloys with Precipitation Strengthening, *Avtom. Svarka*, 1990, no. 11, pp. 19–20.
10. Kazakov, N.F., *Diffuzionnaya svarka materialov* (Diffusion Welding of Materials), Moscow: Mashinostroenie, 1976.
11. Ryabtsev, I.A., Thermodynamic Analysis of the Processes Occurring in Gaps of Multilayered Leak–Free Packages at their Roll Welding, *Avtom. Svarka*, 1987, no. 1, pp. 28–32.

ISSN 1068-3755, Surface Engineering and Applied Electrochemistry, 2008, Vol. 44, No. 4, pp. 335–338. © Allerton Press, Inc., 2008.
© Published in Russian in Elektronnaya Obrabotka Materialov, 2008, No. 4, pp. 98–101.

OPERATING EXPERIENCE

Experimental and Theoretical Investigation of Stress Variation in $AlCu_4Mg_1$ Aluminum Alloy[1]

Alina-Adriana Minea

Gh. Asachi Technical University, Iasi, Romania
Bul. D. Manjeron, Iasi, Romania
E-mail: alina.minea@yahoo.com

Received January 18, 2008

Abstract—This paper presents the results of experimental and theoretical studies regarding the behavior of $AlCu_4Mg_1$ aluminum alloy after a heat treatment. The methodology has been proposed to study improvements in $AlCu_4Mg_1$ aluminum alloy in the process of heat treatment, which included the following steps: (1) adopting the heat treatment technology for the specified alloy, (2) choosing the necessary heat treatment installations to perform the heat treatment of the specified alloy, (3) choosing tools and machines used to study the mechanical characteristics, and (4) planning the experiment and analytical interpretation of the results. On the basis of these experiments and the obtained regression equation, we performed a theoretical study with the aim to determine the heating parameters for quenching and aging in order to obtain a specified stress needed for application of this alloy. We considered two cases for this theoretical study: (1) the stress and quenching temperatures were fixed and we determined the aging temperature; (2) the stress and aging temperatures were fixed and we determined the quenching temperature. Using the determined equations, we assumed the definite characteristics needed for the working part after treatment and calculated the parameters for quenching and artificial aging in the process of the heat treatment. Note that the calculated temperatures should be in the standard limits for the studied alloy. In conclusion, an algorithm was proposed for the process of the optimum heat treatment in order to obtain the necessary properties of the working parts.

DOI: 10.3103/S1068375508040157

INTRODUCTION

Heat treatment in its broad sense refers to any heating and cooling operations performed with the aim to change the mechanical properties, the metallurgical structure, or the residual stress state of a metal product. The general methods of heat treatment of aluminum alloys include the use of molten salt baths, air chamber furnaces, and induction heaters [1, 2]. Air furnaces are used on a wider scale because they permit greater flexibility in the range of operating temperatures. Air furnaces are also more cost effective in the case of small-scale production; it is far more expensive to maintain the temperature of a large volume of salt awaiting parts than to heat an equal volume of air. At the same time, induction methods can provide high heating rates, which affect the transformations. Good temperature control and uniformity throughout the furnace and load are required for all kinds of heat treatment. Materials subjected to heat treatment should always meet specific quality criteria, which include tensile properties and, for certain alloys, adequate durability. All the processing steps during the heat treatment should be carefully controlled to ensure high and reliable performance [3, 4].

A methodology has been proposed to study improvements in $AlCu_4Mg_1$ aluminum alloy in the process of heat treatment that included the following steps:

—adopting the heat treatment technology for the specified alloy;

—choosing the necessary heat treatment installations to perform the heat treatment of the specified alloy;

—choosing tools and machines used to study the mechanical characteristics;

—planning the experiment and analytical interpretation of the results.

The aim of this paper was to study the behavior of $AlCu_4Mg_1$ aluminum alloy at final heat treatment. In order to carry out this study, we performed the process optimization by variation of the heating temperatures within the standard limits. After we fulfilled the planned experiments, we determined the mechanical stress. For the experiments, we used a set of parts that included nine items and a test part. Every part had a specific final heat treatment technology that consisted of quenching and artificial aging by heat treatment within the standard limits. The test part was not subjected to the heat treatment, and its mechanical charac-

[1] The text was submitted by the author in English.

Table 1. Experimental results

Code no.	T_c, °C	T, °C	Stress, Rm
1.1.1.	485	185	276.36
1.1.2.	485	195	392.42
1.2.2.	485	205	331.17
2.2.1.	495	185	329.24
2.1.1.	495	195	436.32
2.2.2.	495	205	355.31
3.2.1.	505	185	367.85
3.1.2.	505	195	224.19
3.2.2.	505	205	316.42

Table 2. The experimental matrix for $k = 2$

Exp. no.	Quenching temp., T_c, °C	Variation, x_1	Aging temp., T, °C	Variation, x_2
1	485	–1	185	–1
2	485	–1	195	0
3	485	–1	205	+1
4	495	0	185	–1
5	495	0	195	0
6	495	0	205	+1
7	505	+1	185	–1
8	505	+1	195	0
9	505	+1	205	+1

teristics were determined in this condition. Every part was assigned a particular code during the experiment.

In order to apply the proposed technology, we used an electric furnace with forced air circulation and we performed the experiments under the same conditions of the furnace preheating. The process of optimization of the final heat treatment was envisaged to determine the minimum number of experiments needed for the correct process description. In this case, when the 3^k factorial experiment model was used, it was enough to perform 9 experiments ($k = 2$ for two variables: the artificial aging temperature and the quenching temperature). Therefore, for each process variable, a base level could be established and the variation area should be determined for a correct description of the heat treatment technology; the experimental results are summarized in Table 1.

1. EXPERIMENTAL

This paper presents the results of experimental and theoretical studies regarding the improvement of heating processes and determining a better heat treatment technology for aluminum alloys with low energy consumption. To perform the mechanical characterization of the studied set of parts and to exactly describe the behavior of each aluminum alloy part after the final heat treatment, experiments were carried out with the aim to do the following:

—determine the exact chemical composition of the used $AlCu_4Mg_1$ alloy in order to establish the proper heat treatment technology;

—study the mechanical parameters of each part from the studied set of parts in order to establish the proper technology for this alloy;

—establish the yield strength variation with the heating temperature;

—find the yield strength variation with the heat treatment technology.

The final heat treatment for this alloy included quenching and artificial aging in the process of heat treatment. The following parameters were used according the standards for aluminum alloys [1]:

—For quenching, the heating temperatures were 480–505°C for all the types of parts. The time of the exposure at the heating temperature depended on the type and dimensions of the working parts. The cooling was performed with a very high rate [6].

—For artificial aging, the standards for $AlCu_4Mg_1$ alloy recommend maintaining heating temperatures of 185–210°C for 6–15 hours [6]. At the end of the process, the variation of the yield strength was studied and the results were compared with the parameters of the test part.

The tridimensional variation of the hardness and stress depending on the heating temperatures was obtained using the results illustrated in Table 1, the 3^k factorial experiment model, and a specific computer program. Furthermore, the regression equation that describes the process was derived:

$$R = 286.88 + 71.927x_1 + 96.02x_2 + 6.71x_1x_2 - 10.693x_1^2 - 31.276x_2^2.$$

The experimental matrix for obtaining the regression dependence is presented in Table 2.

On the basis of these experiments and the obtained regression equation, we carried out a theoretical study with the aim to determine the heating parameters for quenching and aging in order to obtain a specified stress needed for the application of this alloy.

2. RESULTS AND DISCUSSION

For this theoretical study, we considered two cases [7, 8]: the stress and quenching temperature were fixed,

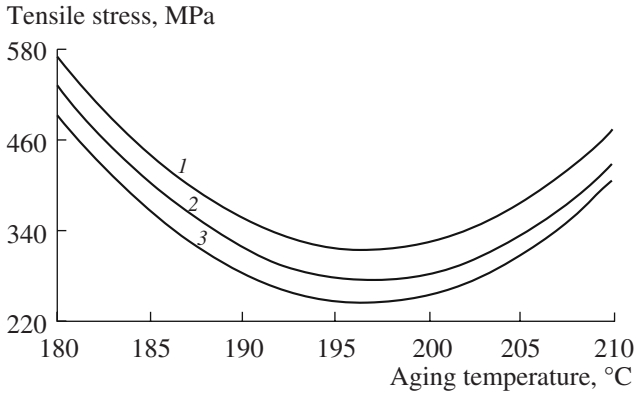

Fig. 1. Graphical determination of the aging temperature for $AlCu_4Mg_1$ alloy. *1*—T_c = 495°C; *2*—T_c = 505°C; *3*—T_c = 485°C.

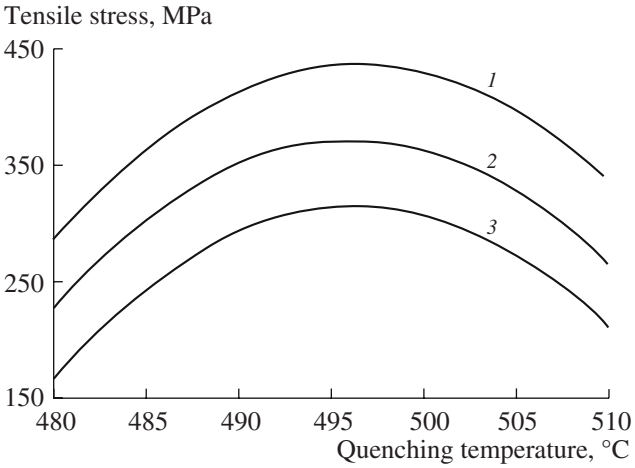

Fig. 2. Graphical determination of the quenching temperature for the $AlCu_4Mg_1$ alloy. *1*—T_c = 185°C; *2*—195°C; *3*—205°C.

and we determined the aging temperature; the stress and aging temperature were fixed, and we determined the quenching temperature.

Case 1. The quenching temperature T_c was known, and we obtained the variation of the aging temperature T with the stress R_m.

$$x_1 = -1, \quad T_c = 485°C; \quad T = 196.65 \pm \sqrt{-267 + 1.1R_m}.$$

This equation has a restriction: $R_m > 242.73$ Mpa.

$$x_1 = 0, \quad T_c = 495°C; \quad T = 196.79 \pm \sqrt{-345 + 1.1R_m}.$$

This equation has a restriction: $R_m > 313.89$ MPa.

$$x_1 = 1, \quad T_c = 505°C; \quad T = 196.93 \pm \sqrt{-299.9 + 1.1R_m}.$$

This equation has a restriction: $R_m > 272.704$ MPa.

The relations are shown graphically in Fig. 1 and demonstrate the variation of the tensile stress of the $AlCu_4Mg_1$ alloy vs. the aging temperature.

Case 2. The aging temperature T_t was known, and we obtained the variation of the quenching temperature T_c with the stress R_m.

$$x_2 = -1, \quad T = 185°C; \quad T_c = 496.59 \pm \sqrt{787 - 1.8R_m}.$$

This equation has a restriction: $R_m < 437.299$ MPa.

$$x_2 = 0, \quad T = 195°C; \quad T_c = 496.37 \pm \sqrt{566.3 - 1.8R_m}.$$

This equation has a restriction: $R_m < 314.657$ MPa.

$$x_2 = 1, \quad T = 205°C; \quad T_c = 496.15 \pm \sqrt{699.7 - 1.8R_m}.$$

This equation has a restriction: $R_m < 372.069$ MPa.

The relations are shown graphically in Fig. 2 and demonstrate the variation of the tensile stress of the $AlCu_4Mg_1$ alloy with the quenching temperature.

CONCLUSIONS

This paper describes how the tensile strength varies with the aging and quenching temperatures. Also, we obtained the equations for theoretical determination of some properties under the standard or special conditions of heat treatment. Using the determined equations, we assumed some characteristics that the final working parts should possess and calculated the parameters of the quenching and the artificial aging by the heat treatment. Also, under some given conditions of the final heat treatment, it was possible to predict the mechanical characteristics of the treated parts; namely, their mechanical stress and hardness. This is a very important problem, because, in practice, it is absolutely necessary to predict the behavior of working parts that can influence the reliability of a machine or a mechanism.

We should mention that the calculated temperatures must be between the standard limits for the studied alloy. In the case when the calculated temperature is not within the standard limits, we cannot impose some characteristics and must use the functions of only one variable. The chosen research methodology allowed us to perform experiments that revealed the following improvements in the final heat treatment technology of the $AlCu_4Mg_1$ aluminum alloy:

—the correct calculation of the parameters of the final heat treatment technology for the studied alloy;

—the selection of an up-to-date furnace and an air chamber furnace with controlled heating;

—the use of up-to-date equipment for testing the final heat treated parts, particularly their yield strength; and

—correctly planned experiments and interpretations.

In conclusion, the paper presents an algorithm for applying the proper heat treatment technology in order to obtain the necessary properties for working parts.

REFERENCES

1. ASTM Handbook: Alloy and Temper Designation Systems for Aluminum, 2004.
2. Banno, T., Heat Treatment Technology—Present Status and Challenges, *Heat Treat. Met.*, 1994.
3. Sheppard, T., *Mater. Sci. Technol.*, 1988, vol. 4, p. 636.
4. Manzini, S.G., Influence of Deformation Before Artificial Aging on Properties of Al–Cu–Mg Aluminum Alloy, *Scripta, Met. Et Materialia*, 1994, vol. 31, pp. 1127–1130.
5. Abis, S., Massazza, M., Mengucci, P., and Riontino, G., Early Ageing Mechanisms in a High-Copper AlCuMg Alloy, *Scripta Materialia*, 2001, vol. 45, pp. 685–691.
6. ASTM Standards for Aluminum and Magnesium Alloys, 2 February, 2005.
7. Taloi, D. and Florian, E., Optimizarea Proceselor Metalurgice, Bucuresti: Tehnica, 1998.
8. Minea, A.A., Minea, O., and Dumitrash, P., Properties of $AlCu_2Mg_{1.5}Ni$ Behavior at Heat Treatment, *Elektron. Obrab. Mater.*, 2003, no. 6, pp. 82–84.

ISSN 1068-3755, Surface Engineering and Applied Electrochemistry, 2008, Vol. 44, No. 4, pp. 339–340. © Allerton Press, Inc., 2008.
Original Russian Text © A.A. Nasirov, 2008, published in Elektronnaya Obrabotka Materialov, 2008, No. 4, pp. 102–104.

OPERATING EXPERIENCE

Surface State Density at the Semiconductor–Glass Interface

A. A. Nasirov

Ulugbek National University, Vuzgorodok, Tashkent, 100174 Republic Uzbekistan
E-mail: aanasirov1962@mail.ru

Received February 14, 2008

Abstract—An investigative technique for the determination of the surface state density (SSD) at the semiconductor–lead-borosilicate-glass interface is proposed. It is shown that this technique involving differentiation of the *C–V* dependence is a more precise and less labor-consuming method, which shows the uniqueness of the solution.

DOI: 10.3103/S1068375508040169

Silicon-based metal–insulator–semiconductor (MIS) structures have gained wide-spread acceptance in recent semiconductor devices and integrated circuits (ICs). Upgrading of the functional complexity of microcircuits and the growth in the packing density of discreet structural elements represent a tendency towards the following advancement of microelectronics. The stable and reliable operation of these devices and ICs is controlled not only by the potentialities of the technology but is primarily defined by the physical processes occurring within near-surface layers of a semiconductor and at interfaces of different materials comprising MIS structures. The energy distribution of the SSD over the energy-gap band of a semiconductor is a fundamental supervised parameter in these structures [1].

To find the energy distribution of the SSD (N_{ss}) over the energy-gap band in a semiconductor, the method of determination of the high-frequency capacity–voltage (*C–V*) characteristics is most commonly used [2–5]. This method is built upon a comparison between the theoretic *C–V* characteristic of an ideal (that is, free of surface states) MIS structure and the experimental characteristic of an actual structure and upon the subsequent differentiation of the result of the comparison [2]. This method ensures the reasonable precision of data on the total SSD, but introduces an essential error into the distribution of the function dN_{ss}/dE over the energy gap width in a semiconductor; this error is conditioned by the operation of the graphical (or numerical) differentiation of the difference of two closely related *C–V* dependences [2]. The method of determination of the distribution $N_{ss}/d\psi_s$, where ψ_s is the surface potential, is outlined in [6]; this method is free of the graphical differentiation of the dependence $dN_{ss}(E)$, where E is the energy gap width in a semiconductor. The essential disadvantage of the method [6] is the complexity of the mathematical relationships; the reason is that the theory [7] of a surface charge is used and the relationships $R(y_s)$ and $\Phi(y_s)$ should be previously plotted [6].

In this paper, a method of determination of the SSD distribution over the energy gap width in a semiconductor is offered; this method is free of the pointed disadvantages.

To obtain the mathematical relationships, we will take expression (2) from [4]; the expression for the ideal MIS structure describes the voltage drop as a function of the dimensionless surface potential *y*. We will find the total voltage drop at an actual MIS structure; in this case, the voltage drop ΔV at the surface states N_{ss} shall be added to the discussed expression. Differentiating this equation with respect to *y* and taking into account expression (1) from [4] and the well-known relationship $N_{ss} = C_0\Delta V/Sq$, where C_0 is the barrier-layer capacitance, S is the structure area, and q is the electron charge, we will obtain

$$\frac{Sq}{C_0}\frac{dN_{ss}}{dy} = \frac{dV}{dy} - \frac{\varepsilon_1}{\varepsilon C_0}\frac{kT}{q}C(y) - \frac{kT}{q}, \qquad (1)$$

where ε and ε_1 are the permittivity of a semiconductor and insulator, respectively; T is the temperature; and $C(y)$ is the MIS-structure capacitance depending on the surface potential.

We will use equation (2) from [4] in the form of

$$\frac{dV}{dy} = \left(\frac{dC_{exp.}}{dV}\right)^{-1}\left(1 - \frac{C_{exp.}}{C_0}\right)^2\frac{dC(y)}{dy}, \qquad (2)$$

where $C_{exp.}$ is the experimentally measured high-frequency MIS-structure capacitance. We will substitute the dependence dV/dy (2) into equation (1) and obtain an expression that presents the variation in the surface charge under changes of the surface potential. In what follows, we take advantage of the relation between the surface potential, the quasi-Fermi level, and the bending of energy bands in a semiconductor and obtain

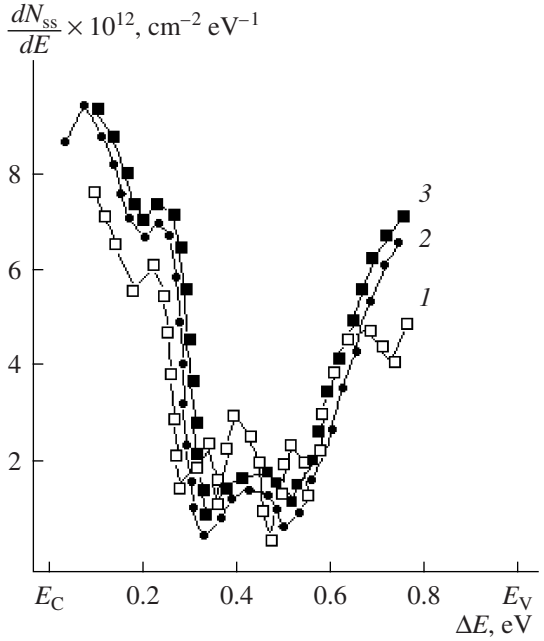

Comparison of the distributions dN_{ss}/dE for a MIS (Al–LBSG–*n*-Si) structure; the curves are plotted with the use of three methods: the method put forward here (curve *2*), the method given in [2] (curve *1*), and the method given in [6] (curve *3*).

$$\frac{dN_{ss}}{dE} = \frac{C_0}{SkT}\left(\frac{C_{exp.}C_1}{dC_{exp.}/dV} - \left(\frac{AC_{exp.}}{C_1} + \frac{kT}{q}\right) + \frac{C_{exp.}C_1}{dC_{exp.}/dV}\left(1 - \frac{BC_{exp.}^2}{C_1^2}\right)\frac{1}{e^y - 1}\right). \quad (3)$$

where

$$C_1 = 1 - \frac{C_{exp.}}{C_0}, \quad A = \frac{\varepsilon_1}{\varepsilon C_0}\frac{kT}{q}, \quad B = \frac{kT}{\varepsilon\varepsilon_0 N_M (qS)^2},$$

N_M is the impurity concentration in a semiconductor, and ε_0 is the permittivity.

As is seen from equation (3), the SSD over the gap band E in a semiconductor can be found if one immediately employs the experimental values of $C_{exp.}$, $dC_{exp.}/dV$, V, and T. The value of y entering into (3) can be obtained from the equation given by $\left.\frac{C}{C_0}\right|_{theor.} = \left.\frac{C}{C_0}\right|_{exp.}$.

The obtained relationships were tested with the test MIS structures prepared by the deposition of lead–borosilicate glass (LBSG) on an *n*-type Si(111) substrate; the single-crystal silicon was produced by the crucibleless floating-zone method. The glass contains SiO_2 (32.9%), PbO (49%), B_2O_3 (15%), Al_2O_3 (2.1%), and Ta_2O_5 (1%); the content of alkali metal oxides (KO and NaO) is under 0.01%. The electrophysical characteristics of the LBSG and the technique of its deposition on a silicon substrate are similar to those in [8]. The formation of the silicon–glass interface occurs at 700°C. The area of the gate in the obtained structure was 0.01 cm^2. The insulator layer thickness found from the MIS-structure capacitance under the enrichment operation was equal to $(2 \pm 0.1) \times 10^{-4}$ cm.

The figure presents the distribution dN_{ss}/dE for the investigated MIS structures; the spectra were obtained with method [2] (curve *1*), method [6] (curve *3*), and with the method put forward in this paper (curve *2*).

It is seen from the comparison between the obtained distributions dN_{ss}/dE over the energy-gap band width of silicon (see figure) that the distribution *2* obtained from equation (3) coincides with curve *3* in the whole energy range and is more smooth as compared to distribution *1*. In the case of distribution *2*, there is no scattering in the values of dN_{ss}/dE; this scattering have occurred if a graphical differentiation were employed; an error in the graphical differentiation manifests itself in separated peaks in the curve given by dN_{ss}/dE.

CONCLUSIONS

The method of electric differentiation with the use of equation (3) is designed to find the distribution of the SSD over the energy-gap band in a semiconductor. This procedure is less labor-consuming as compared to that given in [6] and shows the uniqueness of the solution and higher precision as compared to that given in [2].

REFERENCES

1. Nicollian, E.H. and Brews, J.R., *MOS Physics and Technology*, New York: Wiley, 1982.
2. Terman, L.M., An Investigation of Surface State at Silicon/Silicon Oxide Interface Employing Metal–Oxide–Silicon Diodes, *Solid-State Electron.*, 1962, vol. 5, no. 2, pp. 285–299.
3. Szi, S.M., *Physics of Semiconductor Devices*, New York: Wiley, 1981.
4. Vlasov, S.I., Zainabidinov, S.Z., and Karimov, I.N., Determination of Surface Charge Density at Semiconductor–Insulator Interface, *Dokl. Akad. Nauk UzSSR*, 1985, no. 4, pp. 28–30.
5. Vlasov, S.I., The Effects of Influence of Near-surface Deep Centers on the Parameters of Semiconductor–Insulator Interfaces, *Doct. Sci. (Phys.-Math.) Dissertation*, Leningrad: Physicotechn. Inst., 1991.
6. Gorban, A.P. and Litovchenko, V.G., Investigation of the Fast Surface State Spectrum of MIS Structures by a Differential *C–V* Method, *Phys. Status Solidi A*, 1972, vol. 10, no. 1, pp. 289–296.
7. Garrett, C.G.B. and Brattain, W.H., Physical Theory of Semiconductor Surfaces, *Phys. Rev.*, 1955, vol. 99, no. 2, pp. 375–387.
8. Parchinskii, P.B., Vlasov, S.I., and Nasirov, A.A., Investigation of Slowly Relaxed Charge in Passivating Coatings on the Base of Lead–Borosilicate Glasses with Isothermic Relaxation of Capacitance, *Pis'ma Zh. Tekh. Fiz.*, 2001, vol. 27, no. 18, pp. 65–70.

ISSN 1068-3755, Surface Engineering and Applied Electrochemistry, 2008, Vol. 44, No. 4, p. 341. © Allerton Press, Inc., 2008.
Original Russian Text © On the Memory of Boris Nikiforovich Zolotykh, 2008, published in Elektronnaya Obrabotka Materialov, 2008, No. 4, p. 105.

INFORMATION

On the Memory of Boris Nikiforovich Zolotykh

DOI: 10.3103/S1068375508040170

Boris Nikiforovich Zolotykh, Dr. Sci. (Tech.), professor, member of the editorial board of the journal *Electronic Treatment of Materials*, and cofounder of a new area in the technology of engineering—electroerosion treatment of materials—died on April 17, 2008, after a long illness in the 88th year of his life.

Zolotykh was one of the closest assistants of the Lazarenko, Boris Romanovich and Nataliya Iosifovna, the founders of the electroerosion method. Upon graduating from the Physical Faculty of the Moscow State University (after studying in one group with Academician A.D. Sakharov), Zolotykh began to deal with the problem of electroerosion treatment and dedicated all his life to this prospective area of science. His services to science included the creation of theoretical bases concerning the process of electroerosion destruction of materials, in particular, the development of models describing energy processes in the column of the discharge, the heating processes in the superficial layers of the electrodes, and the hydromechanical processes in the interelectrode interval. He substantiated physical models describing the evacuation of the materials undergoing phase transformations from the surface of the electrode into the volume of the working medium and removal of solid products of destruction out of the interelectrode interval. This scientist's works are distinguished for their high professional level, the organic interconnection between experimental and theoretical research, and their orientation toward achieving a particular final result of practical importance.

Zolotykh repeatedly emphasized the necessity to constantly widen and deepen our theoretical knowledge about the electric erosion process and to further develop the technological basics for this treatment method, without which any effective functioning of contemporary high-tech production is difficult to imagine.

This scientist fruitfully realized his teaching activity for many years, reading lectures and working with graduates and postgraduates at the Department of Electronic Engineering Technology of Moscow State University of Electronics and Mathematics, which was created in 1963.

The development of new industries required creating mechanisms, instruments, and technological systems of a principally new quality. At the same time, the potential of the current mechanical engineering technology became exhausted. It became fundamental to solve problems for the further advancement of the technology of industry and to search for and study novel methods of manufacturing. To solve this problem within electronic engineering, a new specialization—electrophysical and electrochemical methods of sizable treatment—was organized at the department, which was based on form-shaping methods using highly concentrated flows of energy—laser and electronic beams, impulse electric discharges, and others.

The Board of the Presidium of the Federation of Cosmonautics awarded Professor Zolotykh, the new head of the department, the title of Honored Worker of Science and Technology of the Soviet Socialist Republic and the Keldysh, Gagrin, and Glushko Medals for his creative contribution to rocketry and space technology. Training-and-research laboratories for electric erosion, electrochemistry, electronic radiation, magnetic-impulse, ultrasound, and laser technology were created at the department. Research work was conducted for more than ten years jointly with NPO Energiya, which resulted in introducing advanced technology in the manufacturing of elements of cathodes of thermoelectronic converters from tungsten monocrystals.

For nearly 30 years, Zolotykh worked as a member of the editorial board for the journal *Electronic Treatment of Materials* and always took an active part in the work of international forums concerning electronic processing methods. The buoyant memory of Professor Zolotykh will live in the hearts of those who worked and collaborated with him.

His Colleagues